POLITECNICO DI MILANO

School of Industrial and Information Engineering

Master of Science in Chemical Engineering

Department of Chemistry, Materials and Chemical Engineering

"Giulio Natta"

Innovative Oxyflue SO₂ Treatment and Oxidation Plant: Modeling and Experimental Analysis

Supervisor: Prof. Flavio Manenti

Co-supervisor: Ing. Caterina Frau

M.Sc. Thesis of: Riccardo Brazzoli

ID Number: 851450

Academic Year 2016 – 2017

Preface

This thesis has been made possible through a collaboration between Politecnico di Milano[†], in the person of Prof. Flavio Manenti, head of the Sustainable Process Engineering Research (SuPER) team[‡] and Sotacarbo S.p.A.[§] (Carbonia – Italy), where the plant under study is installed and operated.

Ai miei genitori

Ringraziamenti

Table of Contents

List of Figures

List of Tables

Abstract

Pressurized and flameless oxy-combustion of coal is an interesting opportunity to produce low impact electricity with competitive costs. One of the critical point is the treatment of the outlet flue gases coming from this process, burning high sulphur content coal. The aim of this work is to investigate, on a micro-pilot scale, a novel process, called IOSTO (Innovative Oxyflue SO_2 Treatment and Oxidation), that combines different strategic aspects: CO_2 and SO_2 capture and production of sulphuric acid. The project flue gas is composed by: 56% CO_2, 2% SO_2, 39% H_2O, 3% O_2 (molar basis); 4.5 kg/h of total flowrate. The process is mainly composed by: a dehydration section; a catalytic reactor, to convert SO_2 into SO_3; an innovative discontinuous SO_3 absorption column. The first step of the analysis concerns the modeling of the plant with the consequent collection of experimental data. Basing on the literature, a preliminary model in Aspen HYSYS® of the catalytic reactor is proposed. The simulation results show the need of a new kinetic model based on experimental data. A power-law model provides the best data fitting. The consecutive simulations show that the reactor operates in fully chemical regime and it doesn't reach the equilibrium. A design of experiments is applied to the reactor system at two levels. The first one allows to define the experiments to cover the whole operating domain and the second one, a model-based design of experiments, allows to identify optimal additional experimental points. Finally, a dynamic model of the absorption column is provided in Aspen HYSYS®. The model is validated using the project specifications in term of time to produce H_2SO_4 market grade (hundreds of hours starting from 10 kg of H_2O). The outlet gas stream is made by 97% of CO_2 (molar basis), ready for geological storage. Moreover, a deep explanation on the experimental profile of the liquid density and H_2SO_4 concentration, is also provided.

Keywords: innovative SO_2 treatment, low-rank coal, sulphur, sulphuric acid, CO_2 capture, plant modeling, Aspen HYSYS®, reaction rate estimation, regression, design of experiments, dynamic simulation, data analysis.

Sommario

L'ossicombustione pressurizzata e senza fiamma del carbone è un'opportunità interessante per produrre elettricità a basso impatto con costi competitivi. Uno dei punti critici è il trattamento dei fumi di combustione provenienti da tale processo, bruciando carbone ad alto tenore di zolfo. Lo scopo di questo lavoro è quello di indagare, su scala micro-pilota, un nuovo processo, chiamato IOSTO (Innovative Oxyflue SO_2 Treatment and Oxidation) che combina diversi aspetti strategici: cattura di CO_2 e SO_2 e produzione di acido solforico. Il fumo di combustione di progetto è composto da: 56% CO_2, 2% SO_2, 39% H_2O, 3% O_2 (base molare); 4.5 kg/h di portata totale. Il processo è composto principalmente da: una sezione di disidratazione; un reattore catalitico, per convertire SO_2 in SO_3; una colonna di assorbimento di SO_3, innovativa e discontinua. Il primo passo dell'analisi riguarda la modellazione dell'impianto con la conseguente raccolta di dati sperimentali. Basandosi sulla letteratura, viene proposto un modello preliminare in Aspen HYSYS® del reattore catalitico. I risultati di simulazione mostrano la necessità di un nuovo modello cinetico basato su dati sperimentali. Un modello power-law fornisce il miglior fitting dei dati. Le simulazioni consecutive mostrano che il reattore opera in regime puramente chimico e non raggiunge l'equilibrio. Un design of experiments viene applicato al reattore a due livelli. Il primo permette di definire gli esperimenti per coprire l'intero dominio operativo e il secondo, un model-based design of experiments, consente di identificare punti sperimentali aggiuntivi ottimali. Infine, viene fornito un modello dinamico della colonna di assorbimento in Aspen HYSYS®. Il modello viene convalidato utilizzando le specifiche del progetto in termini di tempo per produrre H_2SO_4 commerciale (centinaia di ore a partire da 10 kg di H_2O). Il gas in uscita è composto dal 97% di CO_2 (base molare), pronto per lo stoccaggio geologico. Inoltre, viene fornita una spiegazione dettagliata sul profilo sperimentale della densità del liquido e della concentrazione di H_2SO_4.

Parole chiave: trattamento innovativo SO_2, carbone di basso rango, zolfo, acido solforico, cattura CO_2, modellazione d'impianto, Aspen HYSYS®, stima della velocità di reazione, regressione, design of experiments, simulazione dinamica, analisi dei dati.

Chapter 1
Introduction

The Italian Ministry of Economic Development and ENEA signed on 21 April 2016 the program agreement under which the financial contribution is granted for the implementation of the three-year activities (2015-2017) concerning research and development of general interest projects for the national electric system. The first agreement was signed on 4 March 2013 for three-year activities (2012-2014) concerning the same goals.

This thesis work derives from the collaboration agreement between ENEA and Sotacarbo S.p.A. concerning the creation of the clean coal technological centre in the Sulcis Area (Sardinia – Italy), constituted by agreements signed by the Autonomous Region of Sardinia and the Italian Ministry of Economic Development. It follows the specific project and objectives in which this thesis is involved:

- Project B.2: capture and storage of CO_2 produced with fossil fuels.
- Objective b: CO_2 capture through oxy-combustion of coal.
- Sub-objective b.2: experimentation of a sulphuric acid recovery section from flue gases that come from oxy-combustion of coal.

The oxy-combustion of coal is an opportunity to produce electricity with very low impact on the environment and at competitive costs. It was selected, in particular, the pressurized, flameless oxy-combustion configuration. This technology, nowadays at the pilot-demonstration stage, is very promising on a large scale both from the point of view of the efficiency of the process and from the environmental point of view. For these reasons, it has been selected as one of the most cost-effective technological solutions for the demonstration project "CCS Sulcis" of the near future.

This technology was specifically developed for coal power plant on a size of 5 MW. At the end of a research program concluded in 2010 and of an engineering study for a 350 MW electric power plant, Sotacarbo S.p.A. was committed with the development of this technology related to low rank coal, such as Sulcis coal and support for the diffusion of the technology worldwide.

Later in 2013, Sotacarbo S.p.A. launched, in collaboration with ENEA and Itea (Italian company of the Sofinter Group – Ansaldo Caldaie), a project for the realization of a 48 thermal MW oxy-combustion pilot plant, which will be installed in Sulcis and tested on a significant scale for the first time on a global scale. The aim of the 48 thermal MW oxy-combustion pilot plant is to experiment low-rank coal, and particularly high-sulphur coal (such as the Sulcis coal, 6-8 %w/w of sulphur), to a scale of power that allows the design of large industrial plants (10-20 times larger) with acceptable industrial risk factors.

In 2015, in the experimental area located at the Sotacarbo Research Centre (Carbonia (CI) – Italy), it was installed a 3 $[Nm^3/h]$ micro-pilot plant for the production of commercial grade sulphuric acid from flue gases, that come from pressurized flameless oxy-combustion of coal. The plant, called IOSTO (Innovative Oxyflue SO_2 Treatment and Oxidation), represents a prototype since it is the first example of the application of sulphuric acid production, starting from flue gases with high content of CO_2 and low

concentration of SO_2 and SO_3. The plant consists of two units: the reaction section consisting of a catalytic reactor (working continuously) and the absorption section (working in batch for the liquid phase). This new process seems to be promising since combine different strategic aspects:

- Removal of SO_x from the output stream of a pressurized, flameless oxy-combustion using low rank coal, such as the Sulcis one.
- Production of commercial grade H_2SO_4.
- Production of an output gaseous stream nearly pure in CO_2, ready for geological storage without any other further treatment.

Hence, it allows the abatement of SO_x with a different way with respect to the conventional desulphurization methods; with the production of a valuable chemical (H_2SO_4), produced from non-valuable products with consequential economic benefits; combined with the production of nearly pure CO_2 ready for geological storage avoiding its release in the atmosphere.

Due to the innovative nature of this process, not documented in literature, an extensive experimental and theoretical analysis of the process is needed. The experimental tests are performed at the Sotacarbo Research Centre, where the micro-pilot plant is installed. The data analysis, theoretical study and modeling are performed in Politecnico di Milano and they are the objectives of this thesis work.

Before describing the IOSTO process and the work performed; an extensive analysis of the framework of the process under study is provided. This framework is composed by two main aspect:

- Carbon dioxide capture.
- Commercial grade H_2SO_4 production.

In the following sections, about the first point, they are analysed the techniques of CO_2 capture related with its production in coal power plants, that is the target of the analysis of this work. In particular, the focus is related on the low-rank coal, as mentioned previously. For this reason, the dissertation on CO_2 capture techniques is combined with the review on desulphurization techniques. In fact, one of features of IOSTO process is that it allows the SO_x abatement, combined with the production of nearly pure CO_2 as mentioned many times.

On the other side, about the second point, it is presented the state of the art process for the commercial grade H_2SO_4 production. In fact, one of the key point of the IOSTO process is the production of this commodity chemical, in a rather different way.

These dissertations are necessary in order to introduce and better understand the IOSTO process, since it lays on the basis of these concepts. Analysing all those aspects, it is then possible to point out the similarities and the differences, the pros and cons of the state of the art processes with respect to the IOSTO process and its framework.

1.1. Low Rank Coal

The coal of interest of this work is a low rank coal with a high amount of sulphur, that is very abundant in the southern area of Sardinia, i.e. the Sulcis area. The coal can be defined as at high sulphur content only if the sulphur composition is higher than 3 %w/w. This type of coal is a low-quality coal for at least three reasons:

- Due to the higher presence of sulphur, the heating value obtainable from a burning process of this material is lower than the one obtainable from a coal with a less percentage of sulphur. In fact, the average heating value of coal is about 8000 [kcal/kg][4]. A high sulphur content coal, such as the one available in Sulcis in Sardinia, has an average heating value of only 5700 [kcal/kg][5].

- The sulphur that is present after combustion is transformed in sulphur oxides (SO_x). These species are dragged away through the chimney and show remarkable corrosive characteristics which, if not preventively valuated, could starts corrosion phenomena and, so, bad working of the plant. Due to that, it is easy to deduce the increasing of management and maintenance costs of the site and also the risk to stop the production for extraordinary cleaning and repairing of the reactor and interested components.

- These sulphur-derived molecules are channelized through the chimney, if not specifically treated. Reached and surpassed the chimney, the SO_x molecules diffuse in the air. The major health concerns associated with exposure to high ambient concentrations of SO_2 include breathing difficulty, respiratory illness, and aggravation of existing cardiovascular disease. On the other side, anhydrides have a high propensity to react with the air humidity according to the reactions:

$$SO_{2(g)} + H_2O \rightarrow H_2SO_{3(aq)}$$
$$SO_{3(g)} + H_2O \rightarrow H_2SO_{4(aq)}$$
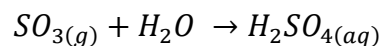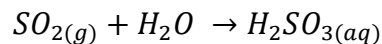
The produced acids stay dissolved in the aqueous vapor in the atmosphere. As soon as this humidity condenses, it precipitates on the ground like acid rain phenomena. This deposition causes acidification of lakes and damage to tree foliage and agricultural crops. Furthermore, acid deposition accelerates the deterioration of buildings and monuments.

The interest in this kind of coal derive from the fact that for Italy it could be an important source of energy, that are in general scarce all around the country. In fact, in the Sulcis basin, the mining field is made by about 2.5 billion tons of coal and it has been mined only the 1% of it [3]. The problem on the other side, as mentioned, is the high amount of sulphur, with the related environmental problem. A development of a clean coal technology is a mandatory constraint for the usage of high sulphur coal. The consequence is the increasing of plant investment and operational costs. The research of new processes

---

[4] US Energy Department Data.
[5] Il Carbone del Sulcis; Botteghi C.; 1979.

and technologies are the only way to reach the goal in a sustainable and economical valuable way.

1.2. Carbon Dioxide Capture

Energy production from fossil fuel combustion results in the emission of greenhouse gases, the dominant contributor being CO_2. Public awareness and legislation have led to a policy of reduction of greenhouse gas emissions in most economically well-developed countries, with the regulations partially driven by international initiatives such as the Intergovernmental Panel on Climate Change [5]. It is well known that greenhouse gas emissions from energy production can be reduced using alternative energy sources such as nuclear power and renewable energy sources. Renewable energy sources are expected to become increasingly important for our future energy demand, however, until these sources can reliably produce significant amounts of energy, the immediate energy demand is likely to be met by conventional fossil fuel combustion, a trend observed in Figure 1.1:
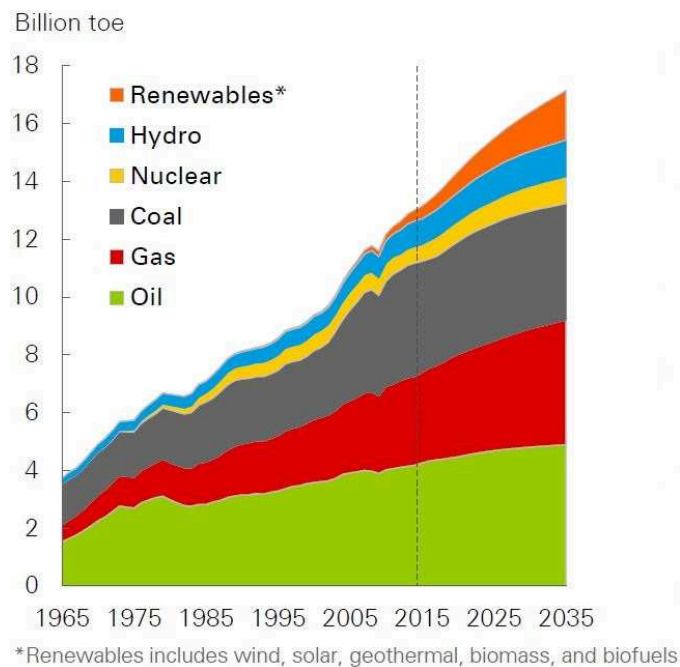
Figure 1. 1 - Primary Energy Consumption in Billion toe[6] by Fuel

Over the past decades, the role of coal as an energy source for the future has gained renewed interest for its proven stability in supply and cost and it is, therefore, very probable that coal will remain in an important position in the energy mix in the future, as clearly shown in Figure 1.1. The effect of greenhouse gasses on global climate change has been acknowledged by many governments worldwide and the reduction of the emissions of these gases is becoming increasingly important. To maintain the position of coal in the global energy mix in a carbon-constrained world, the greenhouse gas emissions, emitted

---

[6] Tonne of oil equivalent (toe) is a unit of energy defined as the amount of energy released by burning one tonne of crude oil.

from its utilization, must be reduced. To reduce greenhouse gas emissions from coal-fired power generation, several possibilities can be perceived:

- Improving efficiency of power plants.
- Introduction of combined cycles, which can reach high thermal efficiencies.
- Replacement of hydrocarbon fuels with renewable resources.
- Capture and storage of CO_2 from conventional plants.

Renewable energies may hold hope for reducing greenhouse gas emissions in an extremely long-time frame. Renewable resources, such as biomass, which can be used to directly replace coal and oil in combustion processes are not available in the quantities required for substantial substitution. With the installation of new capacity which uses modern technologies such as supercritical and ultra-supercritical boilers, the efficiency of this installed capacity continues to increase, a trend occurring worldwide. Incremental reduction of greenhouse gas emissions can be achieved by the stepwise implementation of more efficient coal-fired power plants, however, to make a significant reduction in emissions, the CO_2 generated from coal utilization needs to be captured and stored (sequestered). Several technologies are being developed for CO_2 capture and sequestration from coal fired plants, that include:

- Post combustion CO_2 capture from power plants of conventional design.
- Oxy-combustion. This involves the direct combustion of coal with pure oxygen.
- Pressurized Flameless Oxy-combustion Process. This involves the direct combustion of coal with pure oxygen with high recirculation of flue gas, allowing a volume combustion without the presence of the flame.
- Chemical looping. This involves the oxidation of an intermediate by air and the use of the oxidized intermediate to oxidize the fuel.

The first three processes are considered in the following sections while the chemical looping is not analysed. The reason is related with the fact the post combustion technology is the reference, in case of applying CO_2 capture from existing power plant. On the other side the oxy-combustion and, in particular, the pressurized flameless one is the input for the IOSTO process, object of this work.

1.2.1. Post Combustion CO_2 Capture Processes

Post combustion capture (PCC) refers to the separation of CO_2 from flue gas derived from combusting fossil fuels – coal, natural gas, or oil – in air. In the case of coal-based power plant, as shown in Figure 1.2, coal is combusted in air and the liberated heat is converted to electricity by steam-driven turbines connected to generators. The combustion results in a flue gas mixture consisting of N_2, CO_2, H_2O, O_2 and a host of compounds such as SO_x, NO_x and ashes. Some of these are removed using existing technologies such as selective catalytic reduction (SCR), for NO_x; electrostatic precipitation (ESP), for ashes; flue-gas desulphurization (FGD), for SO_x. A PCC process then aims to selectively separate CO_2 from the remaining gas mixture as shown in Figure 1.2. After capture, CO_2 can be compressed and stored underground, used in some other

processes such as enhanced oil recovery (EOR), or used in some other capacity that does not result in its emission into the atmosphere.
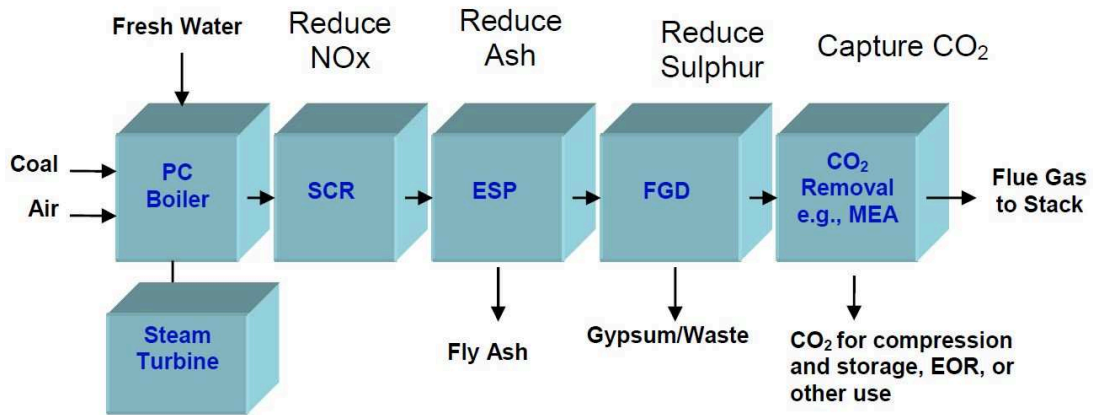
Figure 1. 2 - Typical Post Combustion Carbon Capture Process

Table 1.1 [8] shows the representative concentration of post-combustion flue gas for coal- and gas-fired power plants. There is additional variation around these values depending on the exact composition of the fuel, the efficiency of the plant, types of emission controls installed and other factors, but for purposes of CO_2 capture, 10-15% CO_2 for coal and 4-5% for natural gas are quite representative.

Gas Constituent	Coal	Natural Gas (Gas Turbine)
Nitrogen	70-75 %	73-76 %
Carbon Dioxide	10-15 %	4-5 %
Water Vapour	8-15 %	8-10 %
Oxygen	3-4 %	12-15 %
Trace Gases (SO_x, NO_x, others)	<1 %	<1 %

Table 1. 1 - Typical Composition of Flue Gases

Carbon is the predominant combustion species in coal, while both carbon and hydrogen are combusted in natural gas; thus, for each CO_2 molecule generated during combustion, coal has less energy release. This results in coal power plants typically generating twice as much CO_2 as gas power plants for the same power output, about 1 g CO_2/kWh vs. 0.5 g CO_2/kWh. However, flue gas from coal power plants has more concentrated CO_2 relative to natural gas. This results in CO_2 capture consuming less energy for coal power plants relative to gas power plants, for the same mass of CO_2 captured. Due to the predominance of coal in power production and the likelihood of CO_2-control regulations impacting those most, the overwhelming emphasis of capture process developers has been on coal-fired power plants. Research and development for capture on natural gas fired power plants is relatively scarce, though regulations may require natural gas fired power plants to have CO_2 emission controls similar to that expected for coal fired power plants.

There are several ways to perform CO_2 capture from the gas stream. The most common process is the absorption with amines, for example mono-ethanolamine as mentioned in the Figure 1.2. There are also other processes that they are discussed in the next sections.

1.2.1.1. Absorption Separation

Absorption refers to the uptake of CO_2 into the bulk phase of another material – for example, dissolving CO_2 molecules into a liquid solution, such as an aqueous amine. Absorption is used widely in the chemical, petrochemical and other industries and, as a result, operational confidence in absorption process is high. Indeed, virtually all near-term and mid-term PCC processes under development are absorption based. In a solvent-based PCC process (Figure 1.3), the flue gas is contacted with the solvent which typically contains a reagent that selectively reacts with CO_2. This contact occurs in traditional gas-liquid contactors, and CO_2 transfers from the gas phase into the liquid phase. The CO_2-loaded rich solution is pumped to a regenerator vessel where it is heated to liberate gaseous CO_2 and the lean solution is circulated back to the absorber. The liberated gaseous CO_2 is collected, dried, compressed and transported to a storage reservoir, or it may be used in some other application such as EOR. The most common example of a PCC absorption process is 30 %w/w aqueous mono-ethanolamine (MEA) which has been used commercially capturing up to 1000 tonne/day of CO_2. Current estimates of capture with MEA followed by compression for underground storage impose approximately 30% parasitic load on the net output of a power plant and increase the cost of electricity by 60-90%. These relatively high values result from the relatively large quantity of energy needed to regenerate the solvent.
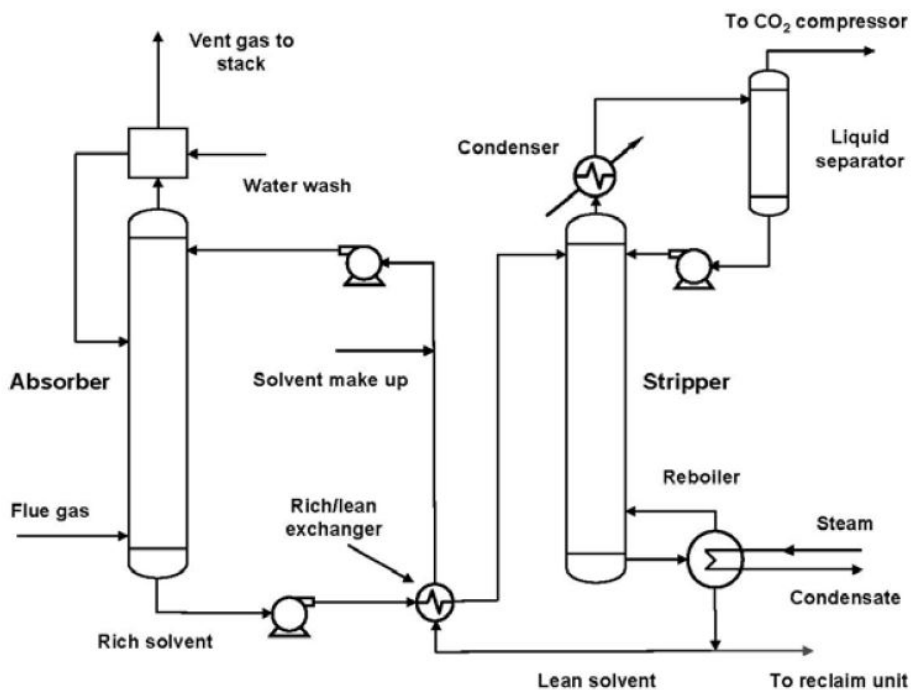
Figure 1. 3 - Absorption-based PCC process

Therefore, much of the current research in absorption-based PCC is focus on development of new solvents that reduce the regeneration energy. Examples of such new chemistries include Alstom's Chilled Ammonia Process which uses a reaction of ammonium carbonate to ammonium bicarbonate as well as a host of proprietary amines from Mitsubishi Heavy Industries, Cansolv. Some early-stage research is also being conducted in more novel chemistries involving ionic liquids, phase separation solvents, and siloxane oligomers.

1.2.1.2. Adsorption Separation

As shown in Figure 1.4 (a), adsorption typically occurs via weak Van der Waals forces for physical adsorption or stronger covalent bonding for chemisorption. Adsorption processes are implemented most often with the adsorbent used in packed beds or fluidized beds. In a packed bed (Figure 1.4 (b)), adsorbent is loaded into a column, flue gas flows through the void spaces between the adsorbent particles, and the CO_2 adsorbs onto the particle surfaces. In fluidized beds (Figure 1.4 (c)), flue gas flows upward through a column at velocities such that the adsorbent particles are suspended in the gas flow. Regardless of the process configuration, the adsorbent selectively adsorbs CO_2 from the flue gas and it is subsequently regenerated by lowering the pressure and/or increasing the temperature to liberate the adsorbed CO_2. In a packed bed configuration, regeneration is accomplished by heating the CO_2-rich adsorbent to liberate CO_2. During this time, flue gas is diverted to a second packed bed which continues to adsorb CO_2 from the gas. By alternating flue gas between two packed beds that alternatively undergo absorption and regeneration in a cycle, CO_2 can be continually removed from flue gas. In a fluidized bed, the sorbent is circulated between an absorber vessel where it contacts flue gas and a regenerator vessel where it is heated to liberate gaseous CO_2.
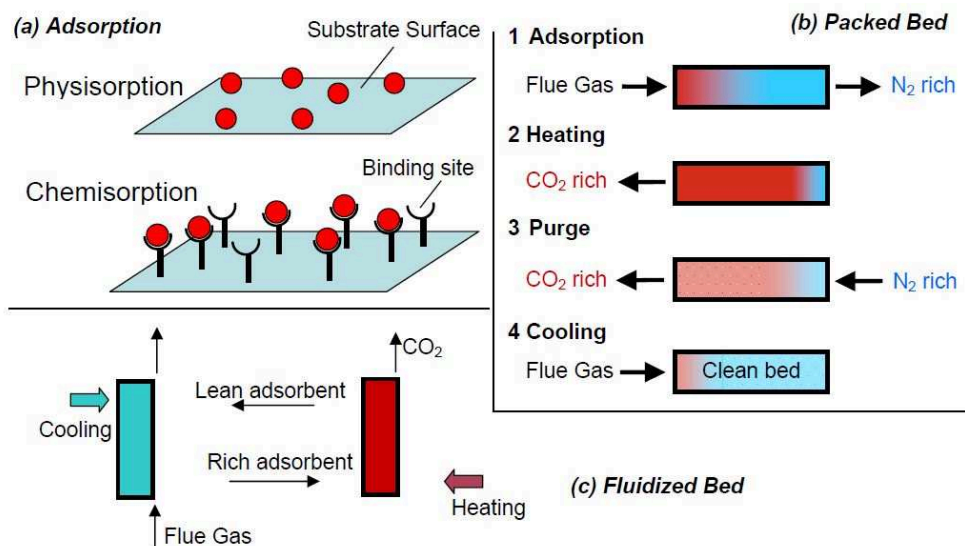
Figure 1. 4 - Adsorption-based PCC process

1.2.1.3. Membrane Separation

Membranes can separate CO_2 from flue gas by selectively permeating it through the membrane material. If CO_2 has a higher permeability (defined as the product of solubility and diffusivity) in the membrane relative to other species in the flue gas, then CO_2 will selectively permeate the membrane. In some cases, chemical agents that selectively react with CO_2 are also added to the membrane to increase the membrane's selectivity for CO_2. CO_2 transports a membrane only if its partial pressure is higher on one side of the membrane relative to the other side. This partial pressure gradient can be obtained by pressurizing the flue gas on one side of the membrane, applying a vacuum on the other side of the membrane, or both, as shown in Figure 1.5. Depending on the selectivity of the membrane, multiple membrane stages may be needed in order to obtain sufficiently high CO_2 purity. Like adsorbents, membranes are claimed to potentially offer low energy capture processes. Additional benefits could include a small foot-print for the capture system and a modular design that may allow for flexible operation. The major challenge for membranes comes from the potential fouling of the membrane surfaces from particulate matter, uncertainty about the performance and cost of large-scale efficient vacuum pumps and compressors required for PCC and the ability to integrate the process into a power plant.
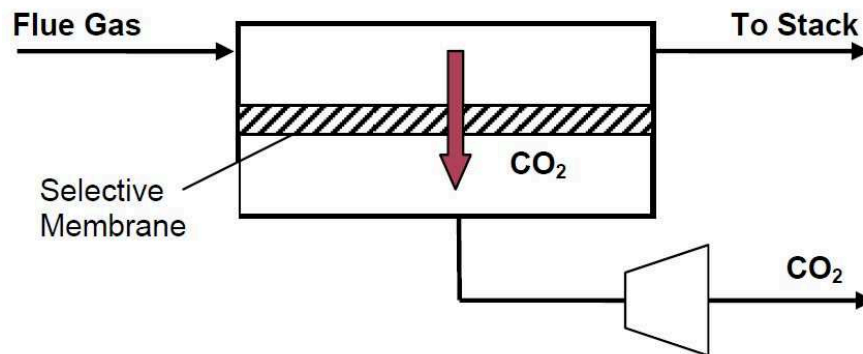
Figure 1. 5 - Membrane-based PCC process

1.2.1.4. Cryogenic Separation

The cryogenic distillation method is the unique method that allows the almost complete selectivity against the CO_2 and permit so its total removal. In the Figure 1.6 the process flow diagram is provided. The flue gas is dried to remove water and then compressed to 5–7 bar. It is then cooled in a de-sublimating heat exchanger where up to 75% of CO_2 become solid and so it is separated; the removal of pollutant (SO_2, NO_2, Hg, HCl) is provided there. The gas is expanded and cooled in a turbine, causing more CO_2 to solidify. At this point, 99% of the original CO_2 has been captured. All the captured CO_2 is pressurized, in liquid form, up to 70-80 bar. The solid CO_2 is in fact melt in the heat exchanger allowing the cooling of the inlet flue gas. This process is very efficient but since requires high pressure and very low temperature is very energy intensive.
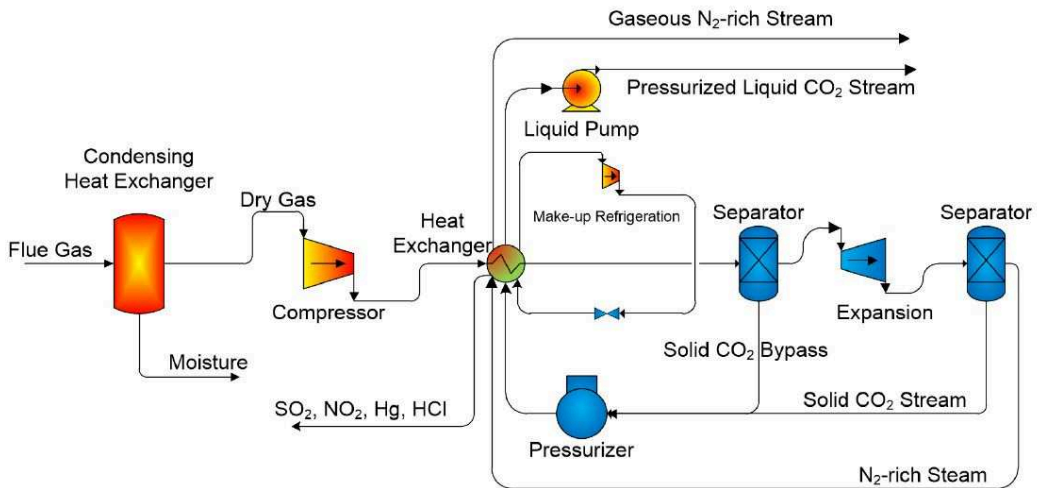
Figure 1. 6 - Cryogenic-based PCC process

1.2.2. Oxy-combustion Process

Conventional coal-fired boilers use air for combustion, in which the nitrogen from the air dilutes the CO_2 concentration in the flue gas. The capture of CO_2 from such dilute mixtures using amines or other technologies is relatively expensive. The principal advantage of oxy-combustion is that it increases very significantly the partial pressure of CO_2 in the exhaust gases from combustion, because it avoids the dilution of exhaust gases with nitrogen. Obviously, an air separation unit (ASU) is necessary to provide almost pure oxygen to the boiler. An oxy-combustion process diagram is shown in Figure 1.7.
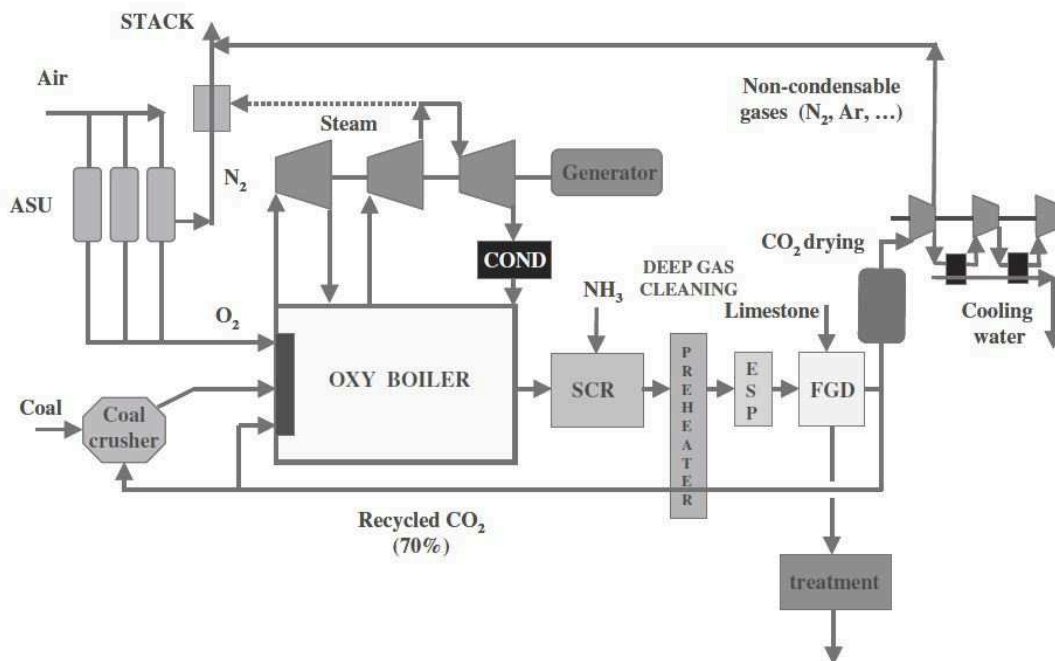
Figure 1. 7 - Oxy-combustion capture

Combustion is made using pure oxygen (up to 97% purity), but in which a small amount of nitrogen and argon remains. A big part of the exhaust gases are recycled in the boiler to maintain the usual flame temperature levels of plants without capture. This avoids full resizing of the boiler and its associated exchangers. The flow of uncycled CO_2 still contains water vapor, impurities (particularly some NO_x and SO_x amounts that remain in the exhaust gas of purification systems, i.e. SCR and FGD) and incondensable gases such as oxygen, nitrogen and argon. These latter are originating from the ASU and parasite air entries due to the lack of seal of the cycle (combustion chamber, de-duster, gas-gas heater, etc.). The content of CO_2 in these exhaust gases is of the order of 75% on wet gas. The next step is to condense the water and purify the CO_2 until 99% pure so that it can be transported in the supercritical state.

1.2.3. Pressurized Flameless Oxy-combustion Process

Up to this moment an overview on general CO_2 capture techniques is provided. Regarding to the pressurized flameless oxy-combustion, that is still a CO_2 capture technique, the aspects to analyse are more detailed. The reason is related with the fact that this kind of technology, as mentioned in the introduction pages, is the previous stage of the IOSTO process; namely the gaseous output of the pressurized flameless oxy-combustion is the input for the IOSTO process.

This technology, now at the pilot/demonstrative scale and developed by Itea, is a modification of the classical oxy-combustion, mentioned in the previous section. In the reactor, under pressure and at a uniform temperature between 1300 and 1500 °C, combustion occurs in a completely different way from traditional one: there is no formation of a flame (flameless) and the oxidation of the material takes place homogeneously throughout the whole reactor chamber in an orderly, foreseeable and controllable manner, with the exclusive production of CO_2 and water vapour. Adoption of the pressurization leads to better performance compared to atmospheric solutions. Reactor temperature is controlled by varying the amount of recycled cold fumes; the ashes melt in the reactor and fall from the bottom of the reactor in a stream of water that causes its instant solidification into inert pearls of vitreous structure. The fumes leaving the reactor at 1300 – 1500 °C consist essentially of water steam and CO_2 and they are cooled to 700 – 800 °C by being mixed with cold recycled fumes; they then enter the boiler that cools them further to about 250 °C. The heat released by the fumes is used to produce steam or for electricity production. On leaving the boiler the fumes are partially recycled to the plant; a portion go to the fumes treatment section that consisting of a condensing section to remove water, a section to remove SO_x (>99% SO_2, <1% SO_3); at the outlet, the fumes consist essentially of clean CO_2, ready for use. In fact, the presence of NO_x, particulate and heavy metals is almost negligible due to process configuration. A schematic representation of the process is provided in Figure 1.8.

This process is particularly considered in this work linked with low-rank coal with high sulphur content; with the possibility of production of energy at competitive price jointly with the reduction of emissions and CO_2 capture at relatively low cost.
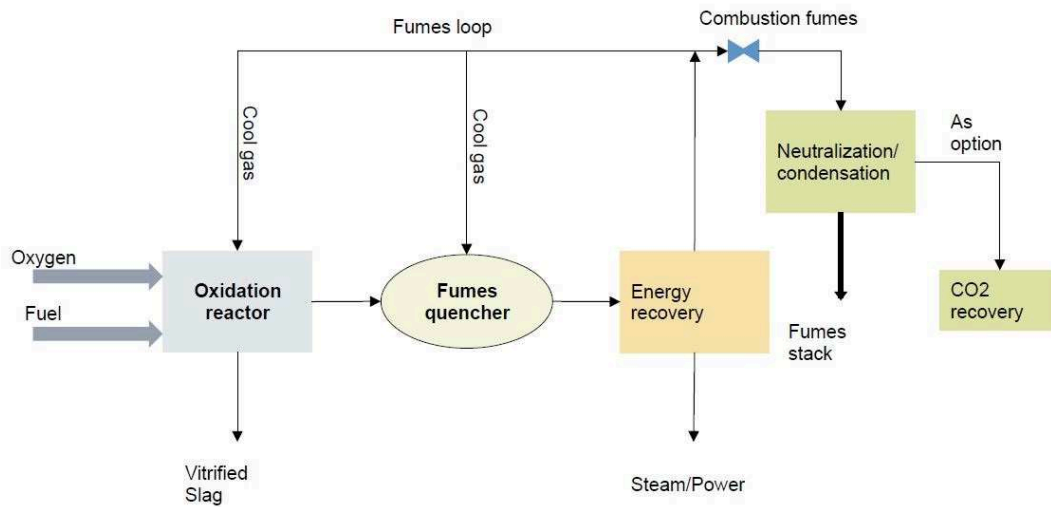
Figure 1. 8 - Pressurized Flameless Oxy-combustion Process

As mentioned above the only after treatment of flue gases is a flue gas desulphurization. There are different techniques to remove SO_x, the most important techniques, implemented industrially, are presented in following section. A promising alternative to conventional desulphurization method is the IOSTO process, that it is described in the next chapter.

It is crucial to define the typical flue gas composition before desulphurization units, referred, of course, to a pressurized flameless oxy-combustion process. The importance derives from the fact that this data are the input and reference data for the IOSTO process, studied in this thesis work. The typical flue gas composition is summarized in Table 1.2:

	Composition [%vol/vol]
Particulate	Absent
Heavy Metals	Absent
NO_x	Absent
CO_2	56%
SO_2	2%
H_2O	39%
O_2	3%

Table 1. 2 - Typical flue gas composition from flameless oxy-combustion process [2]

1.2.4. Comparison of Carbon Capture Techniques

It is worth to compare now the aforementioned CCS techniques. In fact, as said in the first pages of this work, the flameless oxy-combustion technology could be an economical sustainable carbon capture method for coal power plant, in particular referred to low-rank coal, with high sulphur content. They are now provided tangible data to justify what said

above. In Table 1.3 the technologies are compared on the basis of the two most important parameters: Net Plant Efficiency (NPE) (%LHV basis)[7] and CAPEX[8] per KWe_net.

	AC	AC + amine	AOC	FPOC base	FPOC optimized	FPOC CCS ready
NPE (%LHV basis)	40.9	29.3	31.3	36.2	38.6	42.9
CAPEX [€/kWe_net]	1700	3078	4370	4270	2710	1974
AC: air combustion; AOC: atmospheric oxy-combustion; FPOC: flameless pressurized oxy-combustion						

Table 1. 3 - Comparison of Carbon Capture Techniques [15]

The second column indicates the parameter concerning a classical coal power plant. If a PCC is applied, i.e. the commercial amine absorption, there is a drop-in term of efficiency due to the high cost for amines regeneration and an increase of the plant cost. Switching to an oxy-combustion technology the benefit in term of efficiency is clear, but with a huge increase of costs. The nowadays demonstrative flameless oxy-combustion method allows an increase of efficiency and a reduction of costs, but there is still a huge gap of improvement, as mentioned in the sixth column. The last column referred to a "CCS ready" condition, it means a FPOC with the production of a flue gas stream of CO_2 delivered in the atmosphere. These data show that, with respect to the nowadays air combustion, there is the possibility to increase efficiency, with a little bit higher CAPEX.

All these considerations are made in order to consider the valuable and promising framework in which the IOSTO process is present.

1.3. Flue Gas Desulphurization Techniques

The IOSTO process, as mentioned, is a possible and promising way to clean up oxy-combustion flue gases from SO_x. It is an alternative to classical FGD methods. In this paragraph, an overview on such these techniques is provided.

Various technologies exist to remove SO_2 from flue gas produced by coal power plants. Conventionally, FGD processes can be classified as once-through or regenerable, depending on how the sorbent is treated after it has sorbed SO_2. In once-through technologies, the spent sorbent is disposed of as a waste or utilized as a by-product. In regenerable technologies, SO_2 is released from the sorbent during the sorbent's regeneration and the SO_2 may be further processed to yield H_2SO_4, elemental sulphur, or liquid SO_2. No waste is produced in regenerable technology applications. Both once-through and regenerable technologies can be further classified as either wet or dry. In wet

---

[7] Net Plant Efficiency (%LHV basis): efficiency of a plant in percentage of the total energy content of a power plant's fuel that is converted into electricity. LHV stands for Low Heating Value, meaning that the energy of the fuel is referred to its LHV.
[8] CAPital EXpenditure of the plant, i.e. the cost of the plant.

processes, wet slurry waste or by-product is produced and the flue gas, leaving the absorber, is saturated with water. In dry processes, dry waste material or by-product is produced and the flue gas, leaving the absorber, is not saturated. The classification of FGD processes is shown in Figure 1.9.
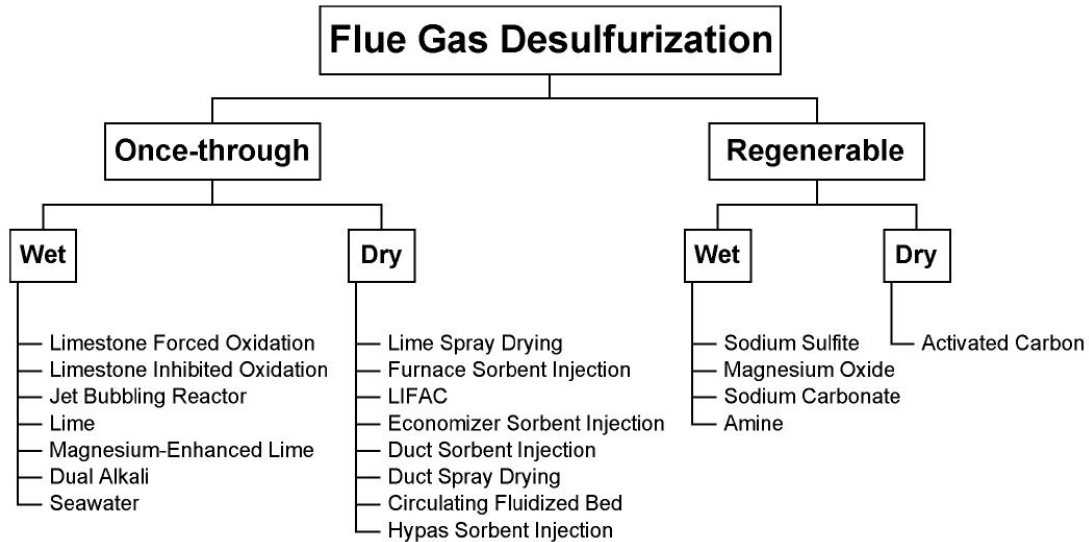
Figure 1. 9 - Classification of FGD processes

At present, regenerable FGD technologies are being used only marginally, as evident from Table 1.4. This may be because these processes involve relatively higher costs compared with other FGD processes. For example, capital costs for FGD technology application on a new 300 MWe plant, burning 2.6% sulphur coal, were estimated at 170 and 217 $/kW for wet once through FGD and sodium sulphite regenerable processes, respectively. Considering the relatively marginal application of regenerable FGD processes, only on once-through FGD processes are considered.

Technology	Generating Capacity [MWe]
Wet	196 892
Dry	24 735
Regenerable	5 192

Table 1. 4 - Generating Capacity equipped with FGD technology of Coal-fired Power Plants

Accordingly, when wet FGD is mentioned in the remainder of this work, it is meant to be once-through wet FGD. Similarly, when dry FGD is mentioned, it is meant to be once-through dry FGD.

In once-through technologies, the SO_2 is permanently bound in the sorbent, which must be disposed of as a waste or utilized as a by-product (e.g. gypsum). For each process, typical SO_2 reduction, advantages and any constraints are described.

1.3.1. Once-through Wet FGD Technology

In these technologies, SO_2-containing flue gas contacts alkaline aqueous slurry in an absorber. The slurry is generally made from either lime [typically 90% or more $Ca(OH)_2$] or limestone (typically 90% or more $CaCO_3$). The most often used absorber application is the counter current vertically oriented spray tower. A generic layout of a limestone-based wet FGD process is shown schematically in Figure 1.10. In the absorber, SO_2 dissolves in the slurry and initiates the reaction with dissolved alkaline particles. The absorber slurry effluent, containing dissolved SO_2, is held in a reaction tank, which provides the retention time for finely ground lime or limestone particles in the slurry to dissolve and to complete the reaction with the dissolved SO_2. As a result of this reaction, sulphite/sulphate crystallization occurs in the reaction tank and alkalinity of the slurry is depleted. Fresh slurry is added to the reaction tank to compensate for this depletion and thereby maintain a desired level of alkalinity. The slurry is recirculated from the reaction tank into the absorber. Reaction products from the reaction tank are pumped to the waste-handling equipment, which concentrates the waste. From the waste handling equipment, the concentrated waste is sent for disposal (ponding or stacking) or, alternatively, processed to produce a salable gypsum (calcium sulphate dihydrate) by-product.
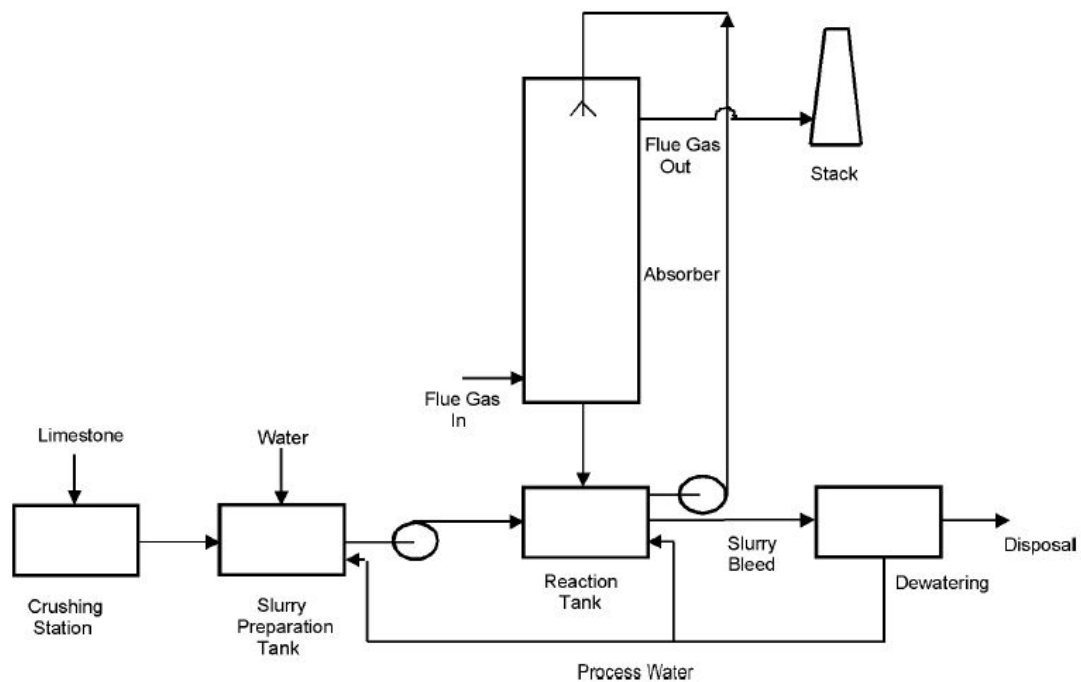
Figure 1. 10 - Wet FGD process

1.3.2. Once-through Dry FGD Technology

In these technologies, SO_2-containing flue gas contacts alkaline (most often lime) sorbent. As a result, dry waste is produced, which is generally easier to dispose of than waste produced from wet FGD processes. The sorbent can be delivered to the flue gas in an aqueous slurry form (LSD) or as a dry powder [furnace sorbent injection (FSI), LIFAC

process, economizer sorbent injection (ESI), duct sorbent injection (DSI), duct spray drying (DSD), circulating fluidized bed (CFB) or Hypas sorbent injection (HSI)]. LSD and CFB require dedicated absorber vessels for sorbent to react with SO_2, while in DSI and FSI, new hardware requirements are limited to sorbent delivery equipment. In dry processes, sorbent recirculation may be used to increase its utilization. A schematic of dry FGD processes involving dry powder injection and DSD is shown in Figure 1.11. In this figure, the flue gas flowsheet, for a plant without FGD, is shown with the solid line. Sorbent injection locations for alternative dry FGD processes with dry powder injection or DSD are shown schematically with broken lines.
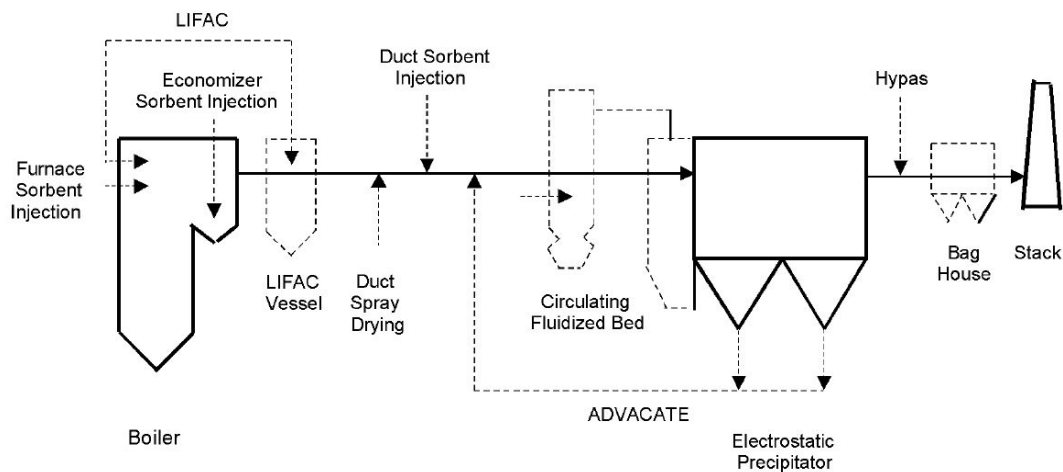
Figure 1. 11 - Sorbent Injection Processes

1.3.3. Comparison of Most Promising FGD Technologies

Limestone Forced Oxidation (LSFO) and LSD represent the most widely applied FGD technologies. Further, Magnesium-Enhanced Lime (MEL) has been used in recent FGD applications. As such, it is useful to assess the SO_2 removal performance potential of these technologies.

In order to compare these three most promising FGD, as done for the carbon capture processes, it is possible to consider the efficiency of SO_2 removal and the cost of the plant.

Most LSFO processes appear to be designed for 90% SO_2 removal; however, the state-of-the-art wet scrubbers are capable of routinely achieving SO_2 removal efficiencies of more than 95%. LSD processed often achieve greater than 90% SO_2 removal. On the other hand, state-of-the-art MEL scrubbers can achieve 98% SO_2 removal while operating at lower L/G ratios than LSFO systems designed to remove SO_2 with the same efficiency.

Regarding the cost of a FGD system, different from the removal efficiency, it depends on the sulphur content of the coal as shown in Figure 1.12. Both LSFO and MEL capital costs are higher than the capital cost for LSD across the range of coal sulphur content. Also, MEL capital cost is lower than that for LSFO across the range of coal sulphur content. These results are consistent with the fact that, in general, the amount of hardware

used decreases from LSFO to MEL to LSD. It is important to precise the size of the plant considered since the FGD plant cost per kWe depends on the size of the plant, for a bigger plant it is lower and vice versa due to scale factors.
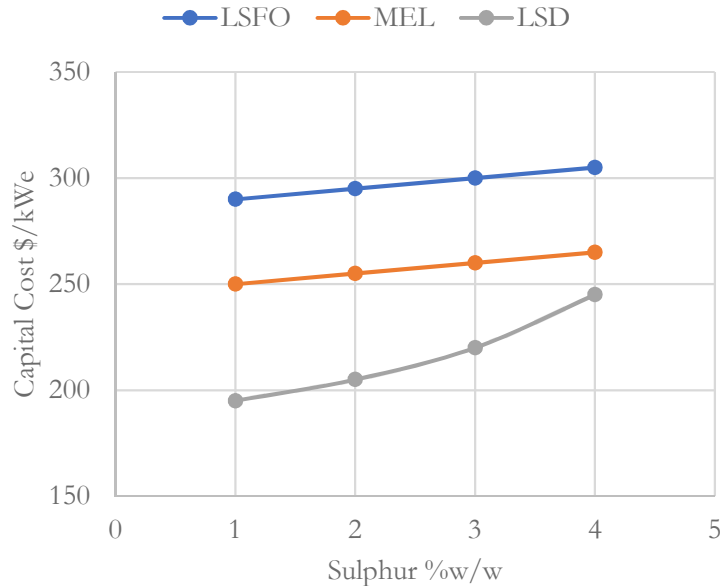
Figure 1. 12 - Capital Cost $/kWe for a 250 MWe Coal Power Plant

1.4. Sulphuric Acid Production

Sulphuric acid is a dense clear liquid. Most of its uses are indirect, in that sulphuric acid is used as a reagent rather than an ingredient. The largest single sulphuric acid consumer by far is the fertiliser industry. Sulphuric acid is used with phosphate rock in the manufacture of phosphate fertilisers. Smaller amounts are used in the production of ammonium and potassium sulphate. Substantial quantities are used as an acidic dehydrating agent in organic chemical and petrochemical processes, as well as in oil refining. In the metal processing industry, sulphuric acid is used for pickling and descaling steel; for the extraction of copper, uranium and vanadium from ores and in the non-ferrous metal purification and plating. In the inorganic chemical industry, it is used most notably in the production of titanium dioxide. Certain wood pulping processes for paper also require sulphuric acid, as do some textile and fibers processes (such as rayon and cellulose manufacture) and leather tanning. Other end uses for sulphuric acid include: effluent/water treatment, plasticisers, dyestuffs, explosives, silicate for toothpaste, adhesives, rubbers, edible oils, lubricants and the manufacture of food acids such as citric acid and lactic acid. Probably the largest use of sulphuric acid in which this chemical becomes incorporated into the final product is in organic sulphonation processes, particularly for the production of detergents. Many pharmaceuticals are also made by sulphonation processes.

Worldwide, about 231 million tonnes of sulphuric acid are produced per year (2012). The world production would be over 250 million tonnes [18] and 260 million tonnes [19] by

2018. On the other side the sulphuric acid market is very fluctuating with very high price volatility, mainly linked with small unbalances between sulphuric acid demand and supply. A recent trend of the sulphuric acid price is provided in Figure 1.13.
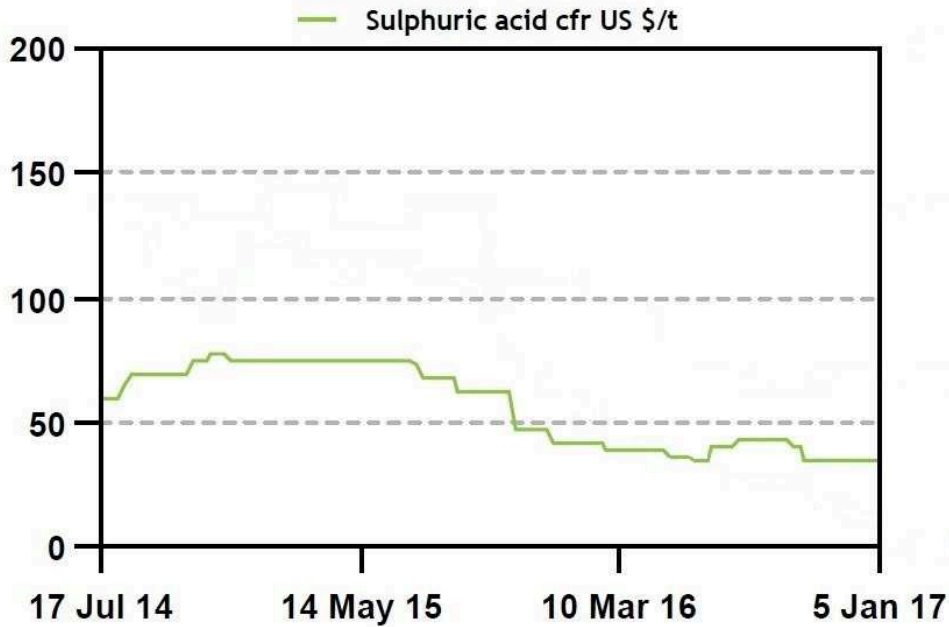
Figure 1. 13 - Sulphuric acid price trend [20]

The raw material for sulphuric acid is SO_2 gas. It is nowadays obtained by:

- Burning elemental sulphur with air.
- Smelting and roasting metal sulphide minerals.
- Decomposing contaminated (spent) sulphuric acid catalyst.

Elemental sulphur is far and away the largest source (70% of the total production). Table 1.5 describes three sulphuric acid plant feed gases. It shows that acid plant SO_2 feed is always mixed with other gases.

	Sulphur burning furnace	Sulphide minerals smelters and roasters	Spent acid decomposition furnace
SO_2 [%v/v]	11	10	9
O_2 [%v/v]	10	11	11
N_2 [%v/v]	79	79	76

Table 1. 5 - Composition of acid plant feed gas entering SO_2 oxidation convert [16]

Sulphuric acid is made industrially from these gases by:

- Catalytically reacting their SO_2 and O_2 to form $SO_3(g)$, i.e. the contact process.
- Reacting product $SO_3(g)$ from the previous step with $H_2O(l)$ in 98.5 %w/w H_2SO_4, 1.5 %w/w H_2O solution.

An example of double contact sulphuric acid flowsheet with the three main sources of SO_2 is provided in Figure 1.14.
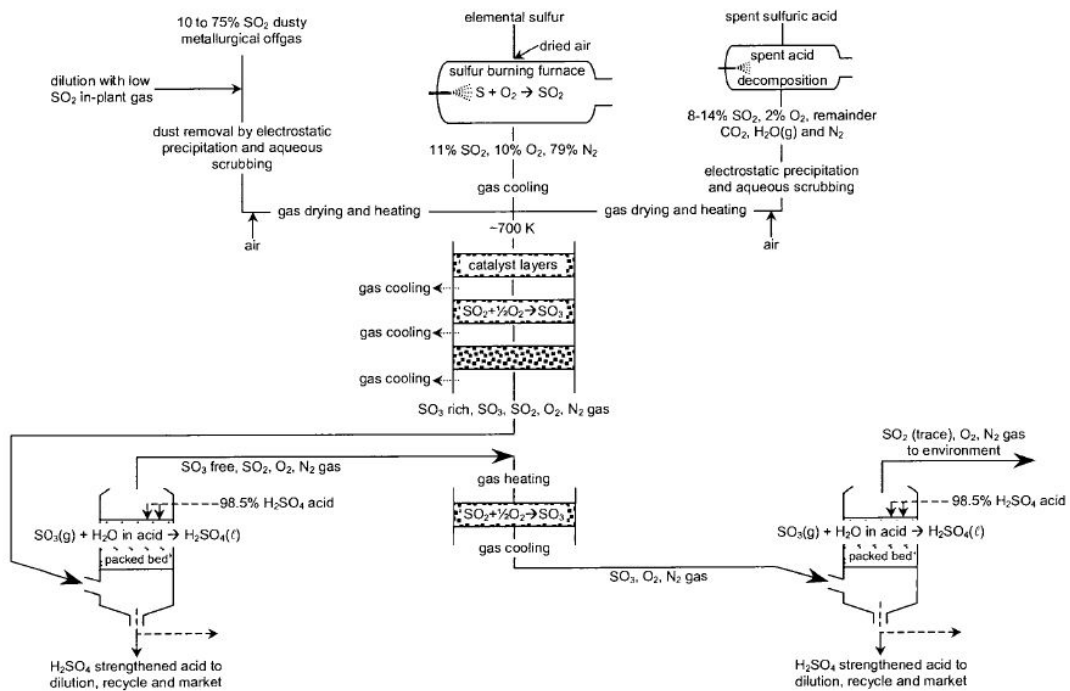
Figure 1. 14 - Double contact sulphuric acid flowsheet

1.4.1. Sulphur Burning

All the sulphur is obtained as a by-product from refining natural gas and petroleum. The sulphur is made into SO_2 acid plant feed by: melting the sulphur, spraying it into a hot furnace (1400 K) and burning the droplets with dried air. The reaction is:

$$S_{(l)} + O_{2(g)} \rightarrow SO_{2(g)} \quad \Delta H° \approx -300 \ kJ \ per \ mol \ of \ S_{(l)}$$
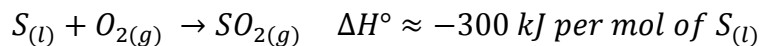
Very little $SO_3(g)$ forms at the 1400 K flame temperature of this reaction. The outlet gases, after cooling to about 700 K, are ready for catalytic SO_2 oxidation and subsequent H_2SO_4 making.

1.4.2. Metallurgical Offgas

SO_2 in smelting and roasting gas accounts for about 20% of sulphuric acid production. The SO_2 is ready for sulphuric acid manufacture, but the gas is dusty. If left in the gas, the dust would plug the downstream catalyst layers and block gas flow. It must be removed before the gas goes to catalytic SO_2 oxidation. It is removed by combinations of: settling in waste heat boilers, electrostatic precipitation and scrubbing with water (which also removes impurity vapours). After treatment, the gas contains about 1 milligram of dust per Nm^3 of gas. It is ready for drying, catalytic SO_2 oxidation and H_2SO_4 making.

1.4.3. Spent Acid Regeneration

A major use of sulphuric acid is as catalyst for petroleum refining and polymer manufacture. The acid becomes contaminated with water, hydrocarbons and other compounds during this use. It is regenerated by:

- Spraying the acid into a hot furnace (about 1300 K) where the acid decomposes to SO_2, O_2 and $H_2O(g)$.
- Cleaning and drying the furnace offgas.
- Catalytically oxidizing the offgas SO_2 to SO_3.
- Making the resulting $SO_3(g)$ into new $H_2SO_4(l)$ by contact with strong sulphuric acid.

About 10% of sulphuric acid is made this way. Virtually all is re-used for petroleum refining and polymer manufacture.

1.4.4. Catalytic Oxidation of SO_2 to SO_3

Catalytic oxidation of SO_2 to SO_3 is a very strong exothermic reaction, its heat of reaction provides considerable energy for operating the plant. The reaction is:

$$SO_{2(g)} + 0.5O_{2(g)} \leftrightarrow SO_{3(g)} \quad \Delta H° \approx -98.3 \; kJ \; per \; mol \; of \; SO_{2(g)}$$

The oxidation occurs only in presence of a catalyst. There are three types of catalysts for this system: platinum (Pt), vanadium anhydride (V_2O_5) and ferric oxide (Fe_2O_3). The activation temperature of each of them (i.e. the temperature below which the catalyst is not active) increases from 300 °C for Pt to about 500 °C of Fe_2O_3. The use of platinum is preferable for the lower work temperature with a consequent increase in conversion, being the reaction an exothermic oxidation and thermodynamically limited. Nevertheless, the most used catalyst is vanadium pentoxide which is more convenient than platinum, especially from the point of view of poison resistance. The working temperature is therefore between 450 and 500 °C, temperature above which the conversion decreases suddenly.

The feed stream must be dried before entering in the catalytic reactor. In fact, the dryness avoids accidental formation of H_2SO_4 by reaction of $H_2O(g)$ with the $SO_3(g)$ product; condensation of the H_2SO_4 in cool flues and heat exchangers and corrosion.

The temperature range at which it is possible to operate is therefore very narrow, below 100 °C. It is not convenient to run the reaction in one pass on the catalyst, which would imply the impossibility of accurate temperature control in the reactor. Therefore, in industrial scale systems, the reactor is composed of several adiabatic layers of catalyst with intermediate cooling, as shown in previous Figure 1.14. Cooling is carried out by means of heat exchangers where the coolant fluid is the mixture of fresh gas entering the reactor, that is preheated, or by direct injection in the catalyst layers of a certain amount of fresh mixture that it is mixed with the partially reacted gases. The used reactant is not pure oxygen but air that allows better temperature control, due to the presence of the nitrogen

that absorbs part of the reaction heat. In particular, excess air is used in such a way to have a $SO_2/O_2 = 1$ input to the reactor instead of the stoichiometric ratio equal to 2. The working pressure is atmospheric, since air is used. Anyway, the increase of conversion that it is possible to obtain with the increase of pressure is modest; although in the reaction there is a decrease of the number of moles (thermodynamic reason). The conversions that are obtained industrially are almost total (97-98%). The operating temperature is mainly due to the type of catalyst used. With platinum, it is possible operate at 300 °C, while the V_2O_5 requires temperatures slightly above 400 °C.

From what it has been described above, it is clear that SO_2 to SO_3 catalytic conversion technology is well established and it does not require any additional experimental activity for a SO_2 and air mixture, typical of the plants currently in use (Table 1.5). In the case of a gas stream coming from an oxy-combustion, large quantities of CO_2 are present in the feed mix (Table 1.2). That is the case of the IOSTO process, a promising typology of sulphuric acid plant but with some modification with respect to the industrial layout. For these reasons, this process is deeply analysed in following chapter, also because it is the object of the thesis work.

1.4.5. H_2SO_4 Production

H_2SO_4 is produced by contacting cooled SO_3, from effluent gas stream of the catalytic reactor, with strong sulphuric acid in an absorbing tower; the reaction is:

$$SO_{3(g)} + H_2O_{(l)} \rightarrow H_2SO_{4(l)} \quad \Delta H° \approx -130 \; kJ \; per \; mol \; of \; SO_{3(g)}$$

$H_2SO_4(l)$ is not made by reacting $SO_3(g)$ with water. This is because the reaction is so exothermic that the product would be hot H_2SO_4 vapour; which is difficult and expensive to condense and create corrosion problems. The small amount of $H_2O(l)$ limits the extent of the reaction and the large amount of $H_2SO_4(l)$ warms only of 25 °C.

The absorption plant is normally made up of two towers, i.e. dual-stage absorption plant. In this kind of process, an absorption stage, usually before the last catalytic section, is installed to increase the efficiency of the conversion process, thus reaching values close to 100%.

Chapter 2
IOSTO Description

The Innovative Oxyflue SO_2 Treatment and Oxidation process, i.e. IOSTO process, is a micro-pilot scale plant for the flue gas desulphurization. This plant is installed at the Sotacarbo Research Centre (Carbonia (CI) – Italy), commissioned from Sotacarbo S.p.A, built from HySyTech s.r.l. on a turn-key basis. A simple sketch of the plant layout is provided in Figure 2.1.
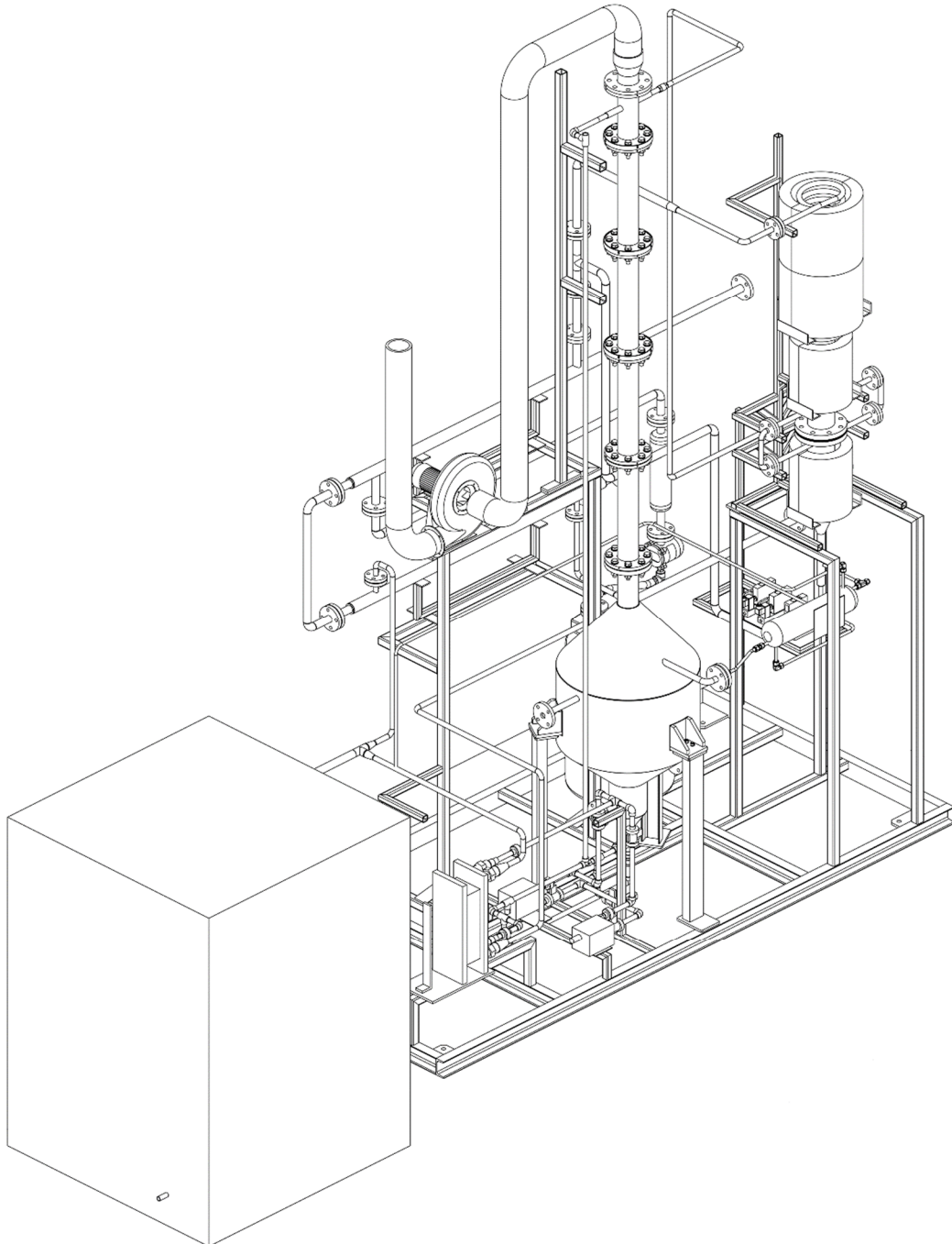
Figure 2. 1 - Sketch of IOSTO layout

The plant represents a prototype since it is the first example of the application of sulphuric acid production, starting from flue gases with high content of CO_2 and low concentration of SO_2 and SO_3. The plant consists of two units: the reaction section consisting of a catalytic reactor (working continuously) and the absorption section (working in batch for the liquid phase).

The flue gases, fed to the system, are the typical effluent of a pressurized flameless oxy-combustor that is fed with low-rank coal, with high sulphur content. In project conditions the feed gas stream comes from a bleed located downstream of a turboexpander, positioned after an economizer boiler. The turboexpander has the function to recover energy decreasing the pressure of oxy-combustion gases, since the IOSTO process works at a pressure little above the atmospheric pressure. The size of the micro-pilot scale plant is 3 Nm^3/h of inlet flue gases. On a service base of 330 days a year (35 days of programmed annual shut-down, not necessarily continuous), the plant has a service factor of 0.90; equal to 7 920 hours per year, not necessarily continuous. Under project conditions, the feed stream (from now on indicated as "Exhausted Gas") has the characteristics indicated in Table 2.1.

Exhausted Gas	
Total Flow Rate	4.5 kg/h (3 Nm^3/h)
Temperature	450 °C
Pressure	0.2 barg
Composition [%vol/vol]	
Particulate	Absent
Heavy Metals	Absent
NO_x	Absent
CO_2	56%
SO_2	2%
H_2O	39%
O_2	3%

Table 2. 1 - Exhausted Gas characteristics

The plant can also be fed with a mixture of synthetic gas at room temperature and atmospheric pressure (from now on indicated as "Simulated Gas"), with the characteristic indicated in Table 2.2.

Simulated Gas	
Total Flow Rate	3.7 kg/h
Temperature	25 °C
Pressure	0.2 barg
Composition [%vol/vol]	
Particulate	Absent
Heavy Metals	Absent
NO_x	Absent
CO_2	91.63%
SO_2	3.16%
H_2O	0%
O_2	5.21%

Table 2. 2 - Simulated Gas characteristics

2.1. Process Description

The process consists of the following steps:

- Dehydration of flue gases (only exhausted gas).
- Heating of dehydrated flue gases entering the reactor at a temperature of 350 °C (exhaust gas and simulated gas).
- Catalytic oxidation of SO_2 to SO_3.
- SO_3 absorption in H_2O to form H_2SO_4.

The process flow diagram (PFD) is provided in Figure 2.2, in order to better understand the following process description. The steps belong to two different principal sections, called Package Units (PU):

- PU-01: dehydration of flue gases, heating of dehydrated flue gases entering the reactor, catalytic oxidation of SO_2 to SO_3.
- PU-02: SO_3 absorption in H_2O to form H_2SO_4.

This conceptual division is done since in the following chapters the two PU are described separately. The interface between the two PU is the stream that pass through the heat exchanger E-104, as it described later on.

The inlet exhausted gases, stream 1, could be substituted with simulated gas, as mentioned previously. The only difference is that, if stream 1 is simulated gas, there is a bypass of the dehydration section, that isn't shown in Figure 2.2.

During the start-up phase, it is necessary to heat the dehydrated stream through an electric heater (F-101) to a suitable temperature for the beginning of the oxidation reaction. It is link with the fact that it is present, in the plant layout, a heat recovery section in which the wet hot flue gases gives heat to the dehydrated stream (E-101). The rest of the heat exchange is done in E-102, where the stream 1.1 is cooled down using cooling water, stream 2. In the case of synthetic gas as feed stream, the electric heater will have to run

for the entire duration of the process, since it is feed from bottles at ambient temperature and at 4 barg.
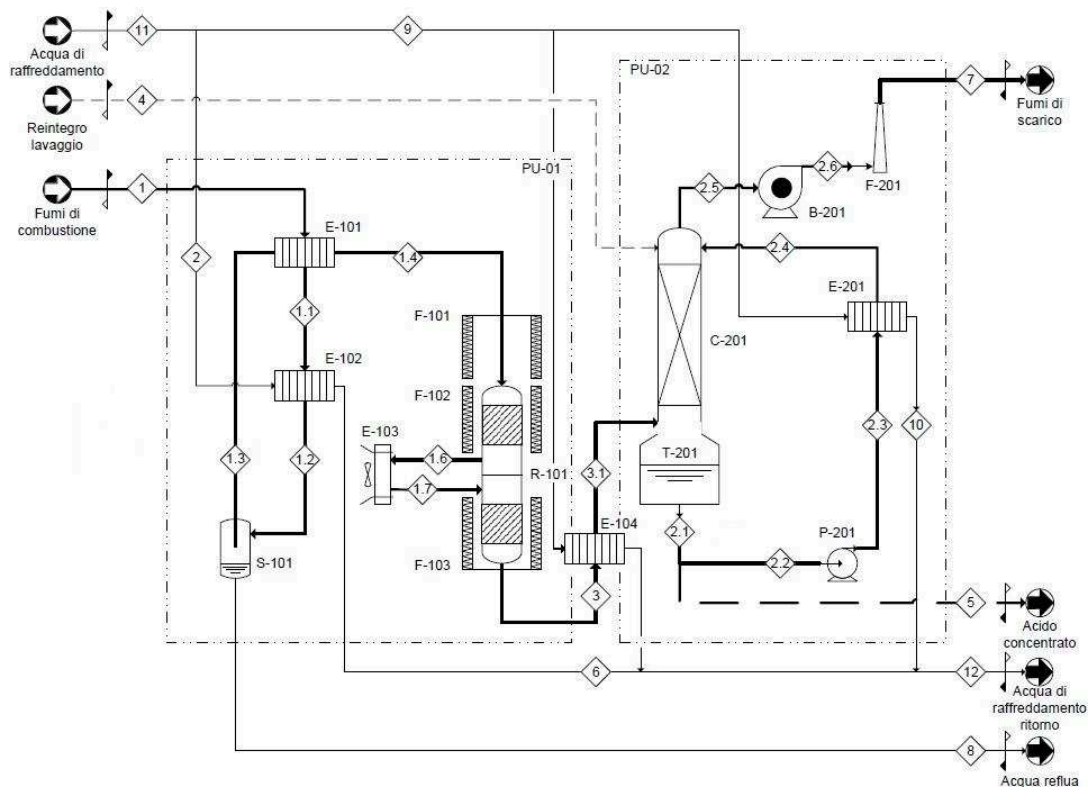
Figure 2. 2 - IOSTO PFD

Oxidation from SO_2 to SO_3 is an exothermic catalytic reaction and it involves the use of a Pt catalyst supported on alumina, with an activation temperature of about 300 °C. The average temperature of the reaction is about 350 °C. The two-stage catalytic reactor is equipped with two electric heaters (one for each stage, F-102 and F-103) in order to maintain the temperature of the reaction at a constant value. Intermediate cooling between the two catalytic stages is provided (E-103), which can be done naturally (natural convection) or forced (by installing aerothermal coolers). The intermediate cooling procedure is link with the fact that this catalytic reaction is exothermic and thermodynamically limited, so the cooling could improve the outlet conversion.

The absorption column (C-201) in PVDF is operated in discontinuous mode. Specifically, at the beginning of the plant working cycle, the bottom column is filled with water or a solution of diluted H_2SO_4, i.e. stream 4, at a lower concentration with respect to commercial grade sulphuric acid.

Exhaust gases from the reactor are cooled before entering in the absorption column, at the interface between the PU in E-104, using cooling water. They cross the column in counter current with the aqueous solution, producing sulphuric acid that is continuously recirculated (streams 2.1 to 2.4) at the top of the column with the use of a pump (P-201), after cooling in a heat exchanger (E-201) with cooling water. The product acid is collected

at the bottom of the column at about 40 °C, in T-201. CO_2-rich gases are purged at about 40 °C from the top of the column, stream 2.5. A blower (B-201) is present in order to allows sufficient gas flow. The absorption column, consequently, works at about 40 °C.

The project specification, from HySyTech s.r.l., states a conversion from SO_2 to SO_3 equals to 99.7% and a total conversion of SO_3 in H_2SO_4; with the production of a gaseous stream (stream 7) with 97 %vol/vol of CO_2, ready for direct geological storage. All the temperature, pressure, flow rate and composition of each stream are provided in Appendix 1, at the end of the text. These values need experimental validation because they are obtained from thermodynamic and kinetic data relating to commercial processes, without considering the effect of low SO_2 partial pressure and the presence of high CO_2 concentration. The batch cycle concludes when sulphuric acid in T-201 reach the concentration of 98 %w/w. Once this condition is reached, the acid is taken in stream 5 and another cycle could start.

In the following chapters, in which it is presented the real content of this work, among all the activities performed, the experimental analysis of the IOSTO plant is shown. The final aim is to experimental validate the project specifications.

2.2. Detind Description of the Plant

The tool needed to have a better understanding of the plant is the P&ID, that it is provided in Figure 2.3, while in Figure 2.4 its legend it is given.

Figure 2. 3 - IOSTO P&ID

Figure 2. 4 - P&ID legend

2.2.1. Simulated Gas Distribution System

The gas distribution system consists of 4 lines, one for each gas: CO_2, N_2, O_2 and SO_2, connected to the four bottles located inside a safety box, Figure 2.5. The feed gases are only CO_2, O_2 and SO_2 but also N_2 is necessary. The N_2 bottle is used to make inertization in the plant and also as substitute of CO_2 in some experimental test, as it is explained in the following chapters.

Figure 2. 5 - Safety box and storage area for gas bottles

The distribution lines are made with pre-treated inox pipes. Each line is equipped with a first stage decompression groups for reducing the pressure to the distribution line value (operating pressure 10 bar, maximum permissible pressure 18 bar).

Downstream of the decompression groups, they are positioned shut-off valves for the pressure reduction, at the required value of the Burkett mass flow controller, Figure 2.6.

Figure 2. 6 - Burkett mass flow controller

2.2.2. Exhaust Gas Dehydration Section

The dehydration section, Figure 2.7, has the function of eliminating the water contained in the exhausted gases and consists of a regenerative exchanger E-101 (hot side from 450 °C to 249 °C, cold side 30 °C to 350 °C), an E-102 condenser (hot side from 249 °C to

30 ° C, cold side from 20 °C to 35 °C), a condensate separator S-101 and a condensate tank V-101. The E-101, E-102, S-101 equipment are highlighted in Figure 2.7.

Figure 2. 7 - Dehydration Section

In particular, the heat exchangers E-101 and E-102 are double-pipe heat exchangers and a simple sketch of the layout is provided in Figure 2.8.
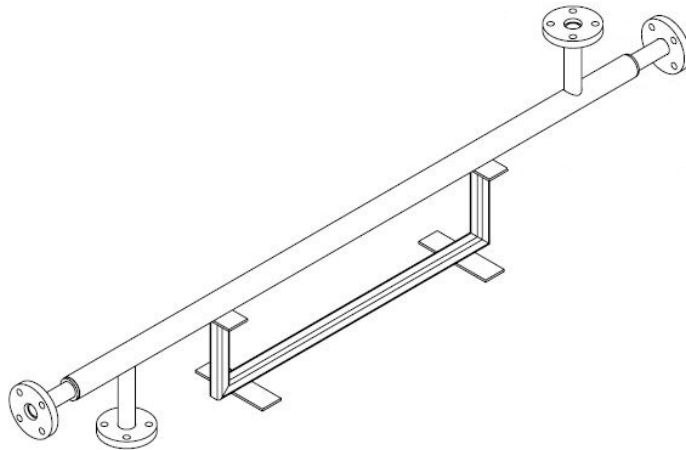
Figure 2. 8 - Sketch of double-pipe heat exchanger

2.2.3. Two-stage Catalytic Reactor

The catalytic reactor, Figure 2.9, has a height of 1 m and an inner diameter of 83 mm and it consists of two inter-refrigerated catalytic stages (natural convection with the predisposition of aerothermal coolers). Each stage is filled with Pt catalyst spheres supported on Al_2O_3, in particular it is an oxidation catalyst (EnviCat® VOC-2531 SPH 3-

5) synthetized by Clariant in a batch of 10 kg for Sotacarbo. The useful catalyst specifications are provided in Table 2.3.

Sphere Diameter [mm]	3 – 5
Catalyst density [kg/m^3]	1373
Surface Area [m^2/g]	110
Pt Density [kg$_{Pt}$/kg$_{cat}$]	0.001
Max. Catalyst Temperature [°C]	650

Table 2. 3 - Catalyst properties

Figure 2. 9 - Two different view of the catalytic reactor

In Figure 2.9 the section of pipe between the two stages is highlighted with white dashed line. It is worth to say that this reactor is quite different from an industrial reactor for the SO_2 oxidation to SO_3. In fact, industrially, the reaction is performed in a multi stage adiabatic reactor, with intermediate cooling, to push the conversion, overcoming the thermodynamic constraint. The logics applied for cooling in this pilot scale reactor are the same for the industrial one. The key point is that, since the reactor is quite small, it has a high surface per unit volume and the dilution of the reactant species is very high. As consequence, the reactor it is more like an isothermal reactor instead of an adiabatic one. The setpoint temperature of each stage, in presence of Pt catalyst, is about 350 °C. In order to reach and maintain the temperature at the pre-established value, there are electric heaters at the reactor inlet (F-101) and around each catalytic stage (F-102 and F-103). The presence of these last two electric heaters is link with the reactor design, in fact,

although the reaction is exothermic, there is the necessity to maintain the temperature due to high thermal dissipation. The high thermal dissipations could be also related to the thermal bridge phenomenon. Even though the reactor is insulated from the external environment, it could exit some connection points that allow to the heat to flow, from the reaction environment to the external ambient. It is reasonable to address this task to the metallic support structure, connecting the reactor to the skid. In fact, this structure is directly linked with the metallic pipe of the reactor and, so, it is exposed to the thermal gradient that allows to the heat to flow, as said. In Appendix 2 it is reported the drawing of the reactor section without the insulation, where the supporting structure is well visible.

2.2.4. Absorption Column

The gases that exit the second stage of the catalytic reactor are cooled down in E-104, Figure 2.10. The absorption column, Figure 2.11, in PVDF (90 mm inner diameter, 4 m height) is a discontinuous equipment operated at 0.2 bar, with random packings. At the beginning of the plant's work cycle, the bottom column is filled with water or a solution of H_2SO_4 at a lower concentration than the commercial one. The project value for the liquid batch is equal to 10 kg of water. The operative temperature of the column is 40 °C. The recirculated fluid is maintained at a flowrate of 0.54 m^3/h with the use of P-201A; the pump P-201B is not used in normal operative conditions and it is set at a value of 1 m^3/h. The liquid stream is then cooled to about 40 °C by a plate heat exchanger. The detail of the pumps and of the plate heat exchanger is provided in Figure 2.12.

Figure 2. 10 - Inlet absorption column gases cooler

Figure 2. 11 - Absorption column

Figure 2. 12 - Plate heat exchanger and recirculating liquid pumps detail

2.2.5. Storage Tank for Commercial Grade H_2SO_4 Product

The storage tank of PVDF (resistant to high concentrations of sulphuric acid), Figure 2.13, has a capacity of 1 000 L. It is equipped with two pumps: one for loading (from the bottom of the absorption column) and one for discharge (to the battery limit of the plant). The tank is equipped with low-level and high-level sensors and a thermocouple to monitor the temperature of the solution inside. Mixing of acid solutions at different concentrations is exothermic and it could cause dangerous temperature increases inside the tank.

Figure 2. 13 - Storage tank for commercial grade H_2SO_4

2.2.6 Sample Ports

The IOSTO plant is an experimental micro-pilot plant. Different from an industrial plant there are several sample ports with the aim of analysing the composition of the process streams and to evaluate the efficiency and performance of the individual equipment. The sampling points for liquid streams are:

- Waste water from exhaust gas dehydration, stream 8.
- Recirculated liquid at the absorption column outlet, stream 2.1.

The sampling points for gas streams are:

- Inlet of exhaust gas line, stream 1.
- Inlet of the first stage of the reactor, stream 1.4.
- Inlet of the second stage of the reactor, stream 1.7.
- Outlet of the second stage of the reactor, stream 3.

- Off gases from the absorption column, stream 2.6.

2.2.7. Operation, Monitoring and Control Plant System

The plant is operated, monitored and controlled directly on an electric panel that is positioned on the plant skid in a safety zone (area not classified, according to ATEX[9] directive), Figure 2.14. This system works both for normal operation (also manual mode) both for emergency operation.

Figure 2. 14 - Electric panel

The system guarantee:

- Monitoring of the process variables.
- Data storage.
- Direct operation on manipulated variables, set-points, valves opening and closing, equipment switch-on and switch-off.

It consists of two parts that allow the control of the plant, keeping of safety conditions and communication with the plant:

- Control system including acquisition modules (Programmable Logic Controller, PLC).
- Emergency shut-down system (ESD).

---

[9] EU Directive describing what equipment and work environment is allowed in an environment with an explosive atmosphere.

The main actions for the normal operation of the plant are carried out by the PLC through a control software with touch screen interface, where all logic operations and sequences are implemented. In an emergency condition, interlocks implemented in the ESD perform actions to restore safety conditions. The system registers, makes visible and manages alarms from the process to ensure operator intervention in case of necessity.

All control loops can be controlled, set up and monitored on the panel through the various control modules, switches and warning light placed on it. Malfunction alarms are displayed by means of special indicators applied to the panel. The system is equipped with appropriate tools and safety components to identify anomalous operating conditions.

2.2.8. Control Loop Summary

It is now provided a brief explanation of the control loops of the process; the aim is to understand which is the control philosophy of IOSTO. For the nomenclature of the loops, the P&ID provides all the information needed.

- Loop 114, 115, 116, 117: control of the inlet flowrate of each stream of simulated gases, N_2, SO_2, O_2, CO_2; manipulating the same flowrate, through a valve.
- Loop 102: control of the outlet gas temperature of E-102; manipulating the cooling water stream, through a valve.
- Loop 103: control of the temperature of gases before the first-stage of the reactor, after the heating in F-101; manipulating the power supply of F-101, through a solid-state relay.
- Loop 104: control of the temperature of gases after the first-stage of the reactor; manipulating the power supply of F-102, through a solid-state relay.
- Loop 105: control of the temperature of gases after the second-stage of the reactor; manipulating the power supply of F-103, through a solid-state relay.
- Loop 106: (only with forced cooling with aerothermal cooler) control of the temperature of gases before the second-stage of the reactor, after cooling; manipulating the power supply of the aerothermal cooler, through a solid-state relay.
- Loop 202: control of the temperature of the recirculating liquid, after the cooling in E-201; manipulating the cooling water stream, through a valve.
- Loop 203: control of the top pressure of the absorption column and if the pressure is too low and it doesn't allow the correct operation of the column, the PLC switch-on the blower B-201 receiving as input the pressure value of the column.

2.2.9. Safety Interlock Summary

It is now provided a brief explanation of the safety interlock logics of the process; the aim is to understand the philosophy of action for the operator protection in case of problems, due to the hazardous nature of the plant. For the nomenclature of the loops, the P&ID provides all the information needed.

- Interlocks I01 – I02 on electrical heaters F-101 A/B for high temperature (700 °C) measured by sensors TT-110 – TT-111. Action: shut-down of the electrical heaters.
- Interlock I03 on electrical heater F-102 for high temperature (700 °C) measured by sensors TT-112. Action: shut-down of the electrical heater.
- Interlock I04 on electrical heater F-103 for high temperature (700 °C) measured by sensors TT-113. Action: shut-down of the electrical heater.
- Interlock I09 on electrical heaters F-102 – F-103 for high process gas temperature measured by TT-104 – TT-105. Action: shut-down of the electrical heaters.
- Interlock I05 for low liquid level of tank T-201. Action: stop of the recirculation pump P-201A.
- Interlock I06 high liquid density of tank T-201. Action: stop of the recirculation pump P-201A.

Chapter 3
Preliminary Analysis towards Design of Experiments

After the description of the framework of the IOSTO process and the explanation of the IOSTO plant itself, there is the necessity to clarify the objective and the content of the work. The principal goal is to verify the feasibility of this innovative process through a series of experimental tests and optimize the process operations for future developments. They are performed several activities concerning: theoretical analysis of the process through literature information, modeling of the plant using commercial software, design of experiments, analysis of data and integration of those data with theoretical studies and model, in order to have a better and coherent picture of the plant behaviour.

In this chapter, the early activities concerning the preliminary modeling of the plant, through general information, are provided. Even though the process is a unique prototype, a literature analysis is performed; in particular related to conventional sulphuric acid plant where some useful information and considerations can be taken into account. The first experimental campaign on IOSTO is then considered, through which it is possible to look the problems and the differences related to the passage from a theoretical and ideal environment to an experimental and real one. This comparison shows the need of an adequate planning of proper experiments, final output of this chapter.

3.1. SO_2 to SO_3 Catalytic Oxidation Literature Analysis

As mentioned in the previous chapter, in the IOSTO catalytic reactor is used Pt as active phase for the catalyst. Platinum, as all the noble metals in general, presents lower activation temperature with respect to transition metals. In fact, regarding to catalytic oxidation of SO_2 to SO_3, it could be performed at a temperature above 300 °C for Pt and 400 °C for industrial V_2O_5 catalyst. The information needed for this work is the reaction rate: a mathematical expression that allows to evaluate the extent of the reaction, through information on the temperature and reactant, eventually also product, concentration inside the reactor.

For the reaction of interest, finding this expression is not too easy since Pt was completely substituted with V_2O_5, in industrial applications, since 1930s. The principal reason is related with economic aspects, in fact Pt is more expensive than V_2O_5 and it is more prone to deactivation, unless it is more active. For this reason, in the literature there are few chemical kinetics studies on Pt, most of them from very old papers.

One recent paper, in which the catalytic oxidation of SO_2 to SO_3 on Pt is analysed (T. Hamzehlouyan et al., 2014 [25]), develops a reaction rate expression derived from experimental data. The reaction rate parameters were established from an optimization procedure (minimizing the distance between the model and the experimental evidence), starting from initial guess from a different paper (J. Dawody et al., 2007 [26]). The rate expression is based on Langmuir-Hinshelwood-Hougen-Watson (LHHW) mechanism, here described.

In LHHW mechanism, the global reaction rate is expressed as sum of single steps that include: adsorption/desorption of reactants and products, reaction on the surface; all considered as reversible reactions.

$$SO_2 + Pt \overset{r_1,r_2}{\longleftrightarrow} SO_2^* \qquad\qquad r_1 = k_1 C_{SO_2}\theta \qquad r_2 = k_2\theta_{SO_2^*}$$

$$0.5O_2 + Pt \overset{r_3,r_4}{\longleftrightarrow} O^* \qquad\qquad r_3 = k_3 C_{O_2}^{0.5}\theta \qquad r_4 = k_4\theta_{O^*}$$

$$SO_2^* + O^* \overset{r_5,r_6}{\longleftrightarrow} SO_3^* + Pt \qquad r_5 = k_5\theta_{SO_2^*}\theta_{O^*} \qquad r_6 = k_6\theta_{SO_3^*}\theta$$

$$SO_3^* \overset{r_7,r_8}{\longleftrightarrow} SO_3 + Pt \qquad\qquad r_7 = k_7\theta_{SO_3^*} \qquad r_8 = k_8 C_{SO_3}\theta$$
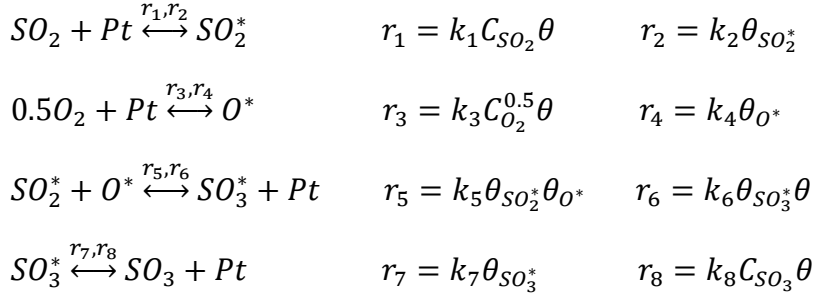
The apex * indicates that the chemical species is adsorbed on the catalyst surface, linked with the active site of the catalyst. The member to member sum of r_1 to r_8 gives the global reaction rate, as mentioned. Each step of LHHW mechanism is considered as an elemental reaction, so the reaction rate is simply the product between the kinetic constant and the concentration of reactant raise to the power equal to the stoichiometric coefficient. In particular θ indicates the fraction of active sites, free or occupied according to the specific subscript. The kinetic constant can be expressed according to the Arrhenius form:

$$k_i = A_i \exp\left(\frac{-Ea_i}{RT}\right)$$

Where A_i is the pre-exponential factor of i-th reaction, Ea_i is the activation energy of the i-th reaction, R is the universal constant of gases and T is the temperature.

The parameters value adopted in this work for the kinetics are taken from Ref. [26] and they are listed in Table 3.1. They are not utilized the optimized parameters from Ref. [25] since in the paper not all the values are disclosed.

Parameter	Value	Parameter	Value
A_1 [mol³/mol/s]	4.8e+7	E_1 [kJ/mol]	7
A_2 [1/s]	1e+15	E_2 [kJ/mol]	150
A_3 [mol³/mol/s]	8.44e+5	E_3 [kJ/mol]	10.40
A_4 [1/s]	9.97e+14	E_4 [kJ/mol]	189.40
A_5 [1/s]	6.4e+14	E_5 [kJ/mol]	179
A_6 [1/s]	6.2e+15	E_6 [kJ/mol]	182
A_7 [1/s]	1e+15	E_7 [kJ/mol]	140
A_8 [mol³/mol/s]	4.7e+7	E_8 [kJ/mol]	4

Table 3. 1 - Kinetic parameter of catalytic oxidation of SO_2 to SO_3 on Pt [25]

It's very important to precise that all the pre-exponential factors are given based on molar amount of active sites. In order to use the reaction rate, these values must be multiplied by the molar amount of active site per kg of catalyst, that for IOSTO catalyst is provided in the previous chapter.

Until now this set of equations is totally unusable, since the reaction rates depend on the fraction of active sites, non-measurable variables. In fact, the LHHW method for the determination of a global reaction rate needs another input data: the rate determining step (RDS) of the scheme, i.e. the slowest reaction. According to literature information (Ref. [25], [26]) the surface reaction can be considered as the RDS. It means that the velocity of the global reaction is equal to the RDS net velocity:

$$r = r_5 - r_6 = k_5 \theta_{SO_2^*} \theta_{O^*} - k_6 \theta_{SO_3^*} \theta$$

This approximation could be also translated considering that all the other reactions are in chemical equilibrium, it means the direct reaction is equal to the reverse reaction:

$$r_1 = k_1 C_{SO_2} \theta = r_2 = k_2 \theta_{SO_2^*}$$

$$r_3 = k_3 C_{O_2}^{0.5} \theta = r_4 = k_4 \theta_{O^*}$$

$$r_7 = k_7 \theta_{SO_3^*} = r_8 = k_8 C_{SO_3} \theta$$

From the three previous equations, it is possible to explicit the fraction of occupied active sites: $\theta_{SO_2^*}$; θ_{O^*}; $\theta_{SO_3^*}$. On the other side, knowing that the sum of all the active sites fraction is equal to one, it is possible to define the balance equation of active sites:

$$\theta_{SO_2^*} + \theta_{O^*} + \theta_{SO_3^*} + \theta = 1$$

From these equations, it possible to explicit the global reaction rate as function of measurable variable only:

$$r = \frac{\left(\frac{k_1 k_5}{k_2} \sqrt{\frac{k_3}{k_4}} C_{SO_2} C_{O_2}^{0.5} - \frac{k_6 k_8}{k_7} C_{SO_3} \right)}{\left(\frac{k_1}{k_2} C_{SO_2} + \sqrt{\frac{k_3}{k_4}} C_{O_2}^{0.5} + \frac{k_8}{k_7} C_{SO_3} + 1 \right)^2}$$

Or in a more compact form:

$$r = \frac{\left(k_{dir} C_{SO_2} C_{O_2}^{0.5} - k_{inv} C_{SO_3} \right)}{\left(k_{SO_2} C_{SO_2} + k_{O_2} C_{O_2}^{0.5} + k_{SO_3} C_{SO_3} + 1 \right)^2}$$

In order to obtain the reaction rate with unit of measure of kmol/m³/s which is compatible as input data of commercial process simulation software, such as Aspen HYSYS®, the input data on the density of the bed is needed:

$$\rho_{bed} = \rho_{cat} (1 - \varepsilon)$$

Where ε is bed void fraction, that is possible to estimate according to the correlation of A.S. Pushnov, 2006 [27]; here defined:

$$\varepsilon = \frac{A}{\left(\frac{D}{d}\right)^n} + B$$

Where D is the diameter of the reactor, d is the catalyst diameter and A, B, n constants for catalyst sphere are respectively 1, 0.375, 2.

The operating conditions under study in Ref. [25] and Ref. [26], however, are related with automotive applications, in which the amount of SO_x is on the ppm order. IOSTO process stay in the middle between automotive applications and industrial applications for H_2SO_4 production, in term of SO_2 concentration. As consequence, it is already possible to say that every reaction rate in the literature is not applicable at 100% to IOSTO process, due to its innovative nature. These values can be considered only as first guess in the simulations and, in order to have reliable estimation on the kinetics, an extensive experimental study on IOSTO process conditions is needed. These aspects are considered in the next chapters.

3.2. Preliminary Simulation of the Process in Aspen HYSYS®

Once the reaction rate is available, it is possible to start a first approximation of the process simulation. The tool used in this works is Aspen HYSYS®, that is a user friendly commercial process simulator. The other reason also links with Aspen HYSYS® usage is related with the fact that this work is in collaboration between Politecnico di Milano and Sotacarbo S.p.A. and, in order to fully transfer the models to Sotacarbo S.p.A., a commercial software is the best solution, with respect to in-house models of each equipment. After the establishment of a correct and working simulation, Sotacarbo S.p.A. could easily works on process variables degrees of freedom in a very easy way, in order to run the process at the wanted operating conditions.

The modeling of sulphuric acid plant in Aspen HYSYS® environment is strongly established and so it is easy to find useful information to set the simulation. Sulphuric acid models have been used to design, de-bottleneck and troubleshoot plants, converter profile optimization, evaluate catalyst purchases and rate present catalyst condition, energy recovery analysis and to simulate gas-gas heat exchanger leaks. Physical properties are the most important part of any simulation, it is critical to have accurate and updated physical properties to perform engineering calculations which eventually dictate the sizing and rating of plant equipment which affects the capital costs, operating costs and safety of the plant [28]. According to different references [28], [29], [30], [31]; to simulate aqueous acids such as sulphuric acid processes it is recommended to turn on the electrolytes feature in Aspen HYSYS®. In Aspen HYSYS®, an electrolyte system is defined as one in which some of the molecular species dissociates partially or completely into ions in a liquid solvent. These dissociation reactions occur fast enough that the reactions can be considered to be at chemical equilibrium. The liquid phase equilibrium reactions that describe this behaviour are referred to as the solution chemistry. Solution chemistry has

a major impact on the simulation of electrolyte systems. Solution chemistry also impacts physical property calculations and phase equilibrium calculations. The presence of ions in the liquid phase causes highly non-ideal thermodynamic behaviour. Aspen HYSYS® provides specialized thermodynamic models and built-in data to represent the non-ideal behaviour of liquid phase components, in order to get accurate results.

In the Properties tab of Aspen HYSYS®, Fluid Packages folder, it is selected the Aspen Properties database. Aspen Properties provides state-of-the-art physical property methods, models, algorithms, and data that enables to easily perform engineering calculations based on rigorous and proven thermo-physical property models and data. Aspen Properties contains the world's largest database of pure components and binary parameter databanks.

The global property method, used in this model, is ELECNRTL. This option set is used for the simulations with non-ideal electrolyte solutions. ELECNRTL calculates liquid phase properties from the Electrolyte-NRTL activity coefficient model. Also, Henry's Law is used to calculate gas (SO_2, O_2, N_2 and CO_2) solubility in sulphuric acid. The ideal gas low is used for vapour phase, in fact using a more advanced equation of state for the gas phase, such as Peng-Robinson or Soave-Redlich-Kwong, the Z-factor value is next to the unit, as the ideal case since the temperature and the pressure of the process are relatively low. Using the Electrolyte Wizard tool, it is possible to automatically generate the aforementioned dissociation reactions, here listed:

$$H_2O + CO_2 \leftrightarrow HCO_3^- + H^+$$

$$HCO_3^- \leftrightarrow CO_3^{2-} + H^+$$

$$H_2SO_4 \leftrightarrow HSO_4^- + H^+$$

$$HSO_4^- \leftrightarrow SO_4^{2-} + H^+$$

$$H_2O + SO_2 \leftrightarrow HSO_3^- + H^+$$

$$HSO_3^- \leftrightarrow SO_3^{2-} + H^+$$
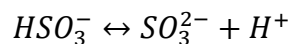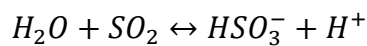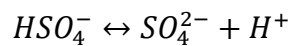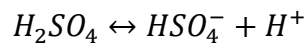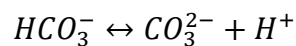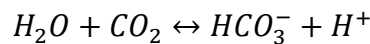
Before entering in the Simulation tab, the last step is to provide to the simulator the reaction that occurs in the process. Since several approaches are used, they are explained in detail in the next sections. Note that all the simulations in this preliminary phase are related to the catalytic reactor of IOSTO process. In fact, the absorption section is operated in discontinuous way and so a more detailed analysis is needed. Only later in this chapter a very rough approximation of the absorption column, related also with experimental data, is provided.

3.2.1. Equilibrium Approach of Catalytic Reactor Simulation in Aspen HYSYS®

Considering the industrial application of catalytic oxidation of SO_2 to SO_3, this reaction occurs in multistage adiabatic reactor with intermediate cooling, since the reaction is exothermic and thermodynamically limited. The IOSTO catalytic reactor, however, does not operate adiabatically but more similar to an isothermal reactor. The first thing to do, after the identification of the real temperature policy inside the reactor, is to understand where is the thermodynamic constraint. In other words, it's interesting to understand which is the thermodynamic conversion, i.e. the maximum allowable conversion according to a specific temperature policy along the reactor.

In Aspen HYSYS® it is possible to use an equilibrium reactor, i.e. a model in which the equilibrium composition is evaluated, given the following input data:

- Inlet composition and flowrate.
- Temperature at which the chemical equilibrium is considered.

In the case of IOSTO process, two different kind of feed stream are present: exhausted gas and simulated gas. In Figure 3.1 and Figure 3.2 the equilibrium conversion function of temperature of the two possible feed streams is shown.
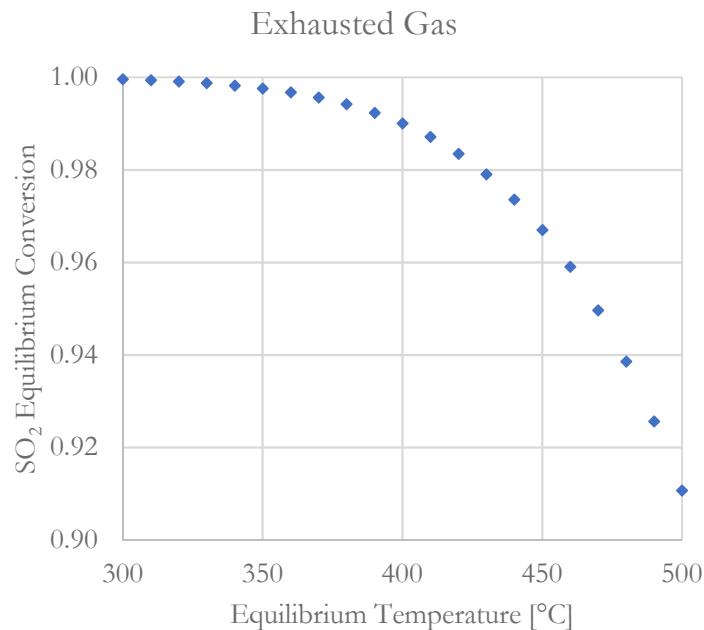
Figure 3. 1 - SO_2 Equilibrium conversion at different temperature (exhausted gas)
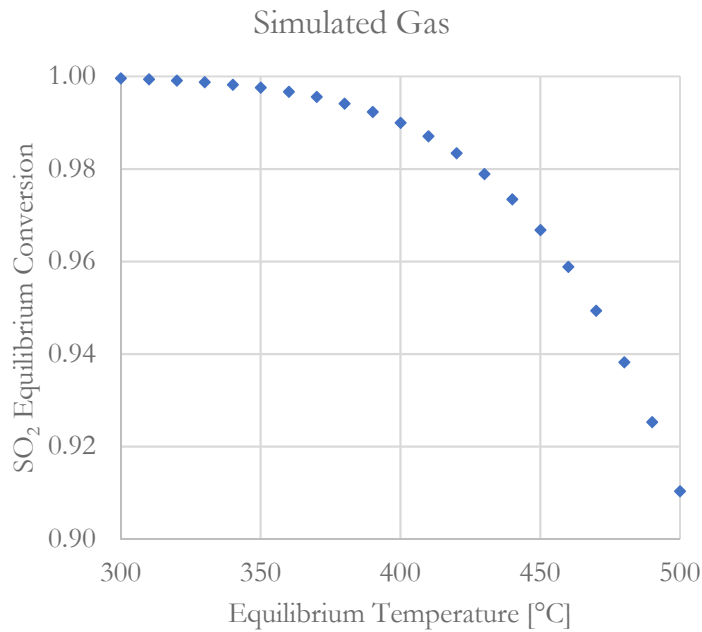
Figure 3. 2 - SO$_2$ Equilibrium conversion at different temperature (simulated gas)

From Figure 3.1 and Figure 3.2 it is possible to obtain some important considerations. First at all, the two plots are practically identical; that is reasonable since the feed gas of the IOSTO reactor should be the same (exhausted vs. simulated). The only real difference is that the dehydration section doesn't allow a perfect separation of water and some of it remains in the exhausted gas. From now on, in this paragraph, only the exhausted gas stream is considered, since similar results are obtainable with the simulated gas stream. The second point to figure out is that, in the temperature range of IOSTO design with Pt catalyst, the equilibrium conversion is very high, greater of 90%. In fact, the real problem of this reaction is when it is run at higher temperature, compatible with active temperature of V$_2$O$_5$ industrial catalyst. This is combined with the fact that the adiabatic conditions bring the reactor at higher temperature, detrimental for equilibrium conversion. That is the reason why the intermediate cooling could be beneficial in those specific cases.

On the other side, for IOSTO process it seems to be that the intermediate cooling would be not so beneficial for the thermodynamic constraint. In fact, if the first stage is set at a temperature of 350 °C, the equilibrium conversion is 99.78%. For instance, cooling the stream at 320 °C, the global equilibrium conversion is 99.92%. In IOSTO plant the intermediate cooling is already in place but, if not, this modification of the plant layout should be considered as minor priority.

Once this thermodynamic analysis is done, it is possible to start to build the plant inside the simulator, still considering the reaching of thermodynamic equilibrium, i.e. assuming that the IOSTO reactor is sufficient long to allow the approach of the chemical equilibrium composition. The plant layout of the simulation of the catalytic section of IOSTO plant is provided in Figure 3.3.
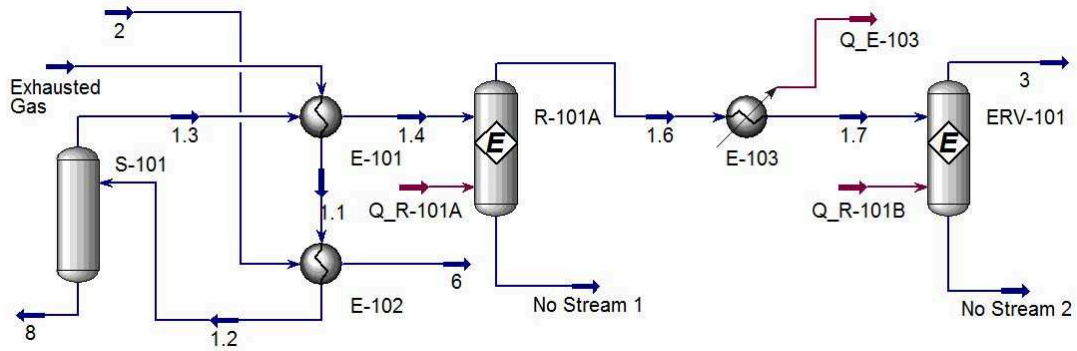
Figure 3. 3 - Catalytic IOSTO section simulation in Aspen HYSYS®, equilibrium reactors

In order to build this simulation, the used reference was the PFD of IOSTO, shown in the previous chapter, in terms of layout and notation. In particular, the two catalytic stages are represented with two distinct equilibrium reactors: R-101A and R-101B. The related heat stream, linked with the reactors, simulates the thermal compensation to maintain an outlet temperature equal to the inlet temperature. The heat of the intermediate cooler E-103 is set to zero, for the reason mentioned above. The output stream 3, represent the best condition that is possible to get in the process, in term of composition. For sure, only a kinetic analysis allows to understand if this condition is reached or not. This is done in the next section.

3.2.2. Kinetics Reaction Rate Approach of Catalytic Reactor Simulation in Aspen HYSYS®

The difference introduced in this section, respect to the previous one, is that a kinetic reaction rate is considered; in particular the one deeply analysed in section 3.1. It is worth to say again that this kinetic equation, although tailored with IOSTO catalyst information, it is only a very rough approximation of the reality, since the parameters are taken from a different catalyst. Practically the only difference is in the substitution of the reactor model. In Aspen HYSYS® the reactor model that fits better for the application is the Plug Flow Reactor (PFR). This model can be integrated, generally, with homogenous reactions set; but under a certain set of hypothesis this model is still valid for heterogeneous gas-solid reactions, this is called pseudo-homogenous model. This model is explained in the next sections, where is also provided a validation of Aspen HYSYS® results with MATLAB®, with the formulation of the governing equations of the reactor.

The plant layout of the simulation, in case of exhausted gas, is shown in Figure 3.4. Also in this case, similar to the equilibrium case, the heat stream linked with the reactors simulate the thermal compensation to get a certain outlet temperature. Compensation means that assigning whatever inlet and outlet temperature; the model of the reactor, once these inputs are received, calculate the heat flow, balancing the heat of reaction and the heat needed to get the pre-establish outlet temperature. Different from the previous equilibrium condition, different temperature solutions are now studied and explained below.
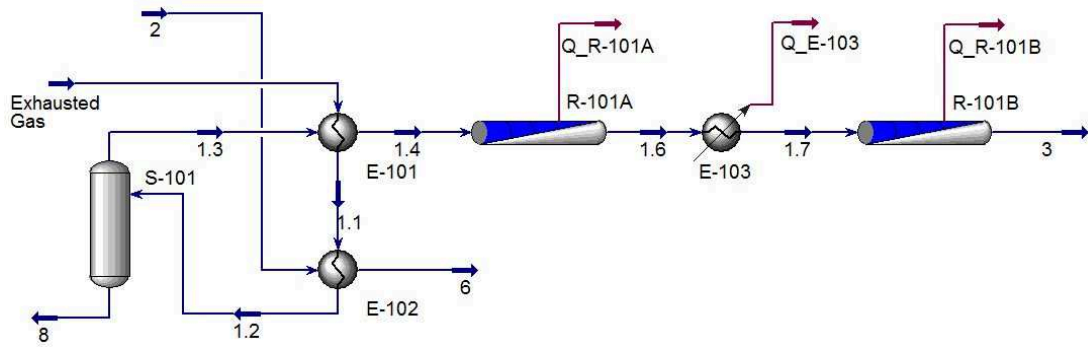
Figure 3. 4 - Catalytic IOSTO section simulation in Aspen HYSYS®, PFR reactors

For sure, in order to model the IOSTO behaviour, the isothermal temperature path is followed. The project temperature of 350 °C is set; the heat related to heat exchanger E-103 is set to zero. This kind of simulation is equal to the modeling of a single reactor with double length with respect to the real one. The dehydration section, on the other side, is kept unchanged. It is worth to mention that the pressure drops are set equal to zero too; it is a reasonable assumption since the reactor is very short, just 0.305 m. The temperature profile, as consequence, is a horizontal line as shown in Figure 3.5. Another interesting plot is the SO_2 flowrate profile along the reactor, illustrated in Figure 3.6.
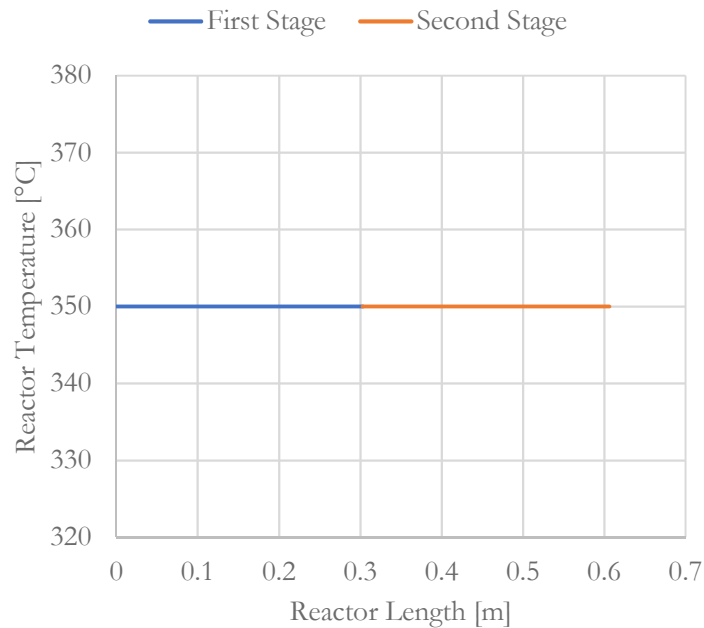
Figure 3. 5 - Temperature profile, 350 °C isothermal condition (PFR reactor)

In both the cases, the two different stages are indicated with different colours of the lines. The most important thing to mention is that the consumption of SO_2 is not very high, in fact the final conversion is 36.55%. Up to now it is not possible to say if the real conversion of IOSTO is that specific value or not, since the kinetic expression is derived from literature. Most probably the rate is not applicable for the system under study and,

as said many times, an experimentation on the IOSTO feed condition and catalyst formulation is needed.
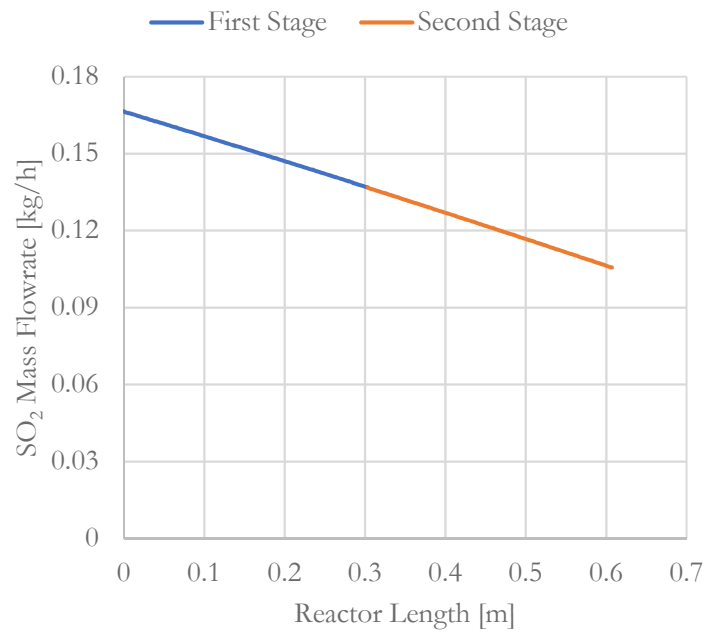
Figure 3. 6 - SO$_2$ mass flowrate, 350°C isothermal condition (PFR reactor)

Since a bad conversion was found, another temperature policy was adopted. In particular to simulate an industrial case, the adiabatic condition is considered. In Figure 3.7 and Figure 3.8 the temperature and SO$_2$ flowrate is indicated.
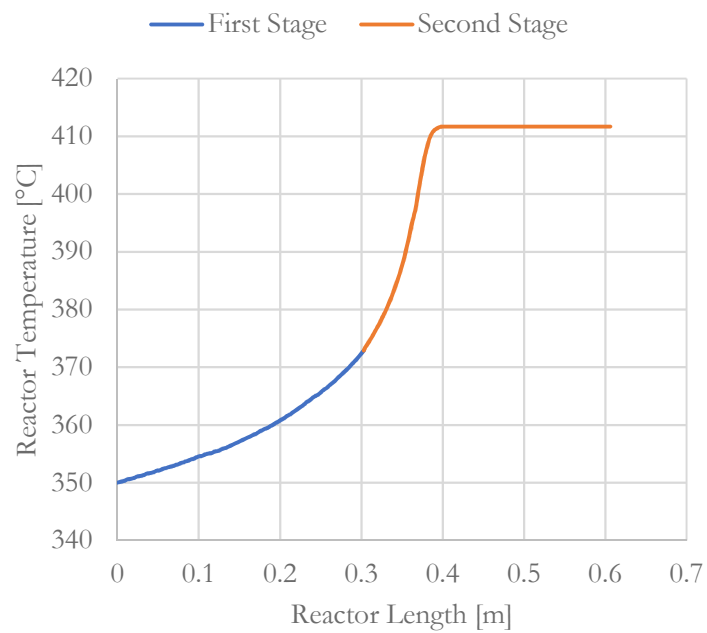
Figure 3. 7 - Temperature profile, adiabatic condition (PFR reactor)
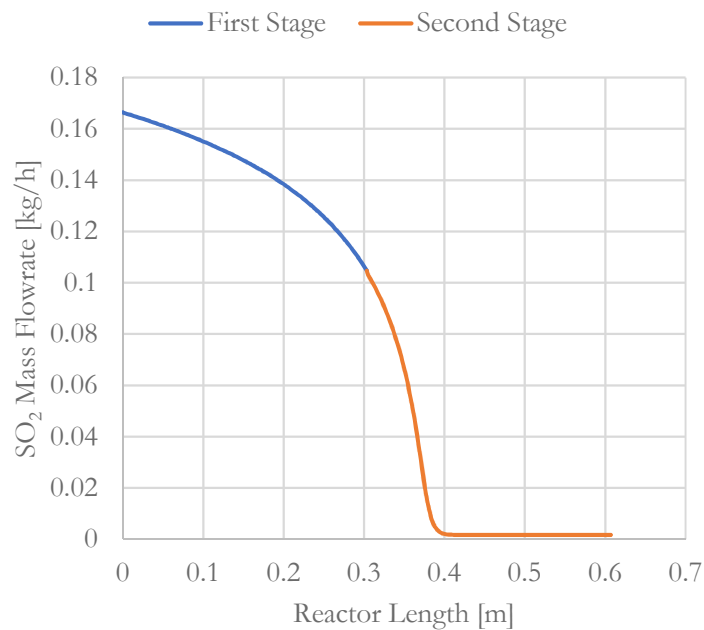
Figure 3. 8 - SO$_2$ mass flowrate, adiabatic condition (PFR reactor)

The first thing that is possible to notice is that there is the reaching of the thermodynamic equilibrium condition, since the profiles become flat at a certain a certain axial coordinate. In order to understand the reliability of the kinetics expression, it is possible to compare the outlet adiabatic conditions, with the equilibrium condition, analysed in the previous section. The comparison is summarized in Table 3.2, imposing a temperature equals to 411.7 °C to the equilibrium reactor, equal to the outlet temperature of the adiabatic reactor.

	Outlet of Adiabatic Reactor	Equilibrium Reactor
SO$_2$ Conversion	0.990	0.988

Table 3. 2 - Comparison of SO$_2$ conversion adiabatic and equilibrium reactor

The values are almost equal, it means that the kinetics expression predict very well the chemical equilibrium, so it is thermodynamically consistent.

The other important results that is possible to identify from the previous graph is that the conversion is much higher with respect to the isothermal case. It is simple explicable looking at the temperature profile: when the SO$_2$ get consumed the energy released from the reaction is converted in sensible heat, with a consequent increase of temperature (no dissipation with the ambient due to the adiabatic assumption). The reaction rate, in the Arrhenius form, has an exponential increase with the temperature. So, there is a sort of self-ignition due to the reaction exothermicity, that brings the system to the final, unchanged, equilibrium condition, in a very short distance.

Coming back to a condition applicable to IOSTO reactor, i.e. isothermal condition, it is possible to run different simulation at different temperature. With only an increase of 20 °C with respect to the project temperature, the results are different as shown in Figure 3.9.
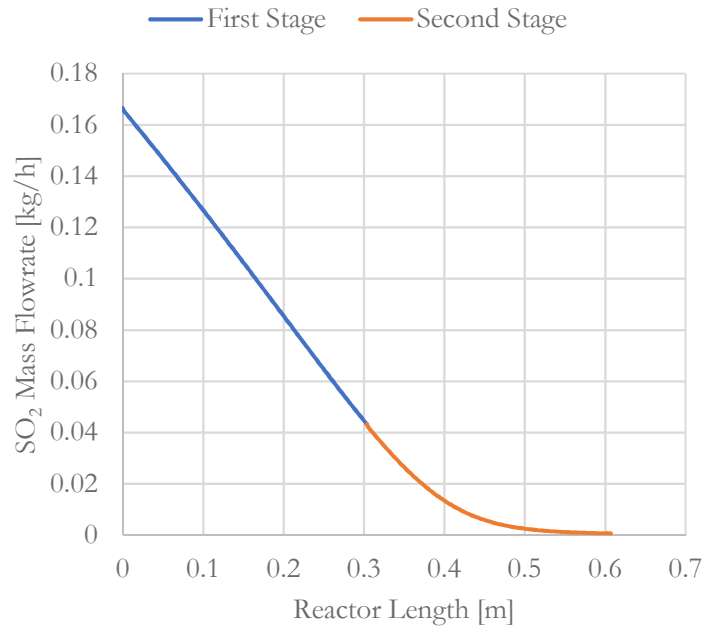
Figure 3. 9 - SO$_2$ mass flowrate, 370°C isothermal condition (PFR reactor)

With this reasonable increase of temperature, the reactor approaches the thermodynamic conditions almost at the end of the reactor. It could be reasonable to run the IOSTO reactor at this temperature, in the event that the kinetic expression is correct. An increase of temperature is beneficial for kinetics but not for thermodynamics but, as said, at this temperature range the equilibrium is completely moved toward the product.

From this preliminary analysis, in fact, the project temperature seems to be too low. On the other side, it is well known that the Pt is active above 300 °C and so another conclusion could be that the reactor is too short for the desired application. From a different perspective, the feed flowrate could be too big, in fact, a decrease of it from 4.5 kg/h to 3.5 kg/h brings the conversion from 36.55% to 47.67%. However, the sensitivity of the conversion to this parameter is clearly lower than the temperature change.

3.2.3. Pseudo-homogenous Model

It could be interesting to indagate deeper the mathematical formulation of the PFR reactor model of Aspen HYSYS®, considering if the hypothesis at the base of the model are reasonable. If no, it is not possible to stay in Aspen HYSYS® environment for all the plant simulation, since it is the only model present for catalytic fixed bed.

The modeling of a fixed bed reactor requires different scale of analysis. Considering a reaction rate, the microscale (catalyst active site) and the mesoscale (catalyst particle) are

considered. So, at the end, what is left is the macroscale, i.e. the scale of the reactor that is mainly determined by hydrodynamics. A given reactor can be modeled in various ways. The basic model, used in most of the studies until now, is the pseudo-homogeneous one-dimensional model, which only considers transport by plug flow in the axial direction [32]. The one-dimensional model is the simplest possible configuration, in which only one dimension is considered, i.e. the axial one. So, no radial gradients are considered; in fact, the introduction of another dimension complicate a lot the mathematical formulation of the reactor. For this work, this level of complication is not necessary. This is manly link with the fact that the IOSTO process in only at the very first phase of study. The other assumption of this model is that the motion of the fluid is a form of plug; it means that the elemental package of fluid does not exchange mass and heat with the elemental package of fluid before and after. This hypothesis is valid according to the criteria of Ref. [33] according to which the axial dispersion is negligible if L/d_p is greater than 30. L is the reactor length, d_p is the particle diameter; for IOSTO catalytic reactor is ratio is equal to 76.25. Moreover, the pseudo-homogeneous notation means that the gradients between the catalyst surface and the bulk phase are negligible. So, the mass and the heat transport are very fast and no gradients around the catalyst particle are established. This is a quite strong assumption and it need verification, in the next section 3.2.3.1. all these aspects are clarified. This assumption leads to the possibility to neglect explicitly the presence of the catalyst itself, considering the reaction occurring in a homogeneous phase. For sure, all the complexity is put inside the reaction rate formulation that takes into account that the reaction does not occurs in all the reaction volume but only on the catalyst surface.

Before describing the mathematical model, it could be of interest to understand if the reactor presents some intraporous limitations; in other words, if the catalyst porous surface is all exploited for the reaction or not. In order to do so the Weisz-Prater Criterion [34] is used. This criterion is based on the satisfaction of the following formula.

$$C_{WP} = \frac{r_{obs}\rho_{cat}r_p^2}{D_{eff}C_{SO_2}} < 1$$

Where:

- r_{obs} is the observed reaction rate in [mol/kg$_{cat}$/s]. In particular to be conservative the most severe condition is considered, that is where r_{obs} is maximum, i.e. at the inlet.
- ρ_{cat} is the catalyst density in [kg/m³].
- r_p is the catalyst radius in [m].
- D_{eff} is the effective diffusivity in [m²/s].
- C_{SO_2} is the sulphur dioxide concentration at the inlet condition (coherent with the reaction rate value) in [mol/m³].

For the system under study it is possible to find a value of about 0.33. In this case the criterion is verified, although the value is not order of magnitude less of the threshold

value. But, as mentioned, this value is the highest possible; so, it is reasonable to say that the reaction does not suffer of intraporous diffusion limitations.

After the declaration of the hypothesis and ancillary considerations, it is possible to write the mathematical model of pseudo-homogeneous one-dimensional reactor. In Figure 3.10 there is the schematic representation of an infinitesimal slice of reactor, needed for the procedure to get the balance equations.
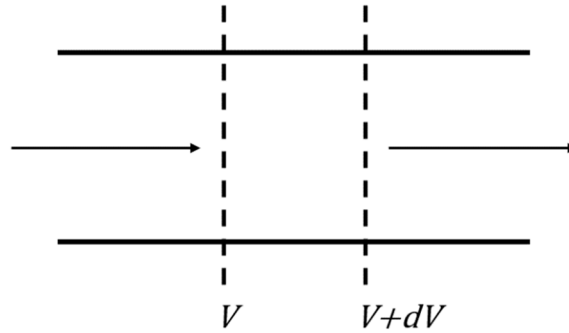
Figure 3. 10 - Schematic representation of an infinitesimal slice of pseudo-homogeneous 1D reactor

The model of the reactor is developed through mass and energy balances, the momentum balance equation is neglected, since the pressure drops are assumed to be equal to zero. As consequence, the arrows represent the inlet and outlet convective fluxes associated with mass and heat. The fluxes are related to the infinitesimal control volume dV. Applying the balance logical statement for that volume and expressing the outlet fluxes as function of the inlet fluxes through a Taylor expansion, it is possible to get the governing equations for the reactor. After some mathematical steps, the equations for an adiabatic reactor are:

$$\frac{d\dot{m}_i}{dV} = v_i r MW_i$$

$$\dot{m}_{tot} \widehat{Cp_{mix}} \frac{dT}{dV} = -\Delta H_R r$$

Where:

- $\dot{m}_i$ is the mass flowrate of the i-th species.
- v_i is the stoichiometric coefficient of the i-th species.
- r is the reaction rate, in [kmol/m³/s] or equivalent unit of measurement. In previous section, it is already explained how to get this expression.
- MW_i is the molecular weight of the i-th species.
- $\dot{m}_{tot}$ is the total mass flowrate of the gas stream.
- $\widehat{Cp_{mix}}$ is the mass heat capacity of the gas mixture.
- ΔH_R is the enthalpy of the SO_2 oxidation reaction.

The resulting model is a set of ordinary differential equations (ODEs), solvable defining initial conditions, that are the inlet reactant mass flowrate and the relative temperature. In

case of isothermal reactor, the system of ODEs is simplified eliminating the energy balance and considering only the material balances. In fact, the energy balance provides, as output, the trend of the temperature along the reactor. If the temperature is constant, it follows that the derivative of the temperature along the reactor is identically equal to zero.

3.2.3.1. Criteria for Transport Limitation Verification

In this subsection, the criteria for transport limitation verification are considered. This dissertation in needed in order to understand if the reactor is in pure chemical regime or suffer of external mass or heat transport limitations. If transport limitations are present the pseudo-homogeneus model is not valid and a heterogeneous model has to be considered. The heterogeneous model takes explicitly into account the gradient between the catalyst particle and the gas bulk phase. In literature, they exist specific criteria to verify this aspect, the most diffused is Mears' Criterion [35]. It follows the mathematical expression for the mass and heat limitation, respectively.

$$C_{M_m} = \frac{r_{obs}\rho_{bed}r_p n}{k_c C_{SO_2}} < 0.15$$

$$C_{M_h} = \left| \frac{-\Delta H_R r_{obs}\rho_{bed}r_p Ea}{hT^2 R} \right| < 0.15$$

Where the variable not mentioned previously are:

-   ρ_{bed} is the bed density in [kg/m³].
-   n is the order of the reaction. It is set an order of reaction equal to 1.5, considering only, as simplification, the direct contribution of the LHHW kinetics.
-   k_c is the external mass transfer coefficient in [m/s], between the bulk phase and the catalyst particle.
-   Ea is the activation energy of the reaction. Similar for the reaction order it is considered only the direct contribution of the LHHW kinetics.
-   h is the external heat transfer coefficient in [kW/m²/K], between the bulk phase and the catalyst particle.

Before illustrating the results, it is worth to mention how the transport coefficient are determined. For fixed bed reactors, the most diffused correlation, to determine transport coefficients, is the Yoshida correlation [36], through which the material Colburn factor J_m is determined:

$$J_m = \frac{0.61}{Re'^{0.41}} \quad with \, Re' = \frac{Gd_p}{6\mu(1-\varepsilon)}$$

On the other side, in order to determine the heat transport coefficient, the Chilton-Colburn analogy is used, it states:

$$J_m = \frac{Sh}{ReSc^{1/3}} = J_h = \frac{Nu}{RePr^{1/3}}$$

The results are resumed in Table 3.3.

	Actual Value	**Absence Transport Limitation**
C_{M_m}	1.01e-2	< 0.15
C_{M_h}	3.54e-3	< 0.15

Table 3. 3 - Mears' Criterion application

Looking at the results, the hypothesis of pseudo-homogeneous reactor is very strong. In fact, the Mears' Criterion values are order of magnitude lower than the threshold value.

3.2.4. MATLAB® Validation of Aspen HYSYS® Pseudo-homogeneous Reactor Model

It is expectable that the MATLAB® and Aspen HYSYS® results are reasonably the same, since the concept behind the formulation of the model equations of the reactor is the same. This validation is more linked with the aim of developing in-house models. In fact, once it is verified that the Aspen HYSYS® PFR model with a heterogeneous kinetics is the same of the pseudo-homogeneus one-dimensional fixed bed reactor; it is possible to use alternatively these two tools. In general, every computational software can be used to this scope. The advantage to have developed this in-house model allows more flexibility in the study of IOSTO reactor. It means that the model can be modified, considering different hypothesis to better fit the reality. Moreover, the model can be used for more advanced calculations, that are impossible to perform in Aspen HYSYS® environment. These concepts will be considered later in this work. The results for the isothermal and adiabatic reactor, are shown in Figure 3.11 and Figure 3.12 respectively.
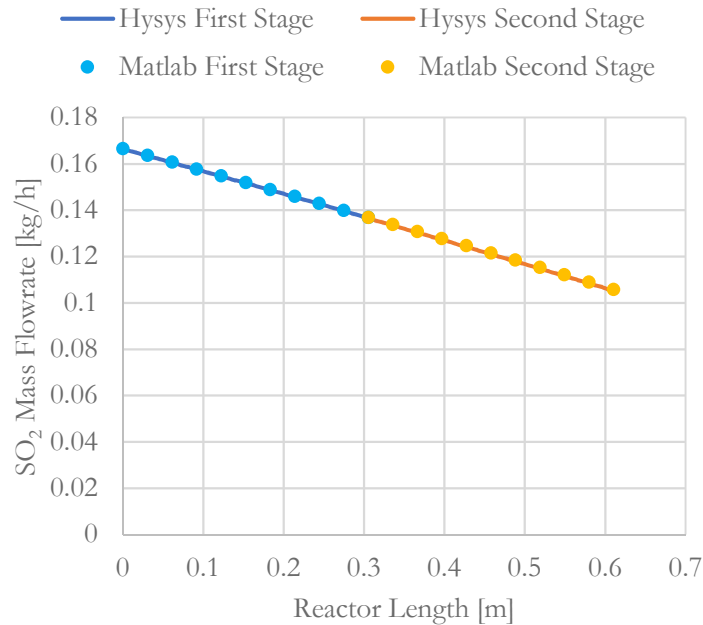
Figure 3. 11 - SO$_2$ mass flowrate comparison between Aspen HYSYS® and MATLAB®, isothermal reactor
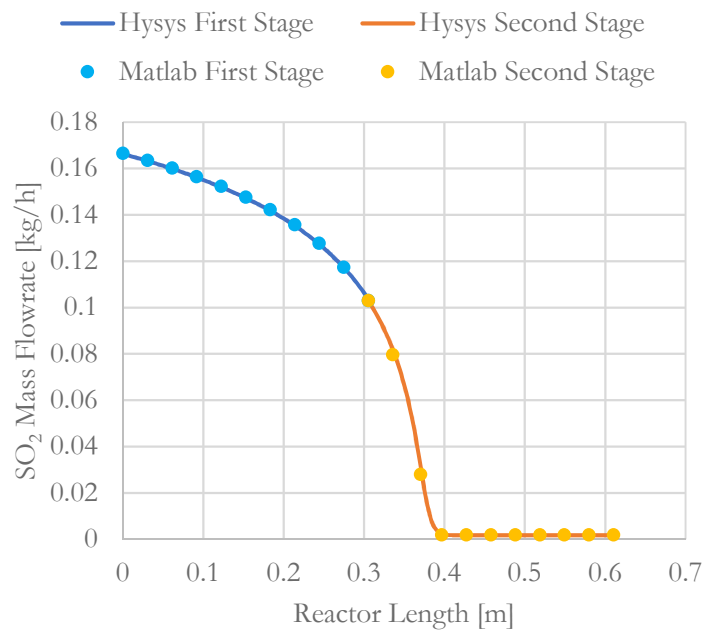
Figure 3. 12 - SO$_2$ mass flowrate comparison between Aspen HYSYS® and MATLAB®, adiabatic reactor

3.3. First Experimental Campaign on IOSTO Process

The experimental tests on IOSTO plant were carried out for the first time in September 2016. This campaign was mainly focused on verifying the operational functionality of the two main sections of the plant (reactor and absorption column), their control loops and their safety control systems. For this reason, IOSTO plant was set at the project conditions; simulated gas feed stream option; presence of the intermediate cooling obtained with natural convection. Moreover, this experimental campaign had also the task to validate the start-up and the shut-down procedure of the plant and to set a preliminary tuning of the controllers. Finally, a sampling system was linked to the plant at the sampling ports, as addition to the sensors already installed on the plant, in order to measure the concentration of the process gas. It is important to underline the fact that it was not present a suitable instrument to measure all the streams of interest. Indeed, it was used a measurement system able to detect only O$_2$ concentration (i.e. a MAGNOS 206 module, paramagnetic type, O$_2$ concentration measurable between 0 %v/v and 25 %v/v). All the other component concentrations were determined through calculation, as it will be shown in the following section.

3.3.1. Measurement of Temperature of the Catalytic Reactor

The real state of the process, referred to the reaction section, is mainly monitored through thermocouples. The temperature system is controlled, as explained in the previous chapter, through modulation of the power to the electrical resistance. For this study, it is important to analyse the behaviour of the reactor in normal operating conditions, regardless to the start-up procedure. It means that, in this section, the plots are related only on the time windows in which the reactant gases are sent to the reactor. In Figure

3.13 the temperature trend of the first catalytic stage is shown. The very first thing that is possible to notice is that the temperature profile is oscillating and the fluctuations are huge, more or less 50 °C of oscillation. It means that the control system is not able to maintain the temperature at the setpoint level. As mentioned, the temperature is controlled through a solid-state relay on an ON/OFF logic. Once the heating elements are turn on, there is an important increase of temperature; once the set point is exceeded, the control sends the input signal to switch off the resistance. The problem is that the tuning of the controller is not optimal and it should be modified, in order to have a faster switch between ON and OFF position and vice versa. Even though the setpoint is not guaranteed, the oscillation is reasonable around the setpoint position. That is truer for the controlling of inlet temperature, less true for the control of the outlet temperature. The reason is simply link with the fact that this last controller has to face with the heat released by the reaction. In fact, the reaction rate is a function of temperature and it is presumable that this oscillation affects the reaction conversion; this aspect is analysed in the following section. Another consequence of the presence of the reaction is likely the presence of micro oscillation of the outlet reactor temperature. The trend of the two profiles is independent, since the control logic of these variables is totally independent; one act on heater F-101 (inlet T) and one on heater F-102 (outlet T). In Figure 3.14 the profiles related with the second catalytic bed are shown.
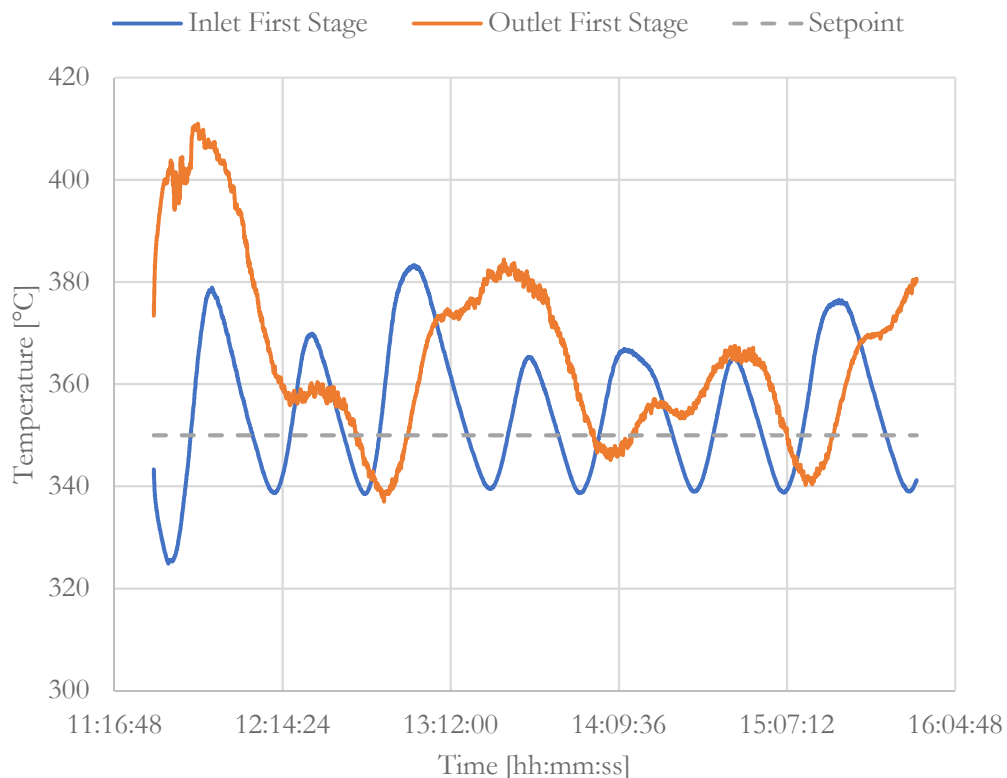
Figure 3. 13 - Temperature profile first catalytic stage during normal operating conditions
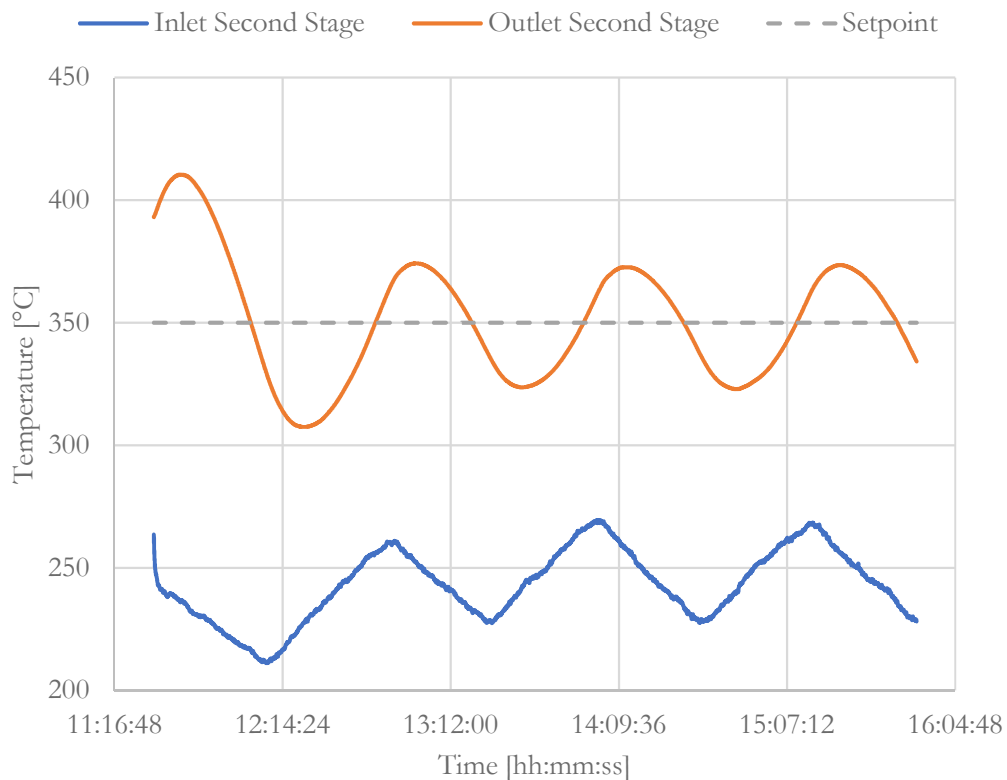
Figure 3. 14 - Temperature profile second catalytic stage during normal operating conditions

In addition to the comments already done it is worth to notice the inlet temperature profile of the second stage. The curve oscillates around 250 °C, more or less 100 °C degree less with respect to the outlet of the first bed. This is due to the natural convection with the ambient between the two stages. It seems to be a very effective cooling and, from this data, the aerothermal cooler is useless. The big problem is that, with this highly intense cooling, the temperature drops below 300 °C, the activation temperature of Pt catalyst. It means that part of the catalyst bed is wasted with consequent decrease of SO_2 conversion. A possible evidence that the reaction extent is very low is the trend of the outlet temperature. In fact, different from the outlet temperature of the first stage, is more regular around the setpoint 350 °C and with the absence of micro fluctuation. The temperature drop between the two stages is too big and it must be limited somehow to improve the IOSTO performances. The model evidence about the catalyst activation will be discussed in next sections. It is possible to find another evidence that explain that the temperature drop is due the heat transfer with the ambient: looking at the Figure 3.13 and Figure 3.14, when the outlet temperature of the first stage reaches a maximum, the inlet temperature of the second stage reaches a minimum and vice versa. The explanation is that, since the ambient temperature is reasonably constant, once outlet temperature of the first stage increases, the heat transfers increases too (proportionality between heat transfers and temperature) with a consequential greater reduction of the inlet temperature of the second stage.

59

3.3.2. Measurement of Concentration of the Catalytic Reactor

The concentration measurements are done through an instrument that is able to determine the volumetric fraction of O_2 only. It is, for sure, a poor instrumentation system; but according to some hypothesis, it is possible to indirectly evaluate the concentration of the other species. This procedure starts with the analysis of the setpoint of the mass flowmeter. According to the project specifications of the simulated gas stream, it is possible to evaluate the molar fraction of the species, listed in Table 3.4. It is important to state that, considering the hypothesis of ideal gas, the volumetric fraction is equal to the molar fraction.

Species	% Molar Fraction
SO_2	3.3
O_2	4.8
CO_2	91.9

Table 3. 4 - Inlet setpoint molar fraction of simulated gas stream

From the analysis of data coming from the measuring instrument, the measured inlet molar fraction of O_2 is 4.7 %; with an error less than 2.1%. It is reasonable to affirm that the inlet composition is equal to its setpoint, being the mass flowrate controller very precise. It is so possible to evaluate the consumption of O_2 and, according to the stoichiometric coefficient of the reaction, the consumption of SO_2 and the production of SO_3 (assuming that the catalytic oxidation of SO_2 to SO_3 is the only reaction that occurs). From these numbers, it is easy to evaluate the SO_2 conversion. In Figure 3.15 it is presented the conversion value during the experimentation time. In particular, as mentioned in the previous section, it is interesting to compare the conversion with temperature profiles, in order to explain better the reaction behaviour.

As expected, the conversion in time is not constant, but oscillating. This is linked with the dependence of the reaction rate with the temperature. Greater the temperature is, higher the conversion is (in chemical kinetics regime). In fact, the level of conversion of about 60%, is far from the thermodynamic limit, near to 100%. The aforementioned conversion vs. temperature trend, from Figure 3.15, is observable only with the outlet temperature from the first stage (marked red line). This evidence validates the hypothesis discussed above about the very low reaction extent in the second reactor. In fact, it seems, from the data, that the greater part of the conversion occurs in the first stage. In the second stage, the greater part of the bed is aimed to the heating of gas stream till the activation temperature and, in any case, once this temperature is reached, the reaction rate is quite small. These concepts will be clearer with the modeling of the reactor in experimental conditions.
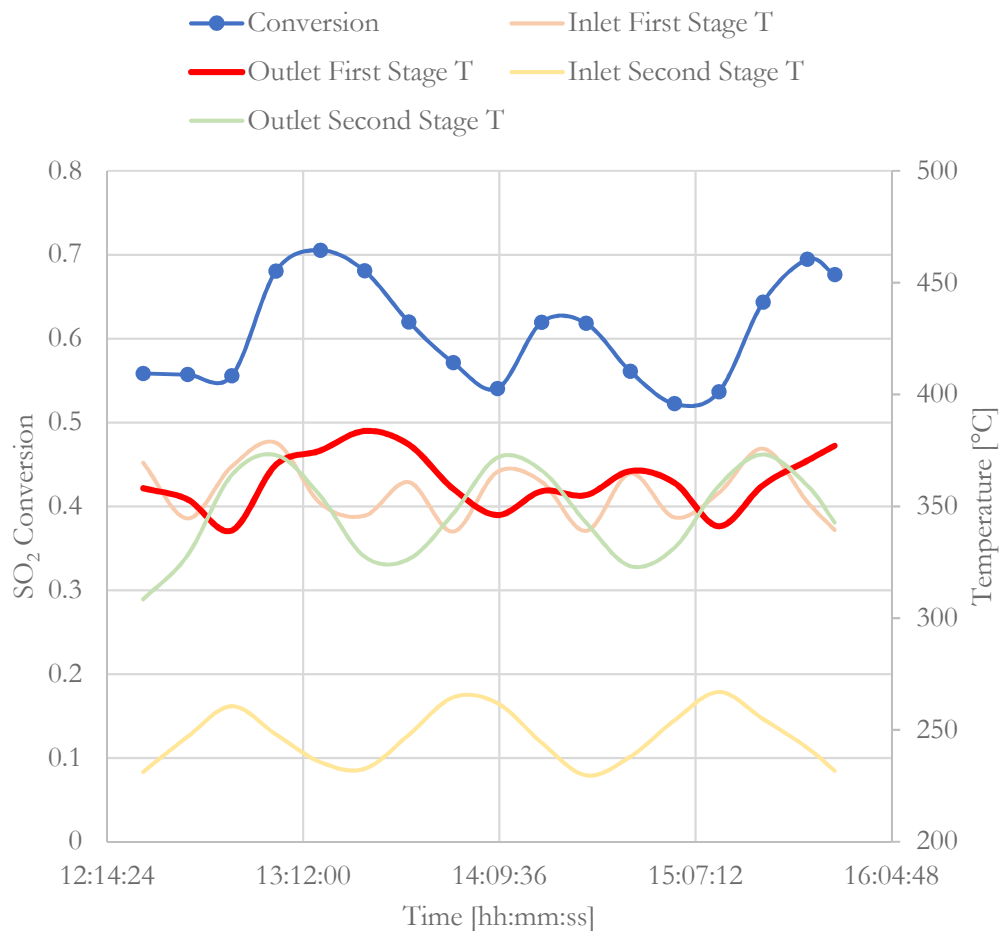
Figure 3. 15 - SO$_2$ Conversion profile and comparison with reactor temperatures

In any case, the fluctuation is totally undesired, since the reactor should work around a stationary condition, with at least few degrees of oscillation. As mentioned, this behaviour is caused by the electric heating elements and there is the need to reduce as much as possible this oscillating nature. In fact, this trend affects the performances of the process, both in the reaction and absorption section.

3.3.3. Modeling Considerations on the Experimental Catalytic Reactor

Starting from the preliminary simulation, it is possible to tailor the reactor models to the experimental evidence. Particularly about the intermediate cooling, since it was set to zero in previous simulations. On the other side, regarding the other big problem of the process, i.e. the temperature oscillation, it is not considered in the model. This because it is an aspect totally unwanted, that must be fixed somehow. In the following chapter, where the dissertation is going deeper in the reactor analysis, this aspect is still neglected. In case the real IOSTO reactor will continue to work in an oscillating way, neglecting this aspect will lead to approximate solution. For future developments, if this worst condition remains

true, it may be reasonable to develop an in-house model which consider the temperature fluctuation.

In the new simulation, the only differences stay in the substitution of the feed stream (from exhausted gas to simulated gas) and in changing of the temperature policy. In Figure 3.16, it is presented the new layout of the simulation, while in Table 3.5 the new setpoints of the temperature are shown. In particular the temperature was selected considering the mean value of the experimental oscillating profiles.
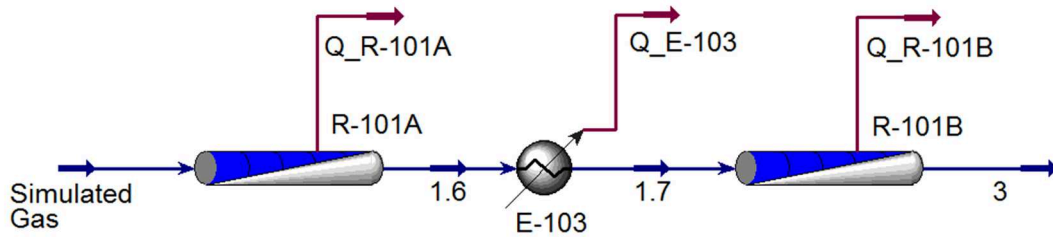
Figure 3. 16 - Simulation in Aspen HYSYS® of catalytic IOSTO section, PFR reactors and simulated gas

Stream	Temperature [°C]
Simulated Gas	350
1.6	350
1.7	250
3	350

Table 3. 5 - Setpoint temperature implemented as input data in Aspen HYSYS®

According to the new temperature policy, the first stage is adiabatic, while the second stage presents a linear increase of temperature thanks to the heating element (Figure 3.17). One interested aspect to show is the SO_2 mass flowrate profile along the reactor (Figure 3.18). This profile validates the hypothesis according to which the reaction occurs mainly in the first stage. In fact, the profile is decreasing in the first stage, where the temperature is constant to 350 °C. But once the gas stream enters in the second stage the reaction does not occurs, since the temperature is very low (about 250°C). As consequence, the SO_2 flowrate remains constant. However, the reactor is heated along its axial coordinate and approximate at a reactor axial coordinate in which the temperature is about 300 °C, the SO_2 re-start to decrease, so the reaction starts again. The kinetic expression is, for this reason, in agreement with the well know activation temperature of Pt catalyst of 300 °C.
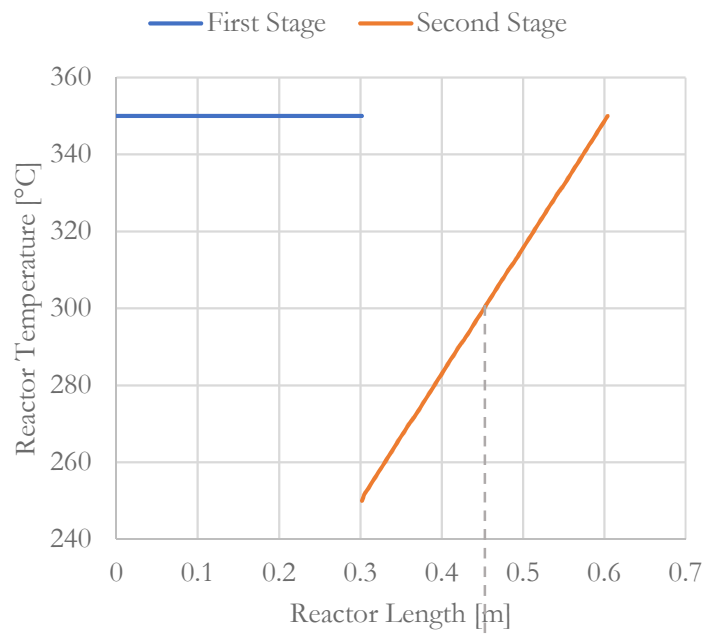
Figure 3. 17 - Temperature profile of Aspen HYSYS® simulation with experimental setpoint
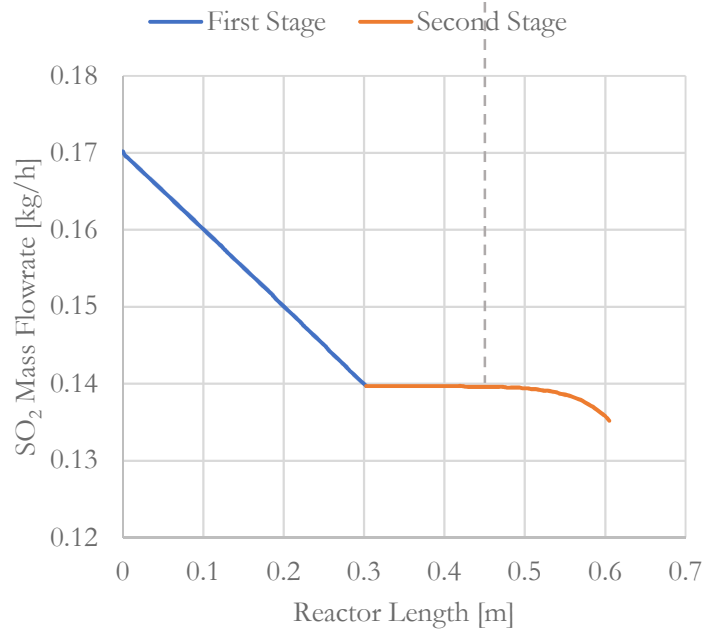
Figure 3. 18 - SO₂ mass flowrate profile of Aspen HYSYS® simulation with experimental setpoint

3.3.4. Summary of the Results of the First Campaign on the Catalytic Reactor

The experimental data presented in the previous sections are referred to the first day of campaign. Three days of successful experimentation were carried out in this phase, all of them under the same operative conditions. It is relevant to represent the conversion results of the different days of experimentation. In particular, since the trend is always oscillating, the results (Table 3.6) are shown in a range definition, highlighting the minimum and maximum value of the wave.

Day	Minimum SO_2 Conversion	Maximum SO_2 Conversion
19 September 2016	0.522	0.705
28 September 2016	0.503	0.714
29 September 2016	0.423	0.686

Table 3. 6 - SO_2 conversion range of different days of the first experimental campaign

The conversion of SO_2 has an average value of about 60%. On the other side, the equilibrium condition at 350 °C is 99.79% of conversion. As conclusion, the reactor is not able to reach the thermodynamic limit; different explanations have been provided in previous section. Moreover, the conversion predicted by Aspen HYSYS® with the literature kinetics is only 20.53 %. As conclusion, although it has been demonstrated that the kinetics is reasonable and physically sound, the rate equation is not predictable for the real system. For sure, one reason is the presence of temperature oscillation, not simulated in Aspen HYSYS® environment. However, the most important reason is that IOSTO process present an innovative nature, not documented in the literature. In particular the high dilution of reactant with CO_2 has an effect on kinetics; combining with competitive adsorption of CO_2 on the catalyst surface. In the next sections, a solution of the problems presented until now is shown, in order to implement actions for the better understanding and operation of IOSTO process.

3.3.5. Experimental Campaign on Absorption Column

Until now, only the experimental evidence on the catalytic section was shown. However, in the first experimental campaign they have been simultaneously performed experiments on the absorption column. Indeed, the outlet gas from the reactor is continuously fed to the absorption section. IOSTO plant is the sum of this two unit and for this reason the experimentation cannot be performed on the individual unit only. The relevant measurement sensor, for the absorption section, is the density sensor at the bottom of the tank T-201, under the column C-201. The instrument is Liquiphant M Density and Density Computer FML621 of Endress + Hauser. In particular, the measurement of the density is done in order to have an evidence on the progress of the absorption reaction and, indirectly, of the oxidation reaction. In fact, if the density increases, the amount of H_2SO_4 in the solution increases (H_2SO_4 is denser than H_2O). They exist experimental correlations that correlate the density of a sulphuric acid solution with the mass fraction

of H_2SO_4 inside the solution itself. It was selected the correlation found in Perry's Chemical Engineers' Handbook [37]. Moreover, in order to have an experimental evidence on the correctness of the Aspen HYSYS® model, developed in previous sections, they have been simulated the solution properties. With the simulation, the value of the density of the solution is calculated; the difference with the experimental density is provided in Figure 3.19. All the data refers to a temperature of 40 °C, i.e. the project operation temperature of the column.
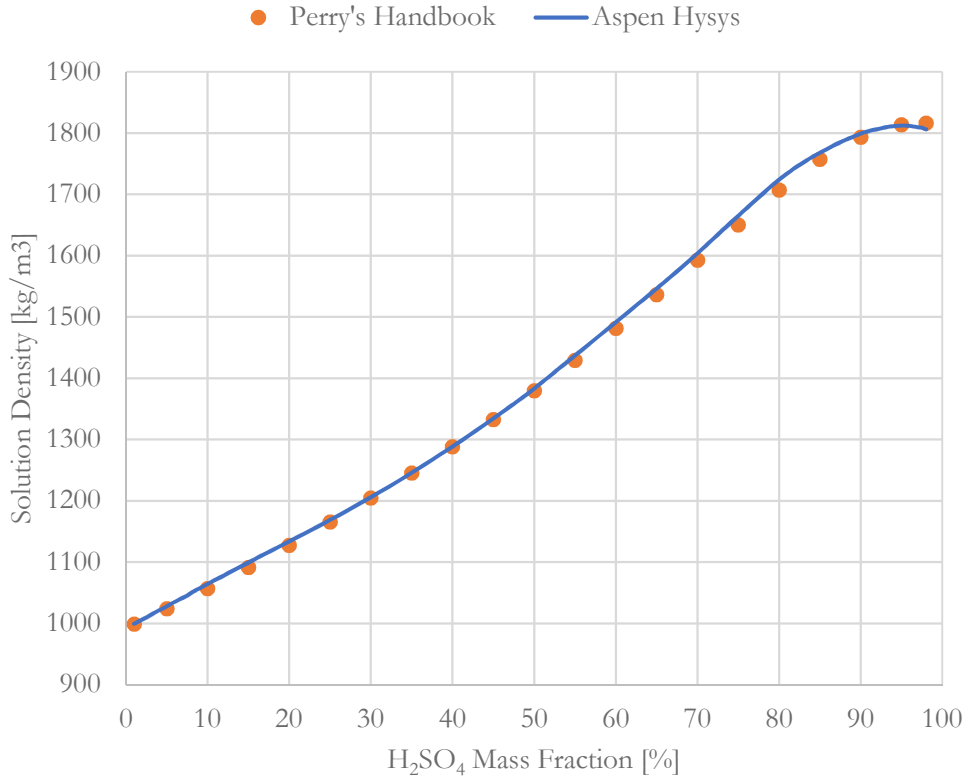
Figure 3. 19 - Solution density function of H_2SO_4 mass fraction

In the application, actually, the density value is the input; while the H_2SO_4 mass fraction is the output. For this reason, it is interesting to change the abscissa and the ordinate, respectively. Moreover, since the values of the experimental density from Ref. [37] are discrete, it is useful to find a mathematical equation that fits at the best the data. From Figure 3.20, it is possible to look that the points reasonably stay on two different pieces of a straight line. The red diamond represents the boundary for the two different models. With a two-pieces straight line model, the calculation of the parameters of the model itself is very simple; the function LINEST of Microsoft Excel® has been used for this purpose. The equation of the straight line is given in the following form:

$$y = mx + q$$

The parameters value and the R^2 value are represented in Table 3.7.

65

	m	**q**	**R²**
First Piece	0.1297	-127.076	0.997
Second Piece	0.1010	-90.022	0.987

Table 3. 7 - Model parameters H₂SO₄ % mass fraction function of the solution density
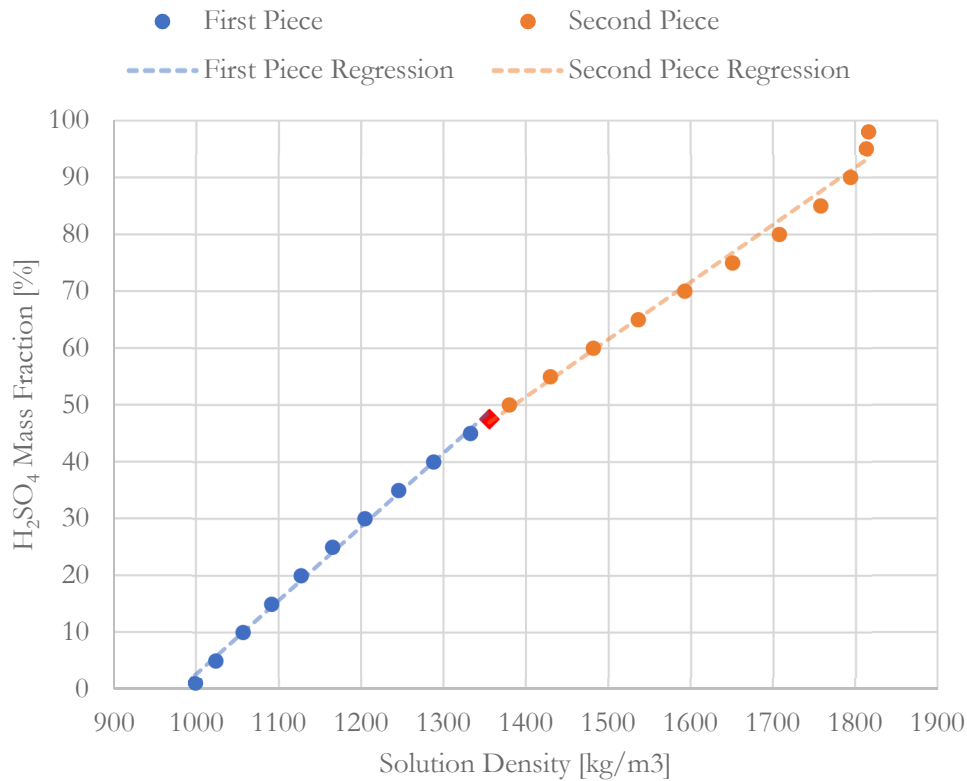
Figure 3. 20 - H₂SO₄ mass fraction function of solution density, with regression trends

The R^2 value of the second piece is not so good as the first one. From Figure 3.20 it is clear that the reason is linked with the value of density at a H_2SO_4 mass fraction next to 98%. The model works well till 97%, after this value the density increases less.

After this necessary introduction, in order to explain how the density measure can be used; it is possible to show the measures done in the first experimental campaign. At this level of experimental study, the process is not run till the reaching of the specification of the H_2SO_4 concentration; but only for 8 hours, of which about 5 hours in normal operative condition feeding the process gas. The feed is very diluted in SO_3 and this amount of time is not sufficient to reach the specification; it takes hundreds of hours to produce commercial grade sulphuric acid, according to the project specifications. In Figure 3.21, it is shown the density trend in time of the same day of experiment in which they have been illustrated some graphs in the previous paragraphs, talking about the catalytic reactor. The curve presents some micro fluctuation, that are linked with the precision of the instrument. Moreover, the line in not perfectly straight line from a macro point of view. In fact, the rate of sulphuric acid production is subjected to the fluctuation in the production of SO_3, in turn linked with fluctuation of the temperature in the reactor.

In this experimental day, the mass fraction of H_2SO_4 is increased from 3.44% to 5.43%. It does not start from zero since, before the first experimental test, the plant integrity was tested with runs without the intent of measuring the concentration of the streams. In all the following days of preliminary experimental test, Sotacarbo S.p.A. started the experimentation with the liquid solution of the previous test, without re-starting with a new batch of water.

19 September 2016
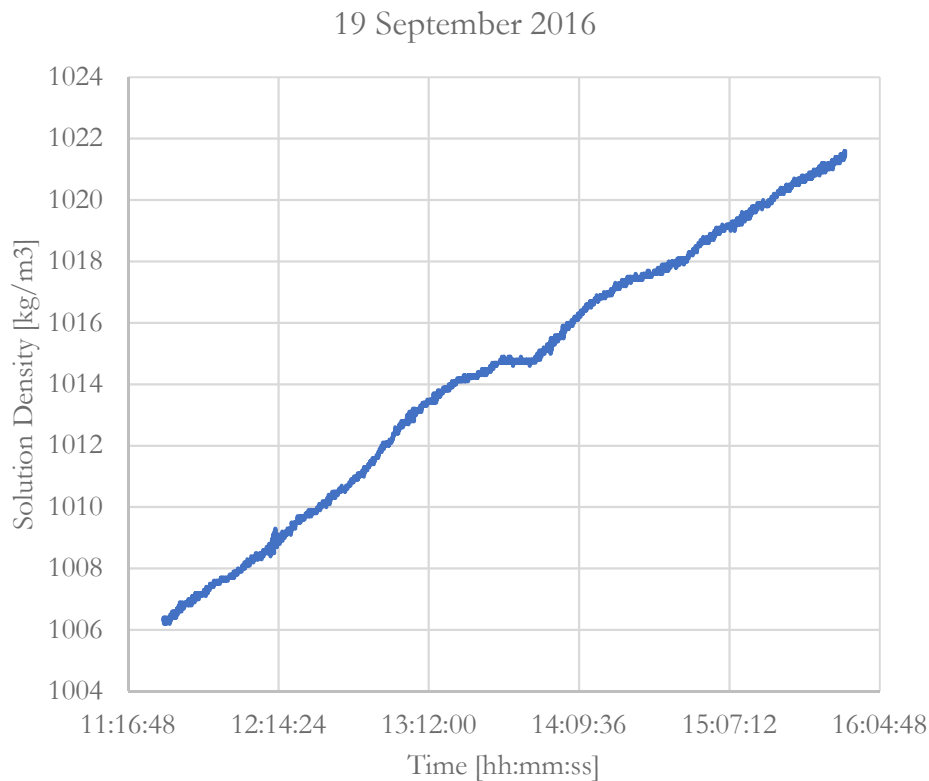
Figure 3. 21 - Solution Density trend in time during normal operative conditions

In parallel to the on-line measurements of density, Sotacarbo S.p.A. monitors, in all the tests, the pH with off-line measurement in laboratory. The pH measure gives information on the progressive increase of acidity of the solution. The pH measure is particularly important in the first phases of the process evolution, because the density sensors does not have the capability of measuring very low sulphuric acid concentration, since it provides as output the density of pure water. So, the evolution of the absorption reaction, in the very first process phase, is traced with the progressive increase of the acidity, i.e. decreasing of the pH.

No measures of the concentration are done on the sample port of the off-gases. The problem of this sample port is that is installed downstream of the blower B-201. This unit, when turned on, sucks the air of the atmosphere, since it is opened, altering the flue gas composition. From final tests, it has been verified that the feed gases have enough pressure to flow inside the system, for this reason the blower has been turned off. In addition, the blower was oversized from the engineering company and, if this unit is not

working, it is beneficial for the process, since it alters the process condition. In particular, the blower drags a considerable amount of liquid water and it reduce the gas residence time in the process, reducing the performance of the plant. However, during the experimentation execution, it has been necessary to turn on the blower for safety reasons. In fact, the amount of unreacted SO_2 exits from the blower hole, at man-level height. With the blower turned on, on the contrary, the gases have enough pressure to be discharged at the top of the chimney.

3.3.6. Modeling Considerations on the Experimental Absorption Column

In this first part of the work, modeling of the absorption column has the role to verify the project specification. In the catalytic section, the project specification has been validated, with the only difference regarding the conversion, linked with the catalyst, as already explained.

The absorption column is a batch process, so a dynamic simulation is needed. Only the liquid phase operates in a discontinuous way. The presence of a time-dependent liquid phase has an effect on the gas phase and, consequently, a time-dependent behaviour is expected also for the gas phase, since inside the column there is the contact between the two phases. As a very rough estimation, in order to avoid using complicate simulation at this first level of study, it is possible to consider a condition of stationarity for the gas phase. This assumption seems to be reasonable since, from the project mass balances, only one value of the off-gas composition is provided. In order to run a stationary simulation, the liquid recycle is not closed, as shown in Figure 3.22. The stream 3a simulates the feed from the catalytic outlet section. It is cooled down to 40 °C and it enters inside the column C-201. The absorber, in this plant layout, is a continuous operation and the feed 2.4a simulated the continuous recycle of liquid. The real column is a packed bed column with random package. In Aspen HYSYS® the model of the absorber is a sequence of stages where the equilibrium is approached. It hasn't put effort to determine the equivalent number of stages linked with a certain height of the real absorber. The reason is linked with the fact that, from the simulation, it is possible to see that with only one stage the SO_3 absorption is complete. This condition is demonstrated with the two asymptotic condition: pure liquid water and pure H_2SO_4. The simulation presents an important difference from the reality: inside the real column two different phenomena occurs, i.e. the physical absorption and the chemical reaction in liquid phase to form H_2SO_4. In this simplification, the two phenomena are split: physical absorption in C-201 and chemical reaction in T-201. According to Ref. [38] the reaction is instantaneous; this information combined with the complete absorption leads to the possibility to consider 100% of SO_3 conversion inside the tank model T-201.
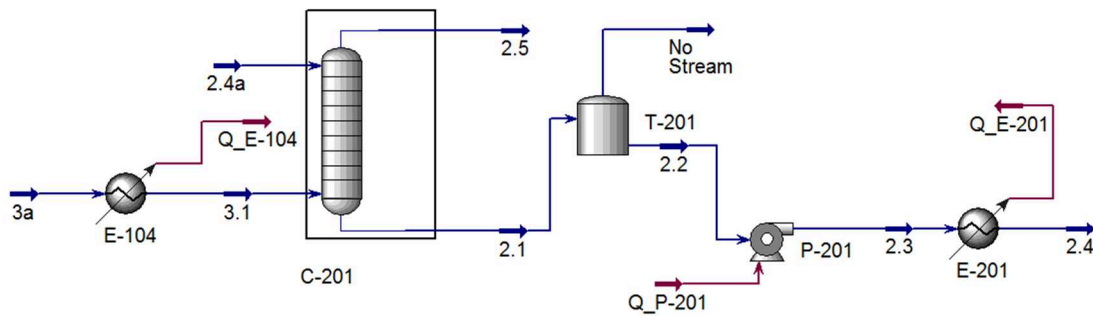
Figure 3. 22 - Simulation in Aspen HYSYS® of the absorption section, stationary assumption

Only the gas phase results can be analysed. In fact, for the consideration on the liquid phase, the recycle must be closed, combined with a dynamic simulation, since the same amount of water is transformed time by time in sulphuric acid. In particular, it is interesting to analyse the gas composition in the two asymptotic conditions (pure water liquid and pure H_2SO_4 liquid) as mentioned above. With pure water in 2.4a, the stream 2.5 is composed by a certain percentage of H_2O. This is a great difference with respect to project data, where no H_2O is declared to be in stream 2.5. The presence of H_2O in off-gases is link with the establishment of vapour-liquid equilibria inside the column. The vapor pressure of water at 40 °C is not negligible and some of H_2O should pass in gas phase. The only way to be sure that assertion is correct is to measure the off-gas composition. While, with pure H_2SO_4 liquid, the amount of H_2O in stream 2.5 is zero. The reason is simply that sulphuric acid has a strong dilution ability and the little amount of H_2O in 3a passes in liquid phase. Moreover, the amount of SO_2 in the off-gases decreases with the increase of H_2SO_4 in the liquid. The explanation is link with the lower solubility of SO_2 in H_2SO_4 with respect to water. As consequence, if some SO_2 does not react in the catalytic reactor, it is absorbed in the liquid or it is purged in the off-gases, according to the liquid composition.

3.4. Preliminary Design of Experiments

This section deals with the definition of new experiments, basing on the model and experimental analysis. The word preliminary stands for the fact that these experiments are the first ones for the determination of the suitable experimental plant model. Sotacarbo S.p.A wants from Politecnico di Milano the simplest model as possible, in order to better understand and manage the process.

Being the first useful experimental points, they need to cover at the best the experimental domain: this is the goal of the preliminary design of experiments procedure. However, it is also important to underline and define what needs to be experimented. In fact, in the following subsection, they are listed all the features which they emerged during the model and experimental analysis. All the features can be translated in nothing more than suggestions and improvements for IOSTO process. Some of them are simply tangible suggestions to implement in a fixed way for the improvements of the plant operation; others one are specifications to implement through the design of experiments.

3.4.1. IOSTO Improvements

In this section, all the improvements suggested from Politecnico di Milano to Sotacarbo S.p.A. are presented. Some of them requires a short dissertation, others a longer one.

1) The experimental tests showed that the kinetics expression available in literature are not able to predict SO_3 production rate, in the conditions of the IOSTO process: low concentration of reactant and platinum catalyst. As consequence, there is the need of finding a proper reaction rate model. The selection of the experimental points, as mentioned, are provided in the following section; while the model is presented, in the deeper analysis of the catalytic section, in the following chapter.

2) Another reason to determine a proper kinetics derives from the fact that the high dilution comes from CO_2. It is not documented the response on the catalyst in presence of a huge quantity of CO_2. The molecule, according to Sotacarbo S.p.A. [1], could form coke on the catalyst surface. However, it is more probable that CO_2 get adsorbed on the catalyst surface, blocking active site for the catalytic oxidation of SO_2 to SO_3. The way to monitor these aspects are different. First, it is possible to analyse in laboratory the catalyst before and after the reaction, in order to see the modification suffered by the catalyst itself. On the other side, it is possible to perform parallel experiments with and without CO_2, with the aim of understand if the SO_2 conversion remains unchanged or not. About this, it is possible to compare two reaction rates, in which in one set of experiments the reactant are diluted by CO_2 (real case) and another set of experiments in which the reactants are diluted by N_2. If this two expressions are identical, the CO_2 has no effect on the activity of the reaction; if there are differences, the causes are related to what said above.

3) From the experimental evidence the intermediate cooling between the catalytic bed lowers down the temperature of about 100 °C, from about 350 °C to 250 °C. Since Pt catalyst is active above 300 °C it was decided to insulate with a removable coat the pipe exposed to the atmosphere. This fact allows to eliminate the cooling of the gas stream, allowing to the reaction occurs also in the second stage, where the temperature is very low.

4) The experimental conversion is lower than the equilibrium conversion at a temperature of about 350 °C. It is proposed to increase the setpoint temperature of the two stages to a value of 400-450 °C. This is beneficial for the kinetics, due to the Arrhenius exponential trend with the temperature. For sure in such this way the equilibrium conversion decreases; however, it is still greater than 98 %.

5) In the previous sections, it was proposed that a possible reason link with the fact that the experimental conversion is lower with respect to the project one, it is connectable to insufficient contact time inside the reactor. It is suggested to decreases the flow rate of feed gases, in order to decrease the gas velocity and increase, as consequence, the contact time.

6) Since the reaction evolves with a decrease of the number of moles, Sotacarbo S.p.A. proposed to pressurize a little bit the plant (few barg). From the thermodynamic point of view, it could be beneficial; but as mentioned in the previous sections, the conversion at 350 °C is already close to one. The results of Aspen HYSYS® varying the pressure are shown in Figure 3.23.
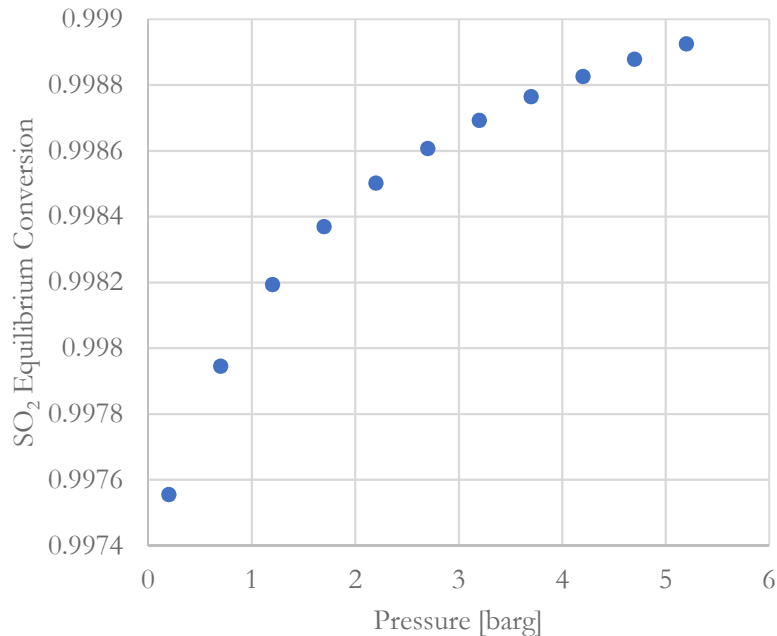
Figure 3. 23 - SO$_2$ equilibrium conversion at different pressure

The difference is on the third decimal digit, practically the value is constant in the pressure range of interest. On the other side the increase of pressure could have also some benefits on kinetics; but at the end, it was decided to consider this implementation with low priority, since the plant is designed to work at 0.2 barg and only little increases are allowed.

7) Industrially the catalytic oxidation of SO$_2$ to SO$_3$ is performed on V$_2$O$_5$ catalyst. Since one of the scopes of IOSTO study is to understand if the process is industrially feasible, it was proposed to perform experimentations also with an industrial V$_2$O$_5$ catalyst.

8) Another big problem of IOSTO operation is the big oscillation in temperature inside the reactor. The cause is the bad management of the ON/OFF logic of the electrical heaters. It is possible to decrease the switch time between ON and OFF position, acting on the controller parameter. With a faster response, the range of the oscillating profile will be lower. As mentioned in Chapter 2, a possible reason for the huge thermal dissipation is the presence of a thermal bridge. It is suggested to properly insulate the process tubes, avoiding any kind of dissipation through the structural connections.

9) In the first experimental campaign, the system of measurement was very poor. In fact, only the concentration of O$_2$ was measured, the other concentrations were

estimate according to the reaction stoichiometry. It is evident that, for more reliable results, a better instrument is needed. Sotacarbo S.p.A. prepared the request for an instrument able to measure the concentration of all the species (SO_2, O_2, SO_3, CO_2, N_2, H_2O) in the range of interest.

10) The concentration of SO_3 after the reactor, even in case of 100% of SO_2 conversion, is low. It takes a lot of time for the batch of water (10 kg) to get concentrated at the level of commercial interest (H_2SO_4 at 98% w/w). In order to simulate experimentally an entire cycle, hundreds of hours of working are needed, that is, for sure, non-economical affordable for research purposes. Moreover, it is not possible to extrapolate the curve of density of the liquid solution in time. In fact, it is almost sure that the trend of density profile is variable in time. It was proposed the purchase of sulphuric acid already concentrated at pre-established values. In this was the density curve is obtainable in discrete, but near, experimental regions.

11) The off-gas composition hasn't been monitored in the first campaign of experiments. As it has been already said, the verification of the presence of water in the off-gases is important to verify the discrepancy between the simulation and the project specification. However, this measure is affected by the presence of the blower that is open. Sotacarbo S.p.A proceeded isolating the blower from the atmosphere. Furthermore, when the blower is turned on, a substantial amount of liquid water is dragged from the top of the column. With the purchase of a demister this phenomenon could be reduced. Finally, although it will be not possible to measure the composition of the off gases, it will be possible to look if, from the sample port of the off-gases, there is or not the presence of water condensate.

12) The blower is turned on only for safety reason; in fact, SO_2 is toxic and above a certain concentration is harmful for the operators in the field. It is under evaluation the purchase of an SO_2 filter that block this gas, avoiding the release in the atmosphere.

3.4.2. Preliminary Design of Experiments Procedure

Once all the modifications and possible implementation had been completed, it has been possible to establish the so called preliminary design of experiment. This procedure refers to the selection of different values of the degrees of freedom of the experimentation. The words "degree of freedom" mean an input variable of the process, that can be modified and causes the modification of the performance (i.e. output) of the process itself. The problem of planning experiments is quite old and well studied since many years [40].

The study of IOSTO is at the first stage. Until now there is no the availability of a real feed stream coming from the pressurized flameless oxy-combustion; as consequence, the feed stream typology is "simulated gas" instead of "exhausted gas". For this reason, the dehydration section is not working and the feed gases are sent directly to the reactor from bottles. The first important things to do is to identify which are the degrees of freedom; their identification is related with the typology of feed, in this case gases from bottles. It is now provided the list and the explanation of the degrees of freedom:

- Catalyst type: test with the current platinum based catalyst and test an industrial catalyst based on V_2O_5. This is the most external degree of freedom; they are done all the tests with Pt first and then consequently all the tests with V_2O_5.
- Dilution gas: tests with a CO_2 rich stream (real case) and test with a N_2 rich stream (fake case). This is the second most external degree of freedom; they are done all the tests with N_2 first and then consequently all the tests with CO_2.

Once these two degrees of freedom are fixed, the preparation of the catalytic section of IOSTO plant is completed, i.e. all the other degrees of freedom (d.o.f.) are modified during the operation of the process. It is reasonable to modify all the d.o.f. that affect the SO_3 production, in particular:

- Setpoint temperature of the catalytic bed: for modeling purposes it is not necessary to select different setpoint for the first and the second bed. In fact, only one setpoint temperature was fixed. For sure, for optimization of the reaction conversion could be reasonable to select different temperature, but, at this level of study, is meaningless.
- Flowrate of the feed stream: at a certain composition, varying the flowrate allows to experience different contact times inside the reactor.
- Concentration of the feed stream: at a certain flowrate, varying the composition allows to understand the effect of the single component on the reaction conversion.

Until now, they have been shown only the degrees of freedom related to the better understanding of the reactor section. In fact, for Sotacarbo S.p.A. the priority is to deep analyse the behaviour of the reactor. Less effort, up to now, is put on the absorption column. Only one degree of freedom is associate with studies on the column:

- Concentration of H_2SO_4 solution inside the tank T-201 and continuously recirculated at the top of the column C-201. In different experimental tests, it can be charged in T-201 a solution of H_2SO_4 with different concentration. For this purpose, solutions with 36% w/w and 78% w/w were selected. The test with different acid solution are programmed at the end of the experimentation of the catalytic reactor. Before that moment, T-201 is charged with a weak acid solution that comes from the first campaign of tests.

Preliminary design of experiment simply means the selection of different combination of d.o.f. in order to cover at the best the experimental domain. The challenge, in this case, is that the experimentation is not done at the lab scale, but on a micro-pilot scale reactor. For this reason, it not affordable to performed lots of test, but the fewest possible number of tests. Moreover, each experimental data, measured by the instrument, is registered only after its stabilization (i.e. reaching of the stationary condition); it is considered a stationary measure, once the variable is constant in three subsequently measure in time. For each d.o.f., the reasonable range for IOSTO application was identified (Table 3.8). It is worth to mention that, in some cases, the variability is not to wide; in fact, it is problematic to

undergo in operative conditions far from the IOSTO original design. As it clear from Table 3.8, only the SO_2 molar fraction range, among all the species, is presented. In fact, it has been selected to operate with a O_2/SO_2 molar ratio constant and equal to 1.65. Doing so O_2/SO_2 molar ratio becomes a d.o.f.; for this reason, in some experiments this ratio was varied according to the same logics as the other variables, the results are shown in the last row of Table 3.9. Regarding the temperature, the minimum and maximum value are expressed in term of a range and, in the following section, it is presented which is the specific value used inside the range as setpoint.

	Minimum	Maximum
Temperature [°C]	320/400	450/500
SO_2 Molar Fraction [%]	1	3.16
Total Gas Flowrate [kg/h]	1	3.7

Table 3. 8 - Experimentation range of the selected d.o.f.

Actually, in this work, two different approaches for the preliminary design of experiment are used. The first one is based on a manually definition of all the possible experimental points to cover at the best the experimental domain. This method is affordable only in the case of few d.o.f. and few experiments, such as this case. However, when the context become more and more complex, an automatic procedure to define the experimental points is needed.

3.4.2.1. First Approach

The first approach is based to a manual combination of all the d.o.f., having defined a minimum, maximum and medium value. The minimum and the maximum value have been already selected and they are the boundaries of the experimental domain. The mean value and the exact maximum and minimum value are shown in Table 3.9. In order to avoid having too many experiment the last d.o.f. (O_2/SO_2 molar ratio) was varied only at the lower temperature of 350 °C and at the maximum total gas flow rate of 3.7 kg/h; for the other temperatures and flowrates this d.o.f. was selected to its maximum value, that is also the project one.

	Minimum	Maximum	Medium
Temperature [°C]	350	450	410
SO_2 Molar Fraction [%]	1	3.16	1.6
Total Gas Flowrate [kg/h]	1	3.7	2
O_2/SO_2 Molar Ratio	0.5	1.65	1

Table 3. 9 - Minimum, maximum and medium value of the different d.o.f.

Actually, the input setpoint that is possible to modify from the PLC, regarding to the feed stream, is the mass flowrate. For this reason, from the SO_2 molar fraction and O_2/SO_2 molar ratio is possible to evaluate the other molar fraction (N_2 or CO_2 according to the test). From the molar fraction, it is possible to calculate the mass fraction and, then, the mass flowrate.

The logics, used for the experimental definition, is the following:

- Select the temperature.
- For each temperature, select the total gas flowrate;
- For each temperature and for each total gas flowrate, select the SO_2 molar fraction.

In this way, the total number of different experiments is 27 (3x3x3). But as said, two additional O_2/SO_2 molar ratio were selected and so 6 (2x3) additional experiments are added. The total number of experiments become 33.

Other 33 experiments are needed for testing the different gas dilution (CO_2 vs. N_2) and additional 66 experiments are required for the V_2O_5 catalyst. The list of 66 experiments (for Pt) is shown in Appendix 3; the list for V_2O_5 catalytic is the same with the only different in the low, medium and high temperature. In this case the minimum and maximum temperature range changes (Table 3.10).

	Minimum	Maximum
Temperature [°C]	420/500	500/550

Table 3. 10 - Minimum and maximum temperature range for V_2O_5 catalyst

It seems to be a huge number of test, 132 at least. However, in each single day, when the plant is running, it is programmed to perform 9 tests (test at fixed temperature). At the end of these experimental tests, it is possible to select the project gas composition or, differently, the composition that maximize the SO_2 conversion, for sure in a feasible range of a flue gas of interest. With this composition, it is possible to test the absorption column through different batch of recirculating H_2SO_4 solutions.

3.4.2.2. Second Approach

The second approach is based on the application of a rigorous and automatic routine for the determination of experimental points, that allow to cover the whole experimental domain, with a limited number of experiments, independently of the problem one is going to solve. This method is based on the utilization of the "GetGoodExperiment" function in the BzzMath library of C++ [39]. It allows to find a good design of experiments, according to what said above: experiments must uniformly cover the experimental domain. This function can be adopted by starting from zero experiments already performed (this case) or from a condition in which it has already been performed a series of experiments.

This function requires three inputs to work; considering NE the number of experiments and NC the number of d.o.f.:

- A matrix with NE rows and NC column, i.e. NE previous experiments in which, for each one, there are defined all the NC degrees of freedom.
- A vector with NC elements, that indicates the minimum value for each d.o.f. in the experimental domain (see Table 3.9).
- A vector with NC elements, that indicates the maximum value for each d.o.f. in the experimental domain (see Table 3.9).

Actually, the real inputs for the PLC of IOSTO process are the mass flowrates; for this reason, they were directly used the component mass flowrates, avoiding the post-processing calculations from SO_2 molar fraction, O_2/SO_2 molar ratio and total mass flowrate. It is possible to arbitrarily decide the number of experimental points, 33 as the previous approach for this study.

3.4.2.3. Comparison between the Two Approaches

It could be interesting to compare somehow the two different approaches. In fact, the theoretical basis behind is the same, i.e. to cover at the best the experimental domain; however, the first one works in a compartmental way (complete combination among minimum, medium, maximum value of each d.o.f.) and the second one assign whatever value inside the pre-established domain.

It is not trivial to find a way to compare the two set of data. In fact, there is no dependence between two pair of vectors containing all the d.o.f. of a single experiment. In other words, the sequence of experimental runs between the two approaches is not correlated. In this work, it is proposed an analytical method to identify how similar are the two approaches. This method is based on the definition of a special mathematical norm:

$$\|\overline{Exp_1} - \overline{Exp_2}\| = \sqrt{\sum_{i=1}^{NC}\left\{\frac{(Exp_{1_i} - Exp_{2_i})^2}{0.5(Exp_{max_i} + Exp_{min_i})}\right\}}$$

Where:

- $\overline{Exp_1}$ is the vector that includes all the d.o.f. defined by the first approach, for a generic experiment.
- $\overline{Exp_2}$ is the vector that includes all the d.o.f. defined by the second approach, for a generic experiment.

It is practically the calculation of the norm of the difference vector between the different approaches. However, since all the d.o.f. (i.e. components of the vector) have different order of magnitude, the value is normalized. The normalization is done, in this case, considering the mean value between the minimum and the maximum of each degree of freedom.

This norm could be calculated for each single pairing between different experimental runs. In this way, it is possible to associate an experimental run of one approach with the respective one of the other approach. This pairing, of course, occurs when the two vectors have the minimum norm. Once all the pairings are estimated, it is possible to calculate a single value that could be the index of the nearness between the two approaches. In this work, it is calculated the sum of all the norm of each pairing and then, divided by the number of experiments. The results are resumed in Table 3.11.

Family of tests	Norm Actual Value	Norm Minimum Value	Norm Maximum Value
N_2 rich	1.02	0	5.39
CO_2 rich	0.91	0	5.36

Table 3. 11 - Norm calculation summary

There are two different family of experiments, based on the second most external degree of freedom, defined in the previous section. In fact, considering a dilution of N_2 instead of CO_2 brings to different norm values. The minimum norm, as definition, is zero, i.e. the two approaches are perfectly superimposed. On the other side, the maximum norm is calculated with the same definition. The only difference is that, the couple of vectors, are composed by the minimum and maximum value of each degree of freedom respectively. From Table 3.11, it is clear that the two approaches are not perfectly identical but they are pretty similar, since the norm is about 1, against a maximum value of about 5.

Chapter 4
Catalytic Section and Data Analysis

A deep analysis of the catalytic section of IOSTO process is provided in this chapter. Due to the innovative nature of the process and the absence of literature data about processes like IOSTO, there is the need of an extensive experimental analysis, accompanied by the theoretical and modeling description. Each step of experimentation is based on what defined in the previous chapter, dealing with the preliminary design of experiments. In this way, there is the possibility to investigate the domain of interest in an exhaustive and complete way, but with a limited amount of test. The problem, as mentioned in previous chapter, is that the system is not a lab scale plant, but a micro-pilot scale plant; with greater consumption of gases from bottles and resulting higher experimentation costs.

The final aim of this chapter is to provide a model for the catalytic section, in Aspen HYSYS® environment. The process flowsheet, used in this work, is already provided in Chapter 3. The only problem was on the reliability of the results, due to the usage of a literature reaction rate. In this chapter, starting from the experiments, different models on the kinetic reaction rate are provided. It will be described, in an extensive way, the numerical procedure to get the kinetic parameters and the consequent selection of the best kinetic model. It is worth to mention that, at this level of analysis, the detailed kinetic mechanism is not needed. There is only the need to establish a global kinetic expression with enough flexibility to fit the experimental data, regardless of what is actually happening at the molecular scale on the catalyst surface.

Another parallel goal is to perform what is technically called model-based design of experiments. It is very different from the preliminary one, but the concept is the same: provide suitable experimental points to test. The difference stays in the goal: in the preliminary design of experiments the goal is to cover at the best the domain of interest; in the case of model-based design of experiments, the goal is to provide only one additional experimental point to test, with the aim of improving the reliability of the fitted kinetic model. This procedure must be performed with the estimation of the kinetic parameters. Based on different criteria, that they will be discussed later on, it is possible to find a certain point of the multidimensional domain in which the model is poor. In this way, an additional experiment consolidates the model itself in that specific zone, increasing the reliability.

4.1. Experimental Tests

Considering the set of experiments established in the previous chapter, only a portion of them is considered in this work. The reason is linked with the fact that the number of experiments is quite high and the runs of the pilot plant are diluted in a long-time frame. Moreover, since the plant is a prototype, Sotacarbo S.p.A. encountered different kind of issues which they had to be solved, in order to run the plant in a safety way. In particular, in this work, the following operative conditions were experimentally tested:

- Platinum catalyst. Pt is the catalyst designed for IOSTO process; however, the testing of V_2O_5 industrial catalyst is required for future experimentations, in order to verify the process feasibility.

- N_2 rich stream. It was decided to start with a fake gas dilution of nitrogen and, only after the complete evaluation with this composition, switch to the real gas dilution of CO_2. The reason is simply based on the keeping of the catalyst at high level of activity; in fact, CO_2 could irreversibly damage the precious platinum catalyst. The understanding of the effect of CO_2 is one of the aim of the experimental study.
- Low temperature range of the catalytic reactors. An increasing of the setpoint temperature has a benefit on the kinetics and, since the thermodynamic equilibrium is very distant, this modification is interesting. Only after testing of the process at lower temperature and verifying the thermal and mechanical integrity of the plant, it is possible to increase the temperature up to 600 °C – 650 °C (design specifications).
- Total insulation of the intermediate cooling with a removable coat; in order to avoid the deep decreasing of temperature, under the activation of Pt catalyst.

Based on these aspects, the runs under study are shown in Table 4.1. It is clear that the variability with different flowrate isn't considered yet. The discussions and dissertations, for these reasons, are rough estimations from a numerical point of view. However, from a theoretical view point, the concepts, shown in these sections, are general. For this reason, for future experimentations, they can be utilized to improve the numerical reliability of the model. The variability of the composition is given in term of mass flowrate, since it is the input required from the PLC; please note that in all the cases the total mass flowrate fed to the reactor is equal to 3.7 kg/h.

Run	SO_2 [kg/h]	O_2 [kg/h]	N_2 [kg/h]	Setpoint T First Stage [°C]	Setpoint T Second Stage [°C]
1	0.083	0.069	3.548	350	350
2	0.132	0.110	3.458	350	350
3	0.254	0.212	3.234	350	350
4	0.083	0.042	3.575	350	350
5	0.083	0.021	3.596	350	350

Table 4. 1 - Different experimental runs under study

Only 5 runs, with respect to the 33 planned in case of Pt catalyst and N_2-rich stream, seems to be very low. Moreover, the temperature setpoint is constant through the different experiments. However, as it will be shown in the next section, the results of these runs were enough for a first estimation of the reaction rate.

In each day of experimentation different runs are performed, in particular run 1, 2 in the first day; while run 2, 3, 4, 5 in the second day (run 2 was repeated). The plant is tested for 8 hours per day and, considering the time to bring the system to the operative temperature, the reactants are fed for about 6 hours per day. The changing of the composition is done after the experimental evidence of the reaching of a steady state condition.

Before showing and describing the measure of the outlet composition, it is worth to show the temperature trend in time, at the inlet and outlet of each stage (Figure 4.1). In particular, Figure 4.1 refers to the second day of experiments, where four runs were performed.
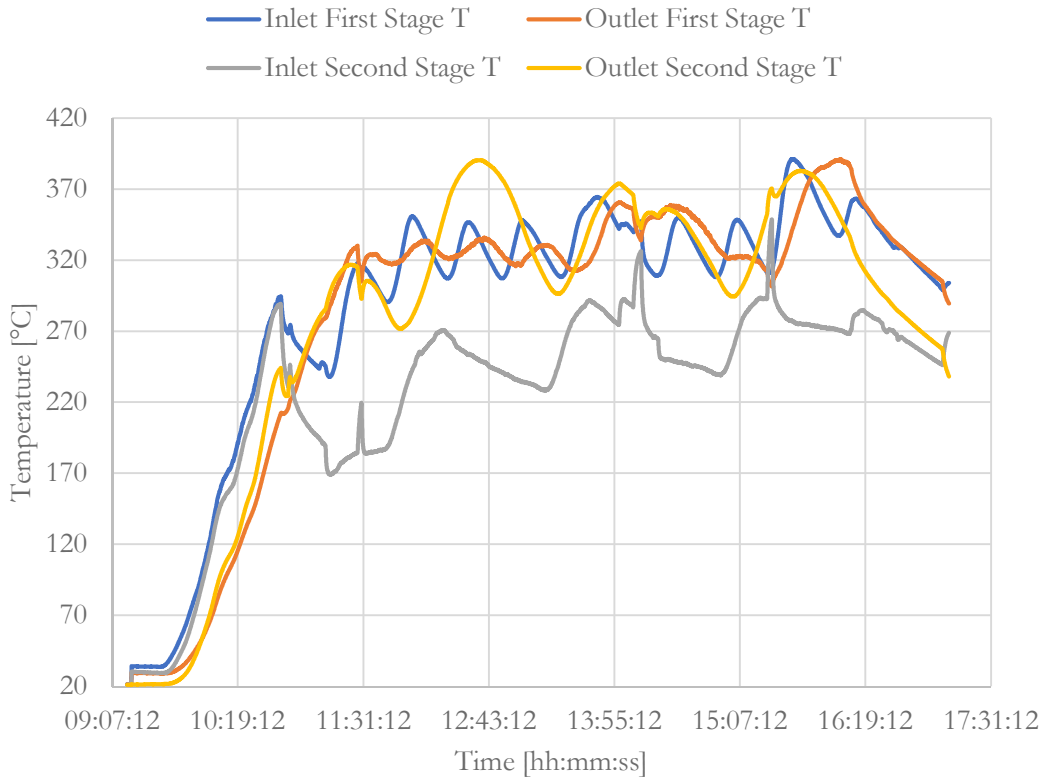
Figure 4. 1 - Temperature profiles in an entire experimentation day (first and second stage)

From Figure 4.1 different considerations can be done. At the very beginning of the experimentation, it is clear the heating phase; while, at the end, the system is shut down and the temperature starts to decrease. The sudden change of the temperature profile is in proximity of the time in which the feed composition setpoint is changed from the PLC. The most important point is that Sotacarbo S.p.A. couldn't decrease the temperature oscillation with a better managing on temperature control loop of the electrical heaters. These oscillations are completely undesired, both from the micro-pilot scale and industrial reactor perspective. All the modeling and theoretical consideration are done by neglecting the oscillations, since there is the possibility to eliminate this trend with a better manage of the controller and of the insulation coat. In this work, however, the presence of the oscillation allows to have a thermal variability. This fluctuation permits to define the variability of the kinetic constant of the reaction rate with the temperature. In fact, in case of constant temperature, this would be impossible. So as conclusion, the oscillations are undesired from the process point of view, but they allow to perform calculations in this work. These concepts are better analysed in the following paragraphs.

The other point is regarding the inlet temperature of the second stage; in fact, although the intermediate cooling was insulated, there is an important decrease of temperature, more or less equal to the previous experimentations, analysed in Chapter 3. The reason is probably linked with a bad insulation system.

It is now the moment to consider the core of the experimentation, i.e. the measure of the gas composition at the reactor outlet. As declared in Chapter 2, describing IOSTO process, there are three sample ports: one at the reactor inlet, one between the two stages and one at the outlet of the second stage. It was used a different instrument to measure the gas composition with respect to the experimentation of the previous year, in this case a gas chromatography instrument was used. The measuring system, also in this case, is very poor; the instrument is able to measure only the N_2 and O_2 concentration and all the other species are calculated, assuming the occurrence of the oxidation of SO_2 to SO_3 only. The calculation performed are explained in the following sections.

As mentioned there are three sample ports, but only one instrument. For this reason, the different measures are not performed at the same time, but alternated. It is possible to select a suitable sampling period for each port. Due to the precision of the mass flowmeter, the frequency of sampling of the inlet port is low, while it was set an equal frequency for the intermediate and outlet port. This idea was based on the consideration to track the composition in a similar way in each stage. The observation of the temperature profiles, however, brings to a negative consequence of this sampling method. Basically, since each temperature profile is oscillating, the conversion at the outlet of the first stage is not constant (although the inlet composition and the temperature setpoint are constant). In this way, since the concentration measures are not contemporary, the outlet composition of the second stage is related with an inlet composition of the second stage that is totally unknown. As consequence, it is not possible to use these data for the reaction rate estimation; it is possible to use only the value of the concentration at the outlet of the first stage, since it is related with a constant inlet composition, equal to the setpoint of the mass flowmeter. For future experimentations, in case of persistent temperature oscillation, it should be desirable to increase the frequency of sampling of the intermediate sample, decreasing or even eliminating the sampling at the outlet of the second stage.

So, as said in the previous paragraph, it is intuitive to think about the oscillation of the reactant composition, upon the temperature fluctuation. In fact, this trend is observable experimentally, as shown in Figure 4.2. In particular, Figure 4.2 refers to a specific case with a certain inlet composition; for this dissertation, it hasn't importance which is the specific run. It is clear that the variation of temperature controls the conversion of the reaction; in fact, with an increase of temperature, the molar fraction of O_2 decreases (i.e. the conversion increases). In particular, this specific trend validates the hypothesis of kinetic regime; in fact, with the increase of temperature there is a speed-up in the reaction rate. It is now clear what said above about the importance of the temperature fluctuation, in order to get more experimental data (at different temperature). For sure the

temperature fluctuations are relatively small, compared to the temperature domain of interest. As consequence, with this method, the reaction rate will be only valid in the lower temperature range. It is again emphasized the importance of performing experiments at different setpoint temperatures, in future tests. It is clear that there is a trend between the temperature and the conversion, so it is not possible to mediate the values in time; each experimental point must be considered independently.

Based on all the considerations made in this section, there is the need to understand the way to use and analyse raw data coming from the instrument. This is done in the next section.
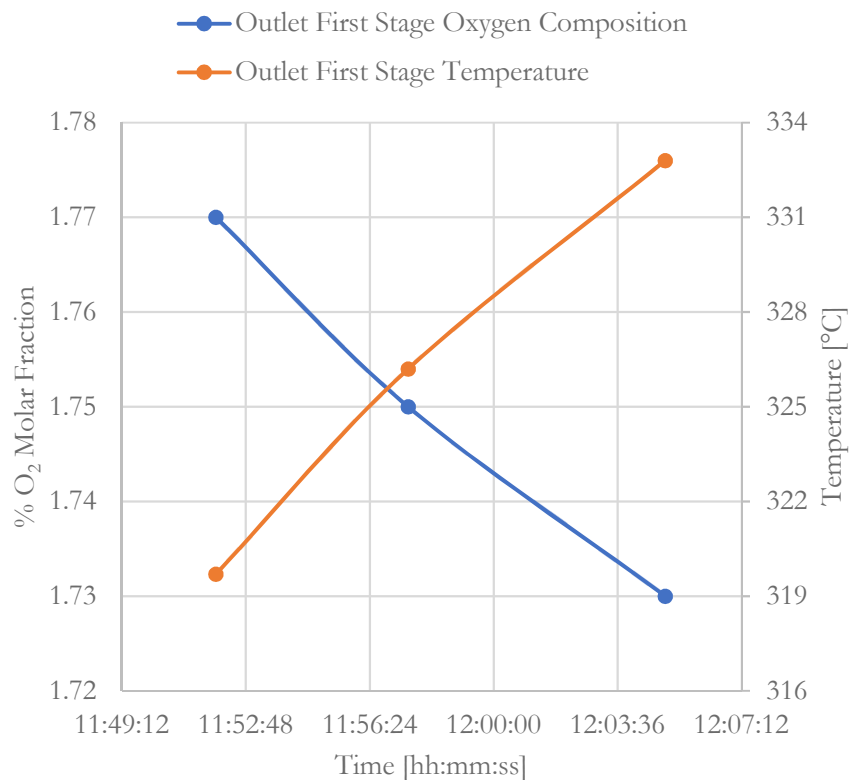
Figure 4. 2 - O$_2$ Molar fraction and temperature trends in time (fixed inlet composition)

4.2 Analysis of Data

The goal of this section is to develop a procedure to take raw data from the gas chromatography instrument, in order to get suitable data that could be used as input for the determination of the reaction rate. In fact, the measuring system is poor and even not all the data can be used.

First of all, as mentioned previously, the composition at the outlet of the second stage cannot be used. Regarding the intermediate gas composition, it is not possible to utilize all the data, since at each instant the inlet and outlet temperature vary independently, belonging to different control loops. However, it is possible to smartly select a proper subsystem of those data. The ideal and wanted behaviour for IOSTO catalytic reactor is

the isothermal condition; so, selecting the specific data, in which the inlet temperature is equal to the outlet temperature, it is implicitly considered a specific instant in which the reactor operates isothermally. This could be done assuming a steady state condition, that is reasonable, since the temperature does not change suddenly but gradually. Moreover, this consideration is true since the contact time inside the catalytic stage is low (1.26 s) and smaller with respect the time resolution of the PLC (5 s). So, it is reasonable to compare the temperature at the inlet and at the outlet of the first catalytic stage, at the same instant (so with no time shift). With this smart choice, the elaborated data, coming from this subsystem, can be inserted inside a routine for the evaluation of the reaction rate, with an isothermal reactor model. It is worth to mention that the tolerance to set the isothermal condition was quite low (ΔT between inlet and outlet less than 15 °C). Moreover, a further data elimination was performed for those data, with higher ΔT, in conflict with other data with lower ΔT. The measured outlet temperature was used, in an arbitrary way, such as the value for the isothermal condition of the reactor.

One of the most important reasons, that is linked with the elaboration of data, stays in the fact that, from the gas chromatography instrument, the only two data (% N_2 and O_2 molar fraction) are normalized, i.e. the sum of the two values is 100 %. In the reaction environment, for sure, there is not only N_2 and O_2 and so there is the need to understand how the instrument works, i.e. understand where is hidden the gas chromatography peak of SO_2 and SO_3. Concerning the inlet composition, in addition to the measured composition, it is possible to have an additional data, the one coming from the mass flowmeter setpoint. In Table 4.2, it is summarized the differences between the two information. In particular, it is provided the ratio of the experimental value with respect to the mass flowmeter value.

Run	N_2 Molar Fraction Ratio	O_2 Molar Fraction Ratio
1	0.998	1.820
2	0.992	1.860
3	0.994	1.833
4	1.000	1.802
5	0.988	7.491

Table 4. 2 - Molar fraction ratio (experimental/mass flowmeter) of N_2 and O_2

The N_2 ratio is next to the unit, it means that the gas chromatography instrument provides exactly the peak of N_2; while the O_2 ratio is greater, it means that the gas chromatography peak of O_2 includes also SO_2. The only difference is run 5 that assume a quite distant value for O_2 ratio. This run belongs to a condition of stoichiometric SO_2 and O_2, unlike all the other case in which oxygen is present in large excess. Due to the lack of data, in order to evaluate the other variables, run 5 is discarded. It is worth to say that, with this approximation, the future reaction rate will be valid only in case of feed with excess of oxygen, that is the typical condition of flue gases coming from a general combustion process. From these observations, it is possible to assume:

$$\begin{cases} n_{N_2}^{exp} = n_{N_2}^{fl} \\ x_{O_2}^{exp}\big|_{data} = x_{O_2+SO_2}^{exp} \end{cases}$$

Where:

- $n_{N_2}^{exp}$ is the experimental N_2 molar flow;
- $n_{N_2}^{fl}$ is the N_2 molar flow of the mass flowmeter;
- $x_{O_2}^{exp}\big|_{data}$ is the experimental O_2 molar fraction;
- $x_{O_2+SO_2}^{exp}$ is the real experimental molar fraction of O_2 plus SO_2.

Being n_{N_2} constant (N_2 is an inert inside the reactor), it is possible to calculate:

$$\begin{cases} n_{tot}^{out} = n_{N_2}/x_{N_2}^{exp,out} \\ n_{O_2+SO_2}^{exp} = x_{O_2+SO_2}^{exp,out} * n_{tot}^{out} \end{cases}$$

And from the definition of $x_{O_2+SO_2}^{exp,out}$, substituting the outlet flowrate as function of the inlet flowrate and SO_2 conversion, it is possible to get:

$$\chi_{SO_2} = (n_{O_2+SO_2}^{fl,in} - x_{O_2+SO_2}^{exp,out} * n_{tot}^{out}) * \frac{2}{3} * \frac{1}{n_{SO_2}^{fl,in}}$$

From the SO_2 conversion, all the outlet molar flowrates are known and, then, the mass flowrates. The inlet and the outlet mass flowrate (first stage) of each experiment of each species is tabled in Appendix 4. With these information, all the input data for the reaction rate determination are in place. In the following section, it is shown all the procedure to hand up with a kinetic expression to insert in the Aspen HYSYS® simulation, that is one of the goal of this chapter.

4.3. Experimental Reaction Rate Estimation

For the kinetic reaction rate equation determination, the first step is to select a proper model. It has been already mentioned that is not interest of this work entering at the molecular scale description. There is the need to identify a global reaction scheme, in particular, in the following section, two different reaction rate equations are proposed. From different input data, like the inlet and outlet mass flowrate and the first guess of the kinetic parameters, it is possible to find the optimal kinetics expression, through a regression method. At the end, after the description of the numerical routine, it is possible to show the results and make some consideration about the different proposed kinetic models.

4.3.1. Proposed Models for the Reaction Rate Equation

The models used in this work are the typical one normally utilized for gas-solid heterogeneous reaction, as documented in many papers [41], [42], [43], [44]. In particular:

- Power-law model.

- Langmuir-Hinshelwood-Hougen-Watson (LHHW) model.

The first one has no theoretical basis; it is only a polynomial formulation, in which the dependence on the concentration of the reactant species and temperature in the reaction rate is decoupled in two different functions:

$$reaction\ rate\ (T, \boldsymbol{C}) = f(T) * g(\boldsymbol{C})$$

The power-law model is used in general for every kind of reaction type and, due to its mathematical flexibility, it fits well the experimental data.

The second model (LHHW) is the most used for heterogeneous gas-solid catalytic reactions. In Chapter 3, the mathematical derivation of this model is already shown. Different from the power-law model, the LHHW model has a theoretical basis, linked with the adsorption-desorption of reactant species on the catalyst surface.

4.3.1.1. Power-law Model

Different from the LHHW, with the power-law there is the need to explicitly say that the reaction is reversible; it means that the reaction rate equation has a direct and indirect term. In the case of N_2-rich simulations, the relative reaction rate expression, for the catalytic oxidation of SO_2 to SO_3 is:

$$r = k_D P_{SO_2}^{\alpha} P_{O_2}^{\beta} - k_I P_{SO_3}^{\gamma}$$

Where:

- $k_D = A_D \exp\left(-\frac{Ea_D}{T}\right)$ is the direct kinetic constant.
- $k_I = A_I \exp\left(-\frac{Ea_I}{T}\right)$ is the inverse kinetic constant.
- α, β, γ are the reaction order for the different species.
- P_i are the partial pressures of the different species. It is the same defining the reaction rate as a function of the partial pressure or of the concentration. For a gaseous species, the partial pressures are a smarter choice.

For a reversible reaction, however, it is better to impose the thermodynamic consistency. It means that the reaction rate should approaches zero when the composition is approaching the equilibrium value, i.e.

$$k_D P_{SO_2,eq}^{\alpha} P_{O_2,eq}^{\beta} - k_I P_{SO_3,eq}^{\gamma} = 0$$

But, at the equilibrium condition, it is possible to define the value of the equilibrium constant:

$$Keq(T) = \frac{P_{SO_3,eq}}{P_{SO_2,eq} P_{O_2,eq}^{0.5}}$$

Being for an ideal mixture of ideal gases the activity value equals to the partial pressure value (reference 1 atm). It is worth to mention that the equilibrium constant is a function of the temperature only.

After some mathematical passage, substituting k_I as a function of k_D, it is possible to get:

$$r = k_D \left[P_{SO_2}^{\alpha} P_{O_2}^{\beta} - \frac{1}{C_e \, Keq(T)} P_{SO_2}^{\alpha-1} P_{O_2}^{\beta-0.5} P_{SO_3} \right] \quad P[kPa] \quad r \left[\frac{mol}{m^3 h} \right]$$

Where $C_e = 10.066$ is a constant for considering that the reference for the equilibrium constant is in atm, while the most comfortable unit of measure of the pressure, for the case under study, is kPa.

In the previous formulation, the reaction rate is useless since it is not defined the value of the equilibrium constant. The Van't Hoff equation correlates the value of the equilibrium constant at a generic temperature with the known value at a reference temperature (usually Tref is 25 °C):

$$Keq(T) = Keq(Tref) * exp\left(\int_{Tref}^{T} \frac{\Delta H_R^0(T)}{R \, T^2} dT \right)$$

But assuming the enthalpy of reaction ΔH_R^0 constant with temperature and equals to a mean value of -98 930 J/mol, it derives:

$$Keq(T) = Keq(Tref) * exp\left(-\frac{\Delta H_R^0}{R} \left(\frac{1}{T} - \frac{1}{Tref} \right) \right)$$

With $Keq(Tref = 25\,°C) = exp\left(-\frac{\Delta G_R^0(Tref)}{RTref} \right) = 2.5633 * 10^{12}$, using the value of ΔG_R^0 defined with a reference pressure of 1 atm.

For the implementation of the reaction rate expression in Aspen HYSYS® it is better to write the equilibrium constant in an Arrhenius form:

$$Keq(T) = K_{eq,0} * exp\left(-\frac{\Delta H_R^0}{R \, T} \right)$$

$$K_{eq,0} = constant = Keq(Tref) * exp\left(\frac{\Delta H_R^0}{R \, Tref} \right)$$

In the case of CO_2-rich simulations, the reaction rate expression is different. In particular, since CO_2 could affect the reaction extent, getting absorbed on the catalyst surface, there is the need to take into explicitly account the effect of CO_2. This is done considering a CO_2 term in the direct and indirect term of the reaction rate, with a specific reaction order:

$$r = k_D P_{SO_2}^{\alpha} P_{O_2}^{\beta} P_{CO_2}^{\delta} - k_I P_{SO_3}^{\gamma} P_{CO_2}^{\varepsilon}$$

And similar to what did before, applying the thermodynamic consistency, it is possible to get this final expression of the reaction rate:

$$r = k_D \left[P_{SO_2}^{\alpha} P_{O_2}^{\beta} P_{CO_2}^{\delta} - \frac{1}{C_e Keq(T)} \frac{P_{SO_2}^{\alpha-1} P_{O_2}^{\beta-0.5} P_{CO_2}^{\delta} P_{SO_3}}{P_{CO_2}^{\varepsilon}} \right] \quad P[kPa] \quad r\left[\frac{mol}{m^3 h}\right]$$

4.3.1.2. Langmuir-Hinshelwood-Hougen-Watson Model

The mathematical derivation of the LHHW model is already provided in Chapter 3. In this case, however, the equation is expressed as function of the partial pressure, instead of the concentration, but with the same structure and hypothesis. This modification can be done since all the parameters will be fitted based on the experimental data and, so, it is formally the same, with the obvious difference in the numerical value of the kinetic parameters. Once an equation of state is defined, it is possible to switch between the equation in partial pressure or concentration, with a proper modification of the kinetic parameters.

In case of N_2-rich simulations, the LHHW kinetic model, in term of partial pressure, is:

$$r = \frac{k_D P_{SO_2} P_{O_2}^{0.5} - k_I P_{SO_3}}{\left(k_{SO_2} P_{SO_2} + k_{O_2} P_{O_2}^{0.5} + k_{SO_3} P_{SO_3} + 1\right)^2}$$

Where k_i is the generic kinetic constant of the LHHW, expressed in the following way:

$$k_i = A_i \exp\left(-\frac{Ea_i}{T}\right)$$

Also in this case, it is better to apply the thermodynamic consistency to the kinetic expression, in order to have a physically sound expression:

$$r = \frac{k_D \left[P_{SO_2} P_{O_2}^{0.5} - \frac{1}{C_e Keq(T)} P_{SO_3} \right]}{\left(k_{SO_2} P_{SO_2} + k_{O_2} P_{O_2}^{0.5} + k_{SO_3} P_{SO_3} + 1\right)^2}$$

A consideration a little but different for LHHW model with respect to the power-law one need to be done for the rate for CO_2-rich simulations. The LHHW model is modifying considering a competitive adsorption of CO_2 on the catalyst surface. It means that the active side can be occupied by the reactant species or by the carbon dioxide as well. With similar mathematical passages like those presented in Chapter 3, the following equation is obtained:

$$r = \frac{k_D \left[P_{SO_2} P_{O_2}^{0.5} - \frac{1}{C_e Keq(T)} P_{SO_3} \right]}{\left(k_{SO_2} P_{SO_2} + k_{O_2} P_{O_2}^{0.5} + k_{SO_3} P_{SO_3} + k_{CO_2} P_{CO_2} + 1\right)^2}$$

4.3.2. Numerical Routine for the Experimental Reaction Rate Estimation

All the elements, for the explanation of the numerical routine for the determination of the reaction rate parameters, are now in place. The experimental determination of these parameters is based on a regression method, i.e. a routine that is able to find the value of the parameters, that minimize the difference between the experimental and the modeling dependent variable, upon a proper set of independent variables. In principle, in the case of interest in this work, with the knowledge of a different set of partial pressure (independent variables) and the relative reaction rate value (dependent value), it is possible to perform a non-linear regression for the determination of the parameters. Actually, the reaction rate value is unknown, since the IOSTO reactor cannot be consider as a differential reactor and so a classical regression method cannot be applied. The known values are: the inlet and the outlet compositions. The relationship between the inlet and outlet composition is the reactor model. For this work an isothermal, pseudo-homogenous model of the catalytic reactor is adopted. So, it is possible to minimize the difference between the outlet experimental composition and outlet modeling composition. In particular, the outlet modeling composition is determined by solving the modeling equations, in this work they are ODEs equations. The modeling equations require the initial conditions (inlet composition and temperature) and the values of the reaction rate parameters, that they are unknown. For this reason, the regression routine (that is an optimization routine) is solved simultaneously with iterative resolution of the model, changing, iteration by iteration, the values of the reaction rate parameters until the identification of the optimal point, i.e. the point in which the difference between the experimental value and the modeling value of the outlet composition is minimized. These concepts may be unclear; so, in Figure 4.3, it is provided a general and conceptual schematization of the adopted approach.
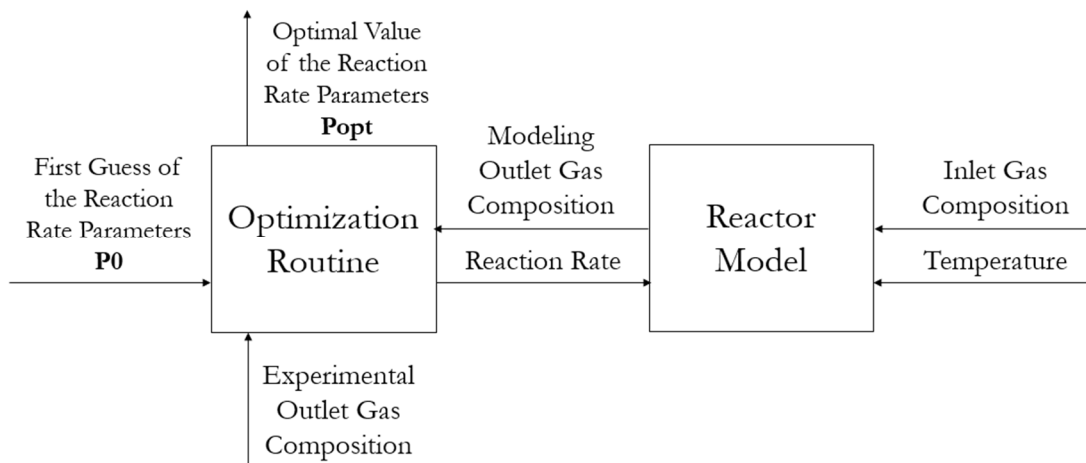
Figure 4. 3 - Conceptual schematization of the reaction rate parameters estimation

After the general description, it is possible to analyse the numerical resolution of the problem. In this work, the numerical problem has been solved through a C++ code using

Microsoft Visual Studio 2013®. In particular, the BzzMath library was used for this purpose. All the codes are provided in Appendix 5a and 5b, for the power-law and LHHW models, respectively. The two codes are very similar and, for this reason, they are explained together, pointing out the few differences.

After the variable declaration at the top of the code, the "main" function is provided. It is worth to mention the importance of setting a proper set of first guess for the reaction rate parameters (P0). For the power-law model reasonable values were selected; for the LHHW model it was used the set of parameters of the literature kinetic expression, provided in Chapter 3, with the obvious modification for the unit of measure. The units of measure of the different parameters of the LHHW model are very different and, for this reason, each parameter was re-scaled between one and ten in absolute values. This procedure allows to have a non-stretched domain, with a consequent ease of convergence for the optimizer. In the "main" function there is the call of the robust optimization routine (BzzMinimizationRobust). For a better convergence, the routine is called five times consecutively, using as first guess the optimized value of the previous call. The results are then printed in a Microsoft Excel® sheet. The optimization routine requires the objective function to be minimized, that is defined in "F3sse" function. In general, for regression problems, the sum of squared errors (SSE) is used as objective function:

$$SSE = \sum_{i=1}^{Nexp} \sum_{j=1}^{Nc} \omega_{i,j} \left(y_{i,j}^{exp} - y_{i,j}^{mod} \right)^2$$

Where ω_i is a suitable weight in order to balance the possible difference in order of magnitude of the different variable to compare. In this work, a more robust definition of the objective function is used:

$$SSE = \sum_{i=1}^{Nexp} \sum_{j=1}^{Nc} \left| \frac{y_{i,j}^{exp} - y_{i,j}^{mod}}{\varepsilon + y_{i,j}^{exp}} \right|$$

Where ε is a suitable small value (1e-4 in this work) to avoid problems if $y_{i,j}^{exp}$ tends to zero. The objective function requires the values of $y_{i,j}^{mod}$, that they are provided as outputs of the "F1odeSol" function. These values are determined with the usage of an ODEs solver (BzzOdeStiff in this work). In particular, since there is only the sample port at the reactor outlet, $y_{i,j}^{mod}$ corresponds to the outlet gas composition from the first stage. The composition, arbitrarily, is compared in term of mass flowrate. The BzzOdeStiff requires the ODEs equations that need to be integrated. The set of model equations is provided in "F2SistDiff" function. In this case the only important thing to say is that, in this function, they are performed all the required calculations for the reaction rate, given the guess of its parameters. In LHHW model, the reaction rate parameters are scaled again to their original order of magnitude, modified for a better optimization resolution.

4.3.3. Model Parameters Results and Comparison

The numerical routine, presented in the previous section, has been applied for the experimental points under study (Appendix 4). For the power-law equation, the numerical value of the parameters is shown in Table 4.3.

Parameter	Numerical Value
A_D	1.5225e+6
Ea_D	4.6024e+3
α	2.006
β	-1.682
r in [mol/m³/h], P_i in [kPa]	

Table 4. 3 - Optimal parameters for the power-law reaction rate equation

While, the results in case of the LHHW model are shown in Table 4.4:

Parameter	Numerical Value
A_D	2.5109e+05
Ea_D	-7.4585e+03
A_{SO_2}	7.9913e-09
Ea_{SO_2}	-1.6258e+04
A_{O_2}	6.5354e-05
Ea_{O_2}	-1.0899e+04
A_{SO_3}	9.3720e-08
Ea_{SO_3}	-1.5573e+04
r in [mol/m³/h], P_i in [kPa]	

Table 4. 4 - Optimal parameters for the LHHW reaction rate equation

The corresponding comparison between the experimental and the modeling results is shown in Figure 4.4 and Figure 4.5 respectively. Please note that the comparison is done in term of conversion, although the SSE function is evaluated in term of mass flowrate. This is done since, in absolute value, the mass flowrate is small. As consequence, in a quite wide range of conversions, the experimental and modeling difference between mass flowrates is smaller than the one between conversions. So, this choice is made based in order to have a better visual impact only. In these figures, it is plotted the deviation of all the experiments, ordered by increasing conversion. For the plots of the composition along the reactor axial coordinate and the relative experimental data, it is possible to look Appendix 6a and 6b; those plots are a different representation of the same problem.
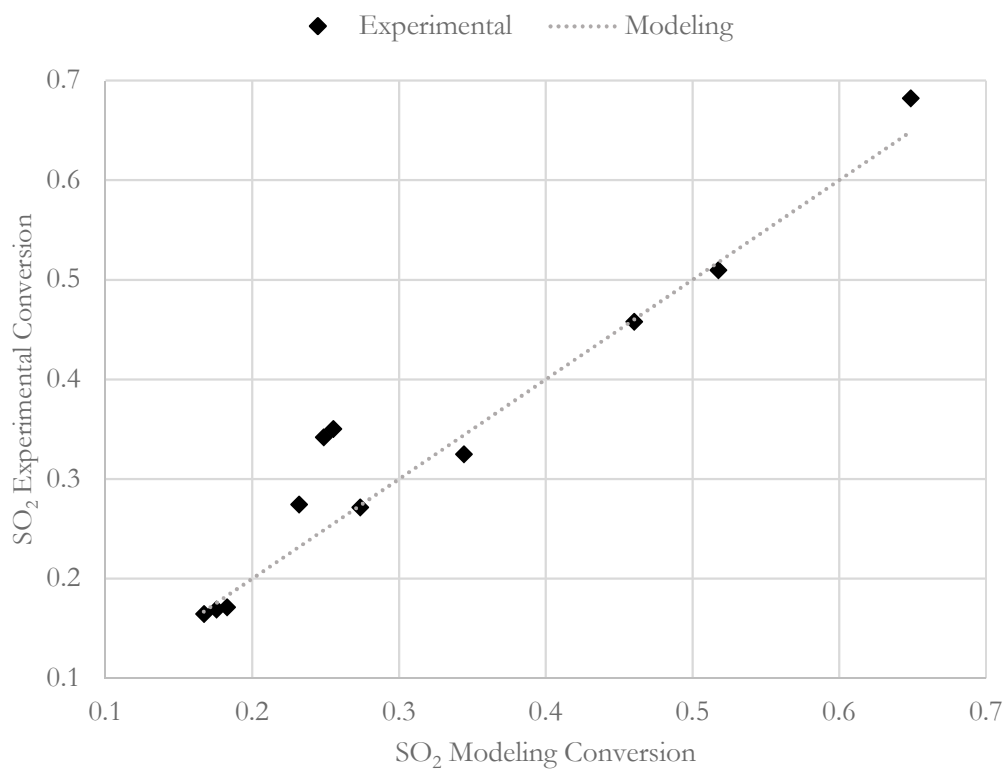
Figure 4. 4 - Modeling and experimental conversion comparison (power-law model)
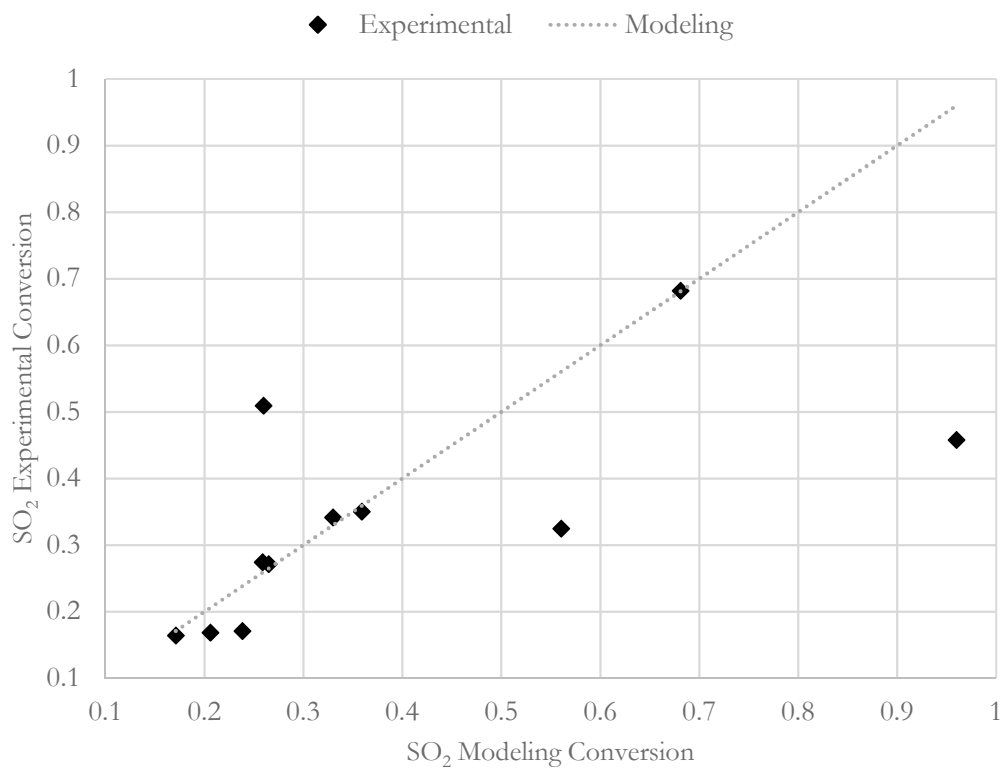
Figure 4. 5 - Modeling and experimental conversion comparison (LHHW model)

Only with a qualitative comparison, it is clear that the power-law model fits better the experimental data than the LHHW one. From a quantitative point of view, this affirmation is validated by the analysis of the final value (i.e. after the optimization) of the SSE function, shown in Table 4.5.

	Final Value of SSE
Power-law Model	1.628
LHHW Model	5.479

Table 4. 5 - Comparison of the final value of the SSE function for the different models

After having pointed out this peculiarity of the different experimental reaction rates, it is important to provide a suitable explanation. Before showing any sort of explanation, it is worth to reaffirms that the experimental domain that it has been investigate is only partially analysed. All the variability (in term of temperature, concentration, flowrate) shown in Chapter 3 (preliminary design of experiments) is only partially investigated. As consequence, any explanation from this set of experimental data cannot be considered as an exhaustive explanation of the behaviour of the system. In fact, with further experimentations, some aspects, now impossible to detect, may arise.

From the data analysis, a key aspect for the explanation of the better results of the power-law model is the oxygen concentration. In particular, it is interesting to analyse the initial condition of run 2 and run 11, compared with the corresponding outlet conversion (Table 4.6).

	SO_2 [kg/h]	O_2 [kg/h]	N_2 [kg/h]	T [K]	Conversion
Run 2	0.083	0.069	3.458	588.05	0.2713
Run 11	0.083	0.042	3.575	588.45	0.5096

Table 4. 6 - Run 2 and run 11 initial condition and the relative outlet conversion

These two runs are selected since the SO_2 inlet flowrate and inlet temperature are the same. The only difference is in the O_2 flowrate and of course in the N_2 flowrate, since the total mass flowrate is always 3.7 kg/h. All the experimentations are done in excess of oxygen, in compliance with the typical condition of the flue gases from an oxy-combustion process. Nitrogen is an inert at the reaction condition, while oxygen reacts with sulphur dioxide to get sulphur trioxide. The reaction is catalysed by a solid catalyst and, on its surface, the reactant species get adsorbed to allow the reaction to evolve. With a decrease of oxygen, the conversion increase. The phenomenon is probably linked with the stronger adsorption power of O_2 compared to the other species. With less O_2 adsorption, since its concentration is less, more active site are available for SO_2 (limiting reactant) and so, the reaction can occur faster. This experimental evidence is correctly interpreted by the power-law model, with a negative order of reaction for oxygen. On the other side, the LHHW model, due to its formulation, has a fixed and positive exponent for oxygen. For sure, the LHHW model considers the different adsorption power with the different constant at the denominator and in fact, the O_2 adsorption pre-exponential factor (A_{O_2}) is orders of magnitude bigger compared to the one of the other species.

However, the effect of the LHHW denominator has a smaller effect compared to the reaction order in the power-law model. For this reason, the power-law reaction rate has a higher mathematical flexibility than LHHW one and so, it fits better the data in the analysed experimental domain.

As conclusion, for the further analysis of the rector model in Aspen HYSYS®, only the power-law model is considered. Moreover, the Weisz-Prater Criterion and Mears' Criteria are verified. The calculations are identical those of Chapter 3 and they are summarized in Table 4.7. The reactor operates in fully chemical kinetics control.

	Actual Value	**Chemical Kinetics Regime**
C_{WP}	1.04e-1	<1
C_{M_m}	4.59e-3	<0.15
C_{M_h}	4.48e-3	<0.15

Table 4. 7 - Weisz-Prater Criterion and Mears' Criteria

4.4. Aspen HYSYS® Simulation and Model Validation

Once the experimental reaction rate is known, it is possible to insert the parameters data inside Aspen HYSYS® environment, in order to perform simulations. The real advantage of using Aspen HYSYS® compared to an in-house pseudo-homogeneous model (developed, for instance, in C++ language) is the heat management. In fact, this commercial simulator has the capability of solving the energy balance of the reactor by imposing the outlet temperature of the reactor as input variable. In particular, referring to Figure 4.6, it is possible to set an arbitrary temperature for stream 1.6 and 3; the simulator evaluates the values of Q_R-101A and Q_R-101B, in order to get the pre-established outlet temperature, given a certain value of the inlet temperature.
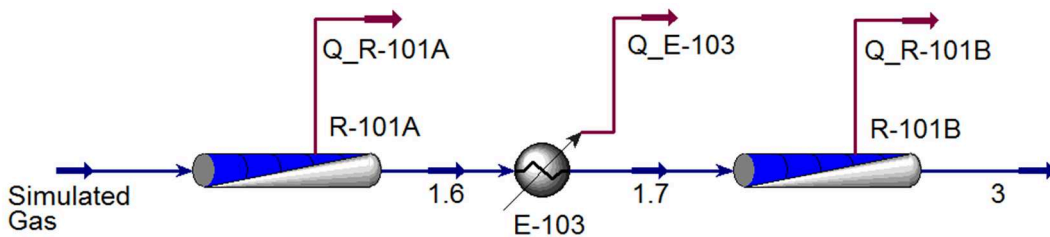
Figure 4. 6 - Aspen HYSYS® flowsheet of the catalytic section

This feature can be used for the model validation. In fact, for the parameters estimation, some data were discarded, since the hypothesis of isothermal reactor wasn't valid. But once the reaction rate is established, it is possible to use it not only for the modeling of an isothermal reactor. Of course, they can be considered only those data that they are inside the experimental domain in which the reaction rate was fitted. According to this logic, six experimental points are available for the reaction rate validation. These data are listed in Appendix 7, where the corresponding initial condition, inlet and outlet temperature and outlet conversion of each experimental run are shown. So, considering

the simulation of the first stage only and imposing the temperature of stream 1.6 as input value (Figure 4.6), it is possible to determine the simulated conversion. The results are shown in Figure 4.7; the plot is similar to Figure 4.4 with the addition of the red triangular points. These points represent the experimental conversion values of Appendix 7 and it is clear that they are represented pretty good by the experimental power-law kinetics (dashed grey line). For sure in some cases the approximation is considerable (at most ± 0.1 conversion points); but considering the fact that the activities in this work are the early stage activity of IOSTO process, it is reasonable to accept those data. For these reasons, it is possible to state that the power-law reaction rate is validated inside the analysed domain. Once a kinetic expression is validated, it is licit to use it for process simulations. With this determination, an important goal of this work is reached.
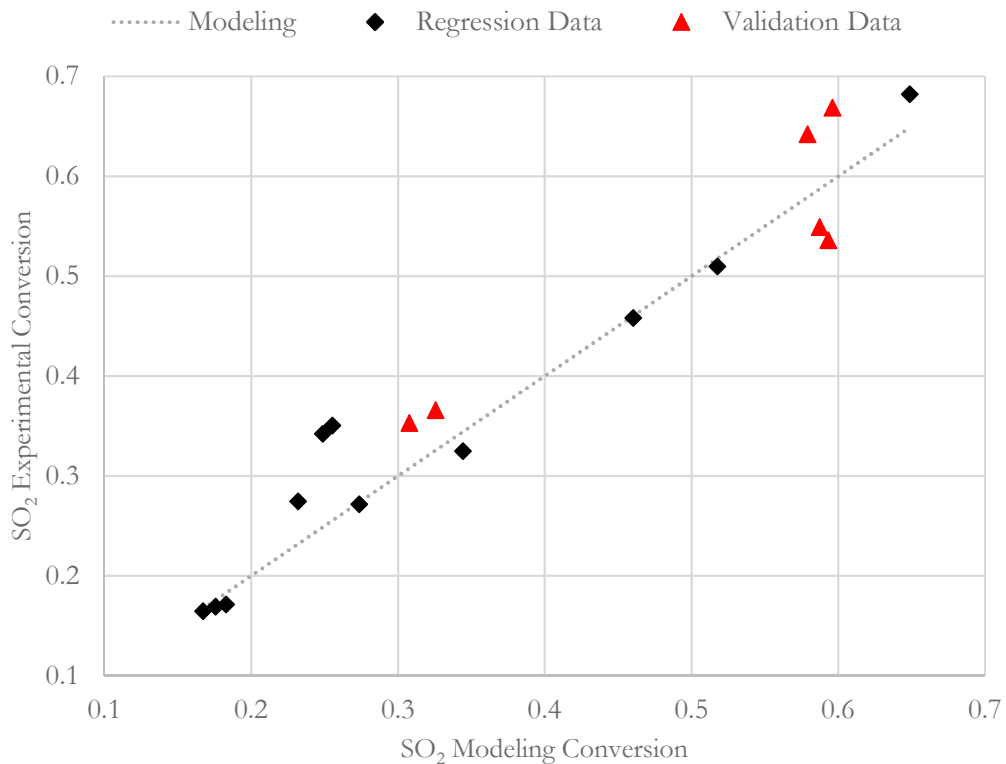
Figure 4. 7 - Modeling and experimental conversion comparison for reaction rate validation

4.5. Optimal Operative Condition inside the Experimental Domain

The knowledge of a validated reaction rate expression allows to perform several simulations in Aspen HYSYS® environment. The logics is to find the best operative condition for the maximization of the SO_2 conversion. The analysed experimental domain is shown in Table 4.8, that corresponds to the d.o.f. variability realized in the different experimental runs.

	Minimum	Maximum
SO_2 [kg/h]	0.083	0.254
O_2 [kg/h]	0.042	0.210
N_2 [kg/h]	3.234	3.575
Temperature [°C]	314.9	377.3

Table 4. 8 - Experimental d.o.f. range

The optimal operative condition comes from the maximization of the outlet SO_2 conversion. This condition could be found changing the d.o.f. of Table 4.8. In particular, it is possible to change the temperatures of stream "Simulated Gas", 1.6, 1.7, 3 (see Figure 4.6), since they belong to different control loops. With Aspen HYSYS®, with the definition of a "Case Study", it is relatively easy to modify the different d.o.f. and perform the corresponding simulation, in an automatized way.

The optimal temperature for each stream, from the simulation results, is the maximum one. This behaviour is reasonable since, at this level of temperature, the equilibrium constant has a big value. The inverse kinetic constant has the following formulation and the parameters are listed in Table 4.9.

$$k_I = \frac{k_D}{C_e\,Keq(T)} = A_I\exp\left(-\frac{Ea_I}{T}\right)$$

Parameter	Numerical Value
A_I	1.2953e+10
Ea_I	1.6502e+4
r in [mol/m³/h], P_i in [kPa]	

Table 4. 9 - Inverse kinetic constant parameters for the power-law model

Comparing the direct and inverse kinetic constants, it is possible to get the results listed in Table 4.10, that allow the explanation of the aforementioned optimal temperature value.

	Direct	Inverse
$k_{350\,°C}$	9.44e+2	4.09e-2
$k_{550\,°C}$	5.68e+3	2.55e+1
Ratio $k_{550\,°C}$ / $k_{350\,°C}$	6.01	622.69

Table 4. 10 - Direct and inverse kinetic constant at different temperature

At the setpoint temperature (350 °C) the direct term is orders of magnitude bigger than the inverse one. This aspect is linked with the great value of the equilibrium constant and it follows that, in the experimental domain, the optimal temperature is the biggest one, as mentioned previously. With an important increase of temperature (550 °C, much greater than the maximum experimental temperature), the direct term is still bigger than the inverse one; but the ratio for the inverse kinetic constant is considerably higher. It means that, with an increase of temperature, the inverse term becomes more and more

important. This feature is in line with the classical trend for an exothermic and reversible reaction.

The conversion increases with a decrease of the total flowrate, at fixed temperature. In fact, there are not present consecutive undesired reactions and so, the contact time inside the catalytic bed can be increased. A possible reason of the distance of the experimental conversion from the equilibrium one, as mentioned in previous chapters, can be linked with an insufficient contact time, assuming reasonable a temperature setpoint level of 350 °C. Or, in an opposite perspective, the reactor volume is insufficient for the inlet gas flowrate.

Regarding the composition, the simulation results are in line with what said from the analysis of the power-law expression, in the previous section (4.3.3.). The conversion increases, increasing the SO_2 concentration, due to its positive order of reaction. The situation is opposite in case of oxygen, in fact its order of reaction is negative. This situation is reasonable since, although O_2 is a reactant, it is present in excess in the feed mixture. Finally, the conversion increases with a decrease of N_2 concentration. In fact, nitrogen is an inert and, with less dilution, the only effect is in the increasing of the partial pressures of the reactant species.

As conclusion of this section, it is worth to say that a specific optimal point is not yet defined. It has been defined only possible changes in the d.o.f. for future experimental runs. In fact, the experimental domain is now to small. Only by continuing the experimentation, it will be possible to find the specific experimental point.

4.6. Model-based Design of Experiments

The purposes of this work are different and not only linked with the theoretical modeling of the IOSTO process. The requested tasks from Sotacarbo S.p.A. concern also the study of the experimental behaviour of the plant. In particular, they have been performed activities concerning data analysis, comprehension of the experimental profiles of the process, troubleshooting, process improvements and design of experiments. This last task concerns the optimal planning of the experimental runs. It can be divided in at least two categories [39]:

- Methods of selection of experimental points to completely cover the experimental field at the best. This category of preliminary design of experiments has been already analysed in the final part of Chapter 3.
- Methods of selection of experimental points in order to improve the parameter estimation of a specific model. This category is the object of this section and it is strictly linked with the definition of a proper kinetic model and its experimental parameter regression.

It can be also considered another category that deals with methods for the selection of experimental points in order to discriminate among alternative models. In this work, there is the clear evidence that, in the analysed experimental domain, the LHHW doesn't work so well and, for this reason, only the power-law model has been considered. It possible to extend, in future developments of this work, the third category of design of experiments, in case of multiple models.

The need of developing rigorous design of experiments comes from the fact that a certain design of experiment, that is optimal for a specific problem, might not be reasonable when considering other problems [39]. In the literature, several strategies are proposed to improve parameter assessment and model discrimination [39]. In order to analyse some criteria adopted to propose new experimental points by exploring features of the selected models, it is suitable to give some definitions. These definitions and the general theoretical background are shown in section 4.6.1., while, in section 4.6.2., the practical resolution of the problem is presented.

4.6.1. Theoretical Background of the Model-based Design of Experiments

Some criteria require a linearization of the model in the neighbourhood of the minimum point. For sake of simplicity, it is supposed to have only one dependent variable y=g(**x**, **b**). Let F_n and F_{n+1} be matrices of the linearized model:

$$F_n = \begin{pmatrix} f_1(\boldsymbol{x}_1) & \cdots & f_p(\boldsymbol{x}_1) \\ \vdots & \ddots & \vdots \\ f_1(\boldsymbol{x}_n) & \cdots & f_p(\boldsymbol{x}_n) \end{pmatrix}$$

$$F_{n+1} = \begin{pmatrix} f_1(\boldsymbol{x}_1) & \cdots & f_p(\boldsymbol{x}_1) \\ \vdots & \ddots & \vdots \\ f_1(\boldsymbol{x}_{n+1}) & \cdots & f_p(\boldsymbol{x}_{n+1}) \end{pmatrix}$$

Where $f_k(\boldsymbol{x}_i)$ coefficients are derivatives of g function with respect to parameters b_k calculated in $\mathbf{x}_i$ (i-th experimental vector) and for the optimal **b**. If there are more than one dependent variable, for each of them there are matrices like F_n and F_{n+1}. In particular, the linearized model has the following expression:

$$y_i = b_1 f_1(\boldsymbol{x}_i) + \cdots + b_p f_p(\boldsymbol{x}_i) = \boldsymbol{f}_i^T \boldsymbol{b} \quad i = 1, \dots, n$$

The matrix $F \in \mathbb{R}^{n \times p}$ with $n \geq p$ can always be factorized in three matrices:

$$F = UDV^T$$

Where the matrices $U \in \mathbb{R}^{n \times n}$ and $V \in \mathbb{R}^{p \times p}$ are both orthogonal; in other words, $U^T = U^{-1}$ and $V^T = V^{-1}$. Moreover, the coefficients of matrix D are the eigenvalue of matrix $F^T F$. It is also possible to get matrix P_n that represent the principal axes (eigenvector matrix) of F_n. From the product of these two $F_n P_n^T$ matrices, the projection of F_n matrix into the space of principal axes can be obtained. The distance between one row of $F_n P_n^T$

matrix and $P_n f_{n+1}$ vector represents the distance between two points in this space. Let X_n be the following:

$$X_n = \begin{bmatrix} \boldsymbol{x_1} \\ \cdots \\ \boldsymbol{x_n} \end{bmatrix}$$

The distance between one row of this matrix and $\boldsymbol{x_{n+1}}$ is the distance between two points estimated in $\boldsymbol{x}$-space. Also, this matrix can be factorized as before to get P_x principal axes. As in the previous case, it is possible to project X_n matrix into the space of its principal axes by $X_n P_x^T$ product. By doing so, the distance between one row of this matrix and $P_x \boldsymbol{x_{n+1}}$ vector is the distance between the two points that are estimated in this space.

Based on the above definition, they exist seven common criteria used in designing experiments, with the aim of improving the model parameter estimation [39]. In the case of linear models, Fedorov (1972, [45]) showed that criterion 1 tends to re-propose the same experiments. Really, such a behaviour belongs to all criteria 1-7 [39]. Even though this cannot be demonstrated, it appears reasonable to introduce the additional experimental points on the frontier of the experimental domain, to improve parameter estimation [39]. These criteria usually select only one or few distinct points. So, the new selected points continuously overlap the other experiments, leading to a very poor experimental design. Beyond previous criteria 1-7, four new criteria were recently implemented in BzzMath library (BzzNonLinearRegression class). These criteria can be considered complementary to the previous one, with the aim of avoiding the overlapping of experiments, by an optimal use of the experimental domain. Inside "BzzNonLinearRegression" class, the user can select one of criteria 1-7; however, criteria 8-11 are ever taken into account. The definition of these criteria is here provided:

- Criterion 8: the new point has to maximize the Euclidean norm of the differences among the new point and the existing one. It doesn't depend on the specific model used, so the chosen points can be used for whatever model is proposed.
- Criterion 9: the new point has to maximize the minimum distance of f_{n+1} from the rows of the matrix F_n. This criterion is similar to the previous one, but it involves the matrix F_n. Indeed, it calculates the Euclidean norm of the differences between each new vector f_{n+1} and each row of the matrix F_n. Such as criterion 8, they fill the domain homogenously, but they do not take into account the problem of multicollinearity (new experimental point may be collinear with previous ones, i.e. closely correlated).
- Criterion 10: the new point has to maximize the minimum distance of $P_x \boldsymbol{x_{n+1}}$ from the row of the matrix $X_n P_x^T$. This is an improvement of criterion 8: instead of calculation the distances among points in the $\boldsymbol{x}$-space, it calculates the distance in the space of principal axes. In this specific space, the scale of each axis is related to the same axis importance. As a result, the distance of those points that are normal to the principal axis is greatly expanded. To get this, the program calculates

Euclidean norm of the difference between each new vector $P_x x_{n+1}$ and each row of the matrix $X_n P_x^T$. It requires the factorization of the matrix X_n in order to get P_x. The usage of this criterion is encouraged by the fact that it covers very well the experimental domain, independent of the model selected.

- Criterion 11: the new experimental point has to maximize the minimum distance of $P_n f_{n+1}$ from the row of the matrix $F_n P_n^T$. The approach of criterion 10 is now applied to f_{n+1} instead of x_{n+1}. It calculates the Euclidean norm of the differences between each new vector $P_n f_{n+1}$ and each row of the matrix $F_n P_n^T$: it requires the factorization of the matrix F_n in order to get P_n. Similar to criterion 10, it avoids the problem of multicollinearity, which affects criteria 8 and 9.

4.6.2. Practical Resolution: Results and Comments

The model-based design of experiments is performed through the function of the BzzMath library "LeastSquaresAnalysisAndExperimentsSearch", that belongs to the class "BzzNonLinearRegression". Therefore, this method is combined with the determination of the kinetic parameters by the minimization of the SSE (classical expression). Different from the in-house routine, explained in the previous sections, in this case the definition of the objective function is inside a black-box loop, without the possibility of modifying the function in the optimized way. The problem of the classical SSE is linked with the fact that it requires the variance of each dependent variable and, if not provided to the code, there is the implicit assumption of considering a constant variance for all the variables in all the experimental domain, that is a quite strong assumption. As consequence, the results will be for sure slightly different from the results of the code in Appendix 5a. The code is fully provided in Appendix 7 and here explained. After the definition of the global variables, in an identical way like codes in Appendix 5a and 5b; it is presented the main function. The class "BzzNonLinearRegression" needs as input: the number of compared models, only one in this case; the X matrix, that is the matrix of the initial conditions, in this work; the Y matrix, that is the matrix of the outlet experimental concentrations, in this work and finally the specific function for the calculation of the modeling Y matrix ("RegressionText"). Inside this function is provided the dedicated solver for the ODEs system, that require the differential system itself, provided in function "F2SistDiff" (identical to codes of Appendix 5a). It is worth to mention that, for a better solvability, both the parameters and the initial conditions are scaled in order to be near to the unity; respectively for a better regression and design of experiments solvability.

The kinetic parameters are evaluated with the least square analysis and they are reported in Table 4.11.

Parameter	Numerical Value
A_D	1.1624e+5
Ea_D	3.1299e+3
α	1.362
β	-1.152
r in [mol/m^3/h], P$_i$ in [kPa]	

Table 4. 11 - Optimal parameters for the power-law reaction rate equation from the least square analysis

The parameters are slightly different from those previously evaluated (optimized SSE), as expected. As consequence, the output results, i.e. the outlet conversion prediction, is slightly different (Table 4.12). In particular, from the comparison with the experimental value, it is possible to see that the Optimized SSE function provides better results. This aspect is in line with that expected.

Experimental Run	Optimized SSE function	Classical SSE function	Experimental
	SO$_2$ Conversion		
1	0.3442	0.3982	0.3246
2	0.2734	0.3384	0.2713
3	0.4601	0.4933	0.4579
4	0.2551	0.2843	0.3502
5	0.2485	0.2790	0.3418
6	0.2317	0.2655	0.2744
7	0.1827	0.1855	0.1712
8	0.1754	0.1802	0.1688
9	0.1669	0.1740	0.1645
10	0.6485	0.6513	0.6820
11	0.5174	0.5424	0.5096

Table 4. 12 - Outlet conversion comparison between different regression methods

Coming back to the least square analysis; first at all, the model is reasonable good. In fact, the mean square error is 7.2802 e-5. The condition number of the model is 3.4513e+2 and, so, the Jacobian matrix is well conditioned. However, the "BzzFile" output summary reports problems of parameter definition and multicollinearity among parameters (variance inflation factor, tolerance index). It is so reasonable to reformulate the kinetic constant in the following form [39]:

$$k(T) = A * \exp\left(-Ea \frac{\frac{1}{T} - \frac{1}{T_{average}}}{\frac{1}{T_{min}} - \frac{1}{T_{max}}}\right)$$

Solving the same problem with this modification, the orders of reaction are equal, while the pre-exponential factor and the activation energy assume different values (Table 4.13). These values provide the same results in term of outlet conversion.

Parameter	Numerical Value
A_D	1.1624e+5
Ea_D	3.1299e+3
r in [mol/m^3/h], P$_i$ in [kPa]	

Table 4. 13 - Parameters of the reformulated kinetic constant

However, although the problem of parameter definition is fixed, the warning message of multicollinearity in the "BzzFile" persists. Since the model is adequate, correctly formulated and it fits the data and the problem is well conditioned; it is reasonable to correlate the multicollinearity cause to an inadequate design of experiment. The experimentations, in fact, are now very poor and similar one to each other, with low variability in term of concentration and flowrate. To understand the reason why this situation can cause problems of multicollinearity, let's think about a model with three parameters and experiments concentrated in only two points. It is obvious that the three parameters of the model cannot be correctly estimated.

It is worth to consider also the problem with optimized SSE function and with the reformulated kinetic constant. The results are analogous to the ones of the least square analysis; so, different pre-exponential factor and activation energy and same orders of reaction. Also in this case, the outlet conversions are identical like in the case of non-reformulated kinetic constant.

It is not yet explained the cause of the different of the reaction order between the classical and the optimized method. It is possible to say that the influence of the reaction orders on the final value of the rate is minor, in fact the feed stream presents a high dilution. Moreover, due to not an optimal design of experiment, these parameters may be not so well defined. As said, in some points, the difference with the experimental value is substantial and, so, it is possible to consider these model parameters as a rough estimation, that could be improved with further runs, as said many times.

After the resolution of the regression problem, the code passes to the resolution of the design of experiments. In this specific code, only one model is considered and so the procedure only concerns the identification of a new optimal experimental point, for the kinetic parameters improvements. The "LeastSquaresAnalysisAndExperimentsSearch" requires two inputs: vectors containing the minimum and maximum value of the interval search for the independent variables. In this case, the program automatically selects a grid to search for the most appropriate point. The user has the possibility to select one of the criteria 1-7 by the function "SelectCriterion", in the code of Appendix 8, for instance, criterion 1 is selected. Independent of this choice, even optimal experiments obtained by criteria 8-11 are provided; these criteria are the most popular and, for this reason, only

these ones are considered in this work. Two possibilities are practicable with the selection of the boundaries:

- Selection of the real experimental boundaries that comes from the complete preliminary design of experiments (Table 4.14). From the original range, defined in the final part of Chapter 3, there is only one deviation in the minimum temperature. In fact, the setpoint minimum temperature was set to 350 °C; however, due to temperature oscillation, some data below the setpoint were analysed.
- Selection of the boundaries of the experimented domain (Table 4.15). This domain is a subset of the previous one, remembering that the current performed experiments are incomplete.

	Minimum	Maximum
SO_2 [kg/h]	0.023	0.256
O_2 [kg/h]	0.019	0.210
N_2 [kg/h]	0.874	3.596
Temperature [°C]	314.85	450

Table 4. 14 - Real input domain

	Minimum	Maximum
SO_2 [kg/h]	0.083	0.254
O_2 [kg/h]	0.042	0.210
N_2 [kg/h]	3.234	3.575
Temperature [°C]	314.85	377.3

Table 4. 15 - Experimented input domain

The results are summarized in Table 4.16 and Table 4.17 respectively.

Criterion	SO_2 [kg/h]	O_2 [kg/h]	N_2 [kg/h]	T [°C]
8	0.256	0.019	0.874	450
9	0.256	0.210	3.596	450
10	0.023	0.210	0.874	450
11	0.256	0.210	3.596	450

Table 4. 16 - Suggested experimental point for the different criteria (real input domain)

Criterion	SO_2 [kg/h]	O_2 [kg/h]	N_2 [kg/h]	T [°C]
8	0.254	0.042	3.234	377.3
9	0.254	0.210	3.575	377.3
10	0.083	0.210	3.575	314.85
11	0.254	0.210	3.575	377.3

Table 4. 17 - Suggested experimental point for the different criteria (experimented input domain)

From Table 4.16, it is clear and evident where the different criteria propose the new experimental point, inside the domain. In particular, from the comparison of Table 4.14 with Table 4.16, it is evident that the new experimental point, for each criterion, is a

combination of points at the boundaries. This is reasonable since there is the need of knowing first the values of the corresponding dependent variables at the boundary, for a better parameter estimation. The results are practically claiming the necessity of expanding the experimental domain, until a reasonable value of interest.

Less evident are the results of Table 4.17. In fact, as the previous case, the different criteria still propose points on the boundary. Differently from the previous case, there is already the presence of some experimental points on the experimented domain; but the criteria insist on proposing non-internal points. From a careful analysis, in fact, the points that satisfy the criteria, with the filling at the best of the domain, are those on the boundary itself. For sure, this statement is valid until all the point combinations at the boundary are completed. For the reader that wants to verify this statement, it is possible to run a very simple example. Let's consider the same code structure of Appendix 8, but considering a very simple linear model. Artificially generating the experimental point, it is possible to get a set of X and Y variables. It is then possible to perform the design of experiments in a certain X range; all the criteria 8-11 propose a point in the middle only if the minimum and the maximum point of the range are already experimented. Generalizing this concept, it has been demonstrated and explained the design of experiments results.

Finally, referring to IOSTO process, once the additional experiment is selected; it is possible to insert these data inside the PLC setpoint. By analysing the outlet composition, an additional row of the dependent variable matrix is obtained. The final part is to update the code for the parameter estimation with the additional experimental point. With this procedure, the reliability of the estimation should be greater. In fact, the point was properly selected in a region of the multidimensional domain where the model reliability was weak.

Chapter 5
Absorption Section and Data Analysis

This chapter deals with the in deep analysis of the absorption section of the IOSTO process. The layout description is already provided in Chapter 2; while, in Chapter 3, the preliminary work on the absorption column is shown. In that chapter, it has been highlighted the necessity of a dynamic model for the comprehension of the column behaviour. Consequently, in this chapter it is provided all the dissertation regarding the dynamic modeling, using commercial software. As first choice, it was selected SimSci DYNSIM® of Schneider Electric as simulation tool; this software is a comprehensive, dynamic process simulator. Despite this, at the end, it was selected the dynamic tool of Aspen HYSYS®. The explanation of this choice and the comparison between them is provided in following sections. Moreover, the results of the dynamic simulation and relative comments will be provided. The final goal, in this case, is to predict the time needed to produce market grade sulphuric acid, that is the economical valuable product of IOSTO process.

The second part of this chapter deals with the experimental analysis of the absorption section. It is explained, in a qualitative way, some experimental evidences. In fact, it is worth to reaffirm that another important goal of this work is the data analysis, with the objective of highlight operational problems, providing troubleshooting and ways to optimize the execution of the plant.

5.1. Simulation Analysis

Regardless the used simulation tools, there are common hypotheses, that are applied to the simulation. As mentioned in Chapter 3, the reaction can be considered instantaneous [38], the absorption of SO_3 is complete (tested with pure H_2O and pure H_2SO_4 liquid recycle). So, as consequence, the modeling of the reactive column can be done, as first approximation, with a simple tank, in which the liquid and gaseous stream get in contact and SO_3 is converted in H_2SO_4 with a unitary conversion. In the following subsection, they are explained all the passages for the establishment of the dynamic simulation in SimSci DYNSIM® and Aspen HYSYS®.

5.1.1. SimSci DYNSIM® Simulation

The very first thing to say about this process simulator is that it tries to simulate the dynamic behaviour of the process with a high level of similarity respect to the reality. It means that is not possible to set an arbitrary initial condition, but there is the need to define a start-up procedure. However, it is not necessary to start every time from the start-up of the plant, but it is possible to set an initial condition, that is a sort of snapshot of a certain instant of previous simulations.

The first thing to do, like in Aspen HYSYS®, is to set a proper set of unit of measures and to set a proper equation of state (EOS). As done in Chapter 3, it is selected the ideal gas EOS for the gas phase, while the NRTL model for the liquid phase. The Electrolyte-NRTL model is more appropriate, but it is not present in this software. After this point, the input variables are defined. Please refer to Figure 5.1 in order to follow this explanation. Each input is, due to the nature of the software, an accumulation (or a source

in the software language), at a certain temperature and pressure. SRC1 is the dummy tank for the batch of water; while SRC2 simulates the gases coming from the catalytic section. INIT stands for initialization, since all the equipment are initialized with nitrogen, i.e. fully of N_2. This procedure helps to avoid numerical problems starting the resolution. Water can enter inside the tank passing through the manual valve XV5. All the valves are sized using the sizing tool of the software, apart from XV5. In fact, an input, needed for the sizing, is the reference mass flow, that is impossible to define for XV5 since it is opened only during the start-up. This valve is sized with a trial and error procedure that allows a suitable dynamic. It is worth to say that each equipment is a pressure node and, so, it needs a pressure drop to work. Since the pressure of the process is 120 kPa, each source is set to 170 kPa. While, the temperature of each source was set to 40 °C, i.e. the mean project temperature of the column. The definition of a mean temperature is reasonable since, although the reaction is strongly exothermic, the liquid flows at a high flowrate (0.54 m³/h), in comparison with the gas stream. So, it is maintained inside the column that temperature, thanks to the heat exchanger than continuously cool the recycled liquid. There is an important difference with the reality for the gas stream. In fact, the gas flowrate that enters inside the tank is preceded by a valve (XV2) with a feedback control loop of the flowrate itself (PID2). This control loop is fictitious and it simulates the presence of an upstream equipment (i.e. the reactor) that provide a constant gas flowrate. The constancy of the flowrate is assured by the mass flowmeter at the beginning of the process. All the PID parameters are set to a value that ensure a suitable dynamic, with a trial and error procedure. Indeed, it hasn't been put much effort in the estimation of the PID parameters and in the sizing of the valve since, in this work, the dynamic simulation is not used to analyse fluctuations caused by whatever disturbance, but to determine the concentration in time of the liquid recycled stream. The process, in fact, is not subjected to fluctuations and the valves, after the initial intrinsic dynamic, set to a certain constant opening value. There is an intrinsic dynamic, for each valve, to go to the setpoint value. This value was set to 10 seconds for XV2 and XV3, zero seconds for XV5, since there is the need to be fast and avoid putting more liquid than needed inside the batch.

The modeling of the absorption column, as said above, is schematized with a simple tank model. It is possible to set the dimension of the tank, in this case it was selected a height of 0.5 m and a diameter of 0.3. It is not so important the dimension and the geometry with respect to the real tank, since it is considered a mean average temperature of 40 °C (no consideration about the heat transfer with the ambient). The only requirement is that the tank must be sufficiently large to contain the correspondent market grade sulphuric acid, starting from 10 kg of pure water. Moreover, it is possible to set the reaction set (i.e. absorption of SO_3 in water) and the relative reaction type (100% conversion in this case). Each feed stream is positioned at a certain height; in particular, the inlet port of the gas is set at the bottom part, in order to allow the flow inside the liquid hold-up.

It is possible to note, in Figure 5.1, that also, at the gas outlet, there is a fictitious control loop. In fact, connecting directly this stream to the sink (i.e. the atmosphere in this case) the software provides an error message. So, the control loop permits to guarantee a

constant pressure inside the tank (120 kPa). There is the need of a certain pressure drop across the valve and, so, the sink is set at 70 kPa. The blower is not modeled since, from experimental evidence, the gases have enough pressure to be discharged from the chimney. This means that the pressure drops are negligible inside the plant. The blower is turned on, in the experimental plant, only for safety and not process reasons.

On the other side, also for the outlet liquid stream, there is a certain idealization from the reality. In fact, it is not present the heat exchanger that cools down the liquid but there is a simple piece of pipe. This fictitious pipe simulates the cooling effect of the heat exchanger and the pressure drop along the liquid circuit. The reason why a heat exchanger is not simulated is the increasing complexity, in case of the presence of the heat exchanger. In fact, this equipment would require an auxiliary fluid, a proper sizing and its temperature control loop. The other reason is that the models of a heat exchanger, compatible with the software, are the industrial one; while, in this case, the plant is a micro-pilot scale plant. The pump is set to a volumetric flowrate of 0.54 m^3/h as the real one, like the real setpoint. In the reality, the pump is activated from the PLC; instead, in this case, it is activated by an ON/OFF switch of the electric motor.
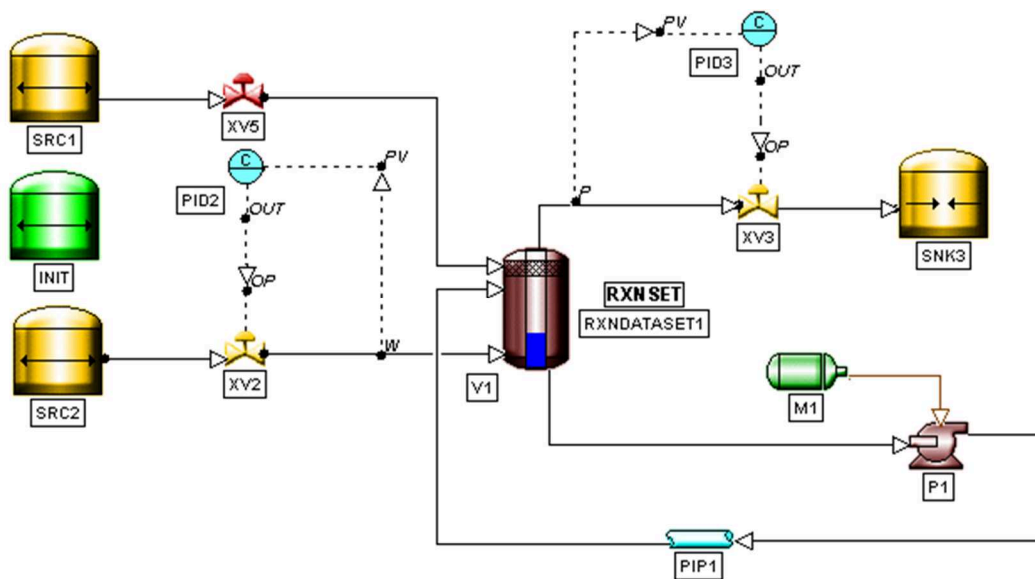
Figure 5. 1 - SimSci DYNSIM® Flowsheet

Figure 5.1 refers to a snapshot of the flowsheet linked with the situation after the start-up of the process. In fact, valve XV5 is closed (red, complete closing), XV2 and XV3 are opened around the setpoint position (yellow, intermediate opening), the motor is turned on (green).

5.1.1.1. Start-up Procedure

The simulated start-up procedure differs from the real one. In fact, at this level of work the goal is the simulation of the time needed for the sulphuric acid production and not the study of the start-up of the process. In principle, it would be possible to simulate the real start-up procedure, but it creates some issues. The gas feed stream reaches its setpoint

value, with the selected sizing and PID parameters, in a relative long time. It could be possible to decrease the time, but with consequently undesired oscillations. Since there is no interest in this phase, the first step of the start-up is to bring the gas flowrate at its set point and to maintain the pressure of 120 kPa. After the reaching of this setpoint, it is possible to feed the liquid batch (10 kg). In order to stop the feed at this level, it is possible to use the "scenario" function. This tool allows to perform automatically different actions with a series of commands written in a text file. Each line of the code is here explained:

- "SET XV5.OP = 1.0;". This command allows to completely open valve XV5.
- "RUN;". Activation of the dynamic simulation.
- "WAIT UNTIL V1.L > 0.141471061;". With this command, the "scenario" function, before performing the following command, waits the satisfaction of the written condition. In particular, the condition is the filling of the tank with 10 kg of pure water, that corresponds to the above tank level value, considering the aforementioned tank dimensions.
- "SET XV5.OP = 0.0;". Once the condition is satisfied, the simulator must immediately close the valve.
- "FREEZE;". After the closing of the valve, with this command, the simulation environment is frozen in the current condition.

Before re-activating the simulation, the motor must be switched on. At this condition, it is interesting to set an initial condition point. Doing so, the time is set again to zero and this allows to determine the real-time evolution of the sulphuric acid production, regardless of the start-up procedure. The results of the SimSci DYNSIM® simulation are reported in the following section 5.1.3.

5.1.2. Dynamic Aspen HYSYS® Simulation

There are similarities and differences between the two different simulators. The big difference is that Aspen HYSYS® analyse the dynamics, starting from a stationary condition. This aspect could seem controversial for IOSTO process, since it is a semi-batch process and it never reaches the steady state condition. However, the discontinuous nature lies in the liquid recycle. From Figure 5.2, it is possible to see the mathematical "recycle" operator, that allows the stationary convergence in presence of a recycle. Setting one iteration as convergence criteria, the simulation works in steady state, of course without reaching the stationary condition. The convergence of the stationary flowsheet is a mandatory step in the dynamic resolution and, doing so, it is possible to use Aspen HYSYS® for a simulation of a semi-batch process (in which the discontinuous nature lies in a recycle). It is worth to mention that the "recycle" operator has no function when the flowsheet is turned in dynamic mode. The similarity, as all the dynamic simulators, is that, every unit, being a pressure node, needs a pressure drop across the unit itself to work. The inputs are material streams; but conceptually, it is the same as the definition of a source in SimSci DYNSIM®. Actually, in stream 3.1 only the pressure is selected, since the flowrate is determined by the control loop with FIC-100 controller. The logic behind this controller is the same as the other software, as well as the definition of the PID

parameters and the sizing of the corresponding valve VLV-100. Identically considerations for the pressure control loop with the controller PIC-100 and its relative valve VLV-101. Likewise, stream 2.6 is conceptually the SimSci DYNSIM® sink. In this case there is not the need to perform a start-up procedure, since it is possible to set in the tank model the initial condition: liquid level, linked with a certain tank dimension. As well as in SimSci DYNSIM®, the conversion reaction set is applied to the tank model, that is a sort of semi-batch reactor, in this simulation structure. Another important difference is in the liquid recycle; in this simulation is not so complicate compared to SimSci DYNSIM®. In fact, it is possible to saturate the d.o.f. of the heat exchanger by imposing the value of the outlet temperature, equal to 40 °C. The simulator, then, calculates the duty, starting from this information and from the inlet temperature, that is determined by the energy balance of the tank. So, the heat exchanger substitutes, both in term of temperature and pressure drop, the fake piece of pipe. Moreover, another little difference is that is not present the motor that actuate the pump. In Aspen HYSYS® there is the possibility of defining a general energy stream, that is evaluated imposing, as d.o.f., the volumetric flowrate across the pump.

Once the steady state simulation is established and the flowsheet converges; it is possible to shift to the dynamic mode, with the specific tab. Aspen HYSYS® offers the "Dynamics Assistant" functionality, that helps in fixing problems. Once the simulation is in dynamic mode, it is possible to run the simulation observing the evolution in time. All the variables can be registered and exported in a Microsoft Excel® spreadsheet. The integrator tool is explained in section 5.1.3.1. Please note that, as mentioned above, the ideal gas law is selected for the gas phase, while the Electrolyte model is used for the liquid phase. In particular, the dissociation reactions, shown in Chapter 3, are neglected. It is possible to numerically determine that this simplification brings to the identically same results, in a much shorter computation time.
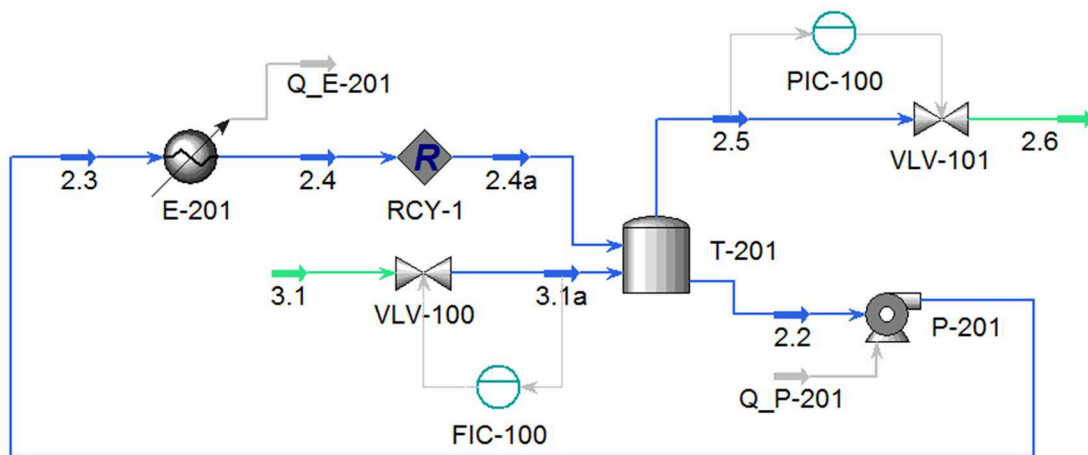
Figure 5. 2 - Dynamic Aspen HYSYS® flowsheet

5.1.3. Final Results

5.1.3.1. SimSci DYNSIM® and Aspen HYSYS® Comparison

As mentioned above, before continuing the dissertation, it is important to properly define the integrator tool. Inside this tab, it is possible to select different parameters: the integration step and the calculation execution rate, i.e. the rate of evaluation of the mass and energy balances per integrator time step. Performing a simulation with the default values and another one with more precise values, it is clear than the computational time increases a lot. This aspect is crucial inside this process: the reactant gas stream is extremely diluted and the mass of water to transform in sulphuric acid is substantial, if compared to the gas stream. As results, the process time is of the order of hundreds of hours. As consequence, also the computational time is big. It is interesting to compare the computational time in case of the SimSci DYNSIM® simulation and in case of Aspen HYSYS® simulation (default and detailed integration). The results are shown in Table 5.1; it indicates the process time, simulated in one real minute of computation. Regarding SimSci DYNSIM® the time refers to the maximum allowable acceleration, while in Aspen HYSYS® the "real time factor" depends on the solver capability of resolution of the model.

	Simulated Process Time [min]
SimSci DYNSIM®	29.23
Aspen HYSYS® - Default Integration	387.97
Aspen HYSYS® - Detailed Integration	41.97

Table 5. 1 - Computational time comparison among the different resolution methods (one real minute)

It is evident that the default setting of Aspen HYSYS® solves the system in a faster way with respect to the two other methods. The detailed integration of Aspen HYSYS® is better than SimSci DYNSIM® but, in both the cases, one order of magnitude slower than the default method of Aspen HYSYS®.

From this evidence, it is interesting to compare the relative prediction in term of the desired output, i.e. the mass fraction of H_2SO_4 in time. These aspects are analysed considering an inlet flowrate to the catalytic reactor equals to run 1 of the preliminary design of experiments. Moreover, it has been considered a unitary conversion inside the reactor. These hypotheses are arbitrarily since, at this level, is not important the absolute value of the variable, but the comparison between the different methods. The results are shown in Figure 5.3.
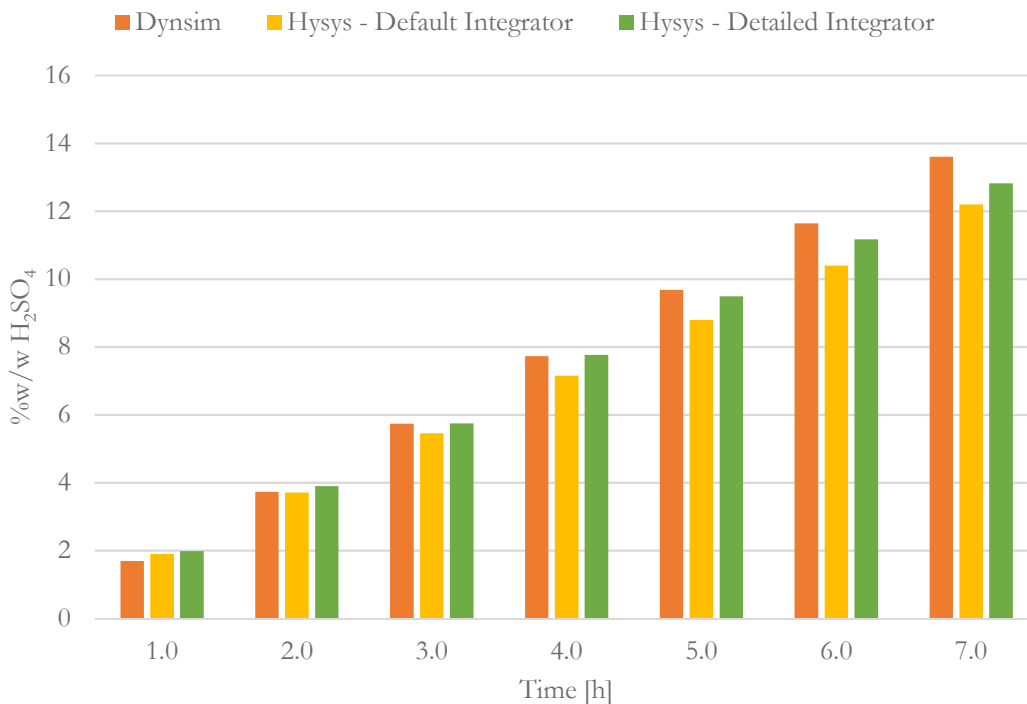
Figure 5. 3 - Comparison of the prediction among the different resolution methods

First at all, it has been simulated, for the comparison, only the first seven hours of the process. The reason is simply linked with the high calculation time consumption. The first evidence is that the differences among the different bars of the histogram increases with time. The explanation is very simple and it is based on the following consideration: a difference in the bar at a certain instant is linked with a different sulphuric acid production. This variance can only grow with time, due to the liquid recycle and the different profiles tends to diverge.

It must be explained the difference among the results. For sure the difference between the default and detailed integrator of Aspen HYSYS® is basically linked with the numerical approximation that, in this case, contributes to reduce the H_2SO_4 production. It means that the truncation of the integration is made in defect. Moreover, there is a difference between the two different software resolution. In particular, the difference could be attributed to: different numerical algorithms for the model's resolution, different model equations, different equation of state (NRTL vs. Electrolyte-NRTL) and also for the different set up of the simulation itself, i.e. different flowsheet.

Finally, it is essential to discuss if it is or not licit use of the default configuration of Aspen HYSYS®. As observable in Figure 5.3, the mass fraction of sulphuric acid is underestimated, or, from the opposite perspective, the time is overestimated. It means that the results, that comes from this method, are the upper limit in term of time prediction. That is reasonable for this level of study of IOSTO process, where a lot of assumption are considered. Moreover, the overestimation allows to analyse the worst case

for the feasibility study of IOSTO process. On the other side, the usage of the other models, from an industrial view point, is not the best solution. In fact, the output results are obtained only after tens of hours of simulation. It could be more feasible to develop a specific model of this absorption section and perform the calculation with advanced numerical tools.

In the following section, it is provided an extensive analysis and explanation of the simulation results.

5.1.3.2. Aspen HYSYS® Results and Profiles

This section deals with the simulation results using the default integrator of Aspen HYSYS®. The studied composition is the project one (simulated gas - Table 5.2).

Simulated Gas	
Total Flow Rate	3.7 kg/h
Composition [%vol/vol]	
N_2	91.63 %
SO_2	3.16 %
H_2O	0 %
O_2	5.21 %

Table 5. 2 - Simulated inlet gas composition

The dilution is made by N_2, as clear from Table 5.2. The results in case of CO_2 dilution, i.e. the real process condition, are similar. The N_2 dilution is studied since the experiments done, at this level of study of this work, are only with streams rich of nitrogen. The difference lies in the different solubility of CO_2 with respect to N_2. In particular, CO_2 is more soluble than N_2 in water. It means that, although the sulphuric acid production is the same, its mass fraction is lower in case of CO_2 due to its greater solubility. But, at the end, the composition will be the same, since the solubility of both CO_2 and N_2 is approximately zero in pure sulphuric acid. Sulphuric acid dissolves only SO_3, forming oleum. These considerations are simply done by a solubility study using Aspen HYSYS®.

It is possible to set an important degree of freedom for the input of the dynamic simulation, i.e. the SO_2 conversion inside the catalytic reactor. It is clear, from Chapter 3 and Chapter 4, that the conversion profile is oscillating in time. As said many times, there is not the interest to model the fluctuation, since it is totally undesired. As consequence, it is possible to select a proper level of conversion for the modeling of the absorption section. It is reasonable to start with a comparison of the sulphuric mass fraction of the liquid hold-up with different level of conversions (Figure 5.4). Each curve represents a different case study; once the target is reached, the dynamic simulation is stopped.

This plot is very interesting since it allows to understand the variance on the process output performance (i.e. sulphuric acid production) with a variation of the reactor performances. In fact, the difference of time needed for reaching the target, for the different cases, is considerable. The batch cycle is not a linear function of the SO_2 conversion, as clear from Figure 5.5. It is a sort of exponential trend: at lower conversion

range, the final time increases much more than at higher conversion range. Moreover, the different batch cycle time, varies of tens of hours for each % point of conversion. So, the process needs, for its feasibility, high performances in the catalytic reactor.

From Figure 5.4, another important aspect is the trend of each case study. The production of sulphuric acid in time is not linear, but with a decreasing derivative. It is simply explained from the analysis of the amount of water in the outlet gases (Figure 5.6). The simulator predicts a decreasing H_2O evaporation term with an increase of acid solution concentration. It means that the H_2SO_4 concentration is controlled by two different terms: the absorption reaction between H_2O and SO_3 and the evaporation of water. Once this last term decreases, the velocity of sulphuric acid formation is lower. On the other side the reaction term is assumed constant, due to the hypothesis of complete absorption.
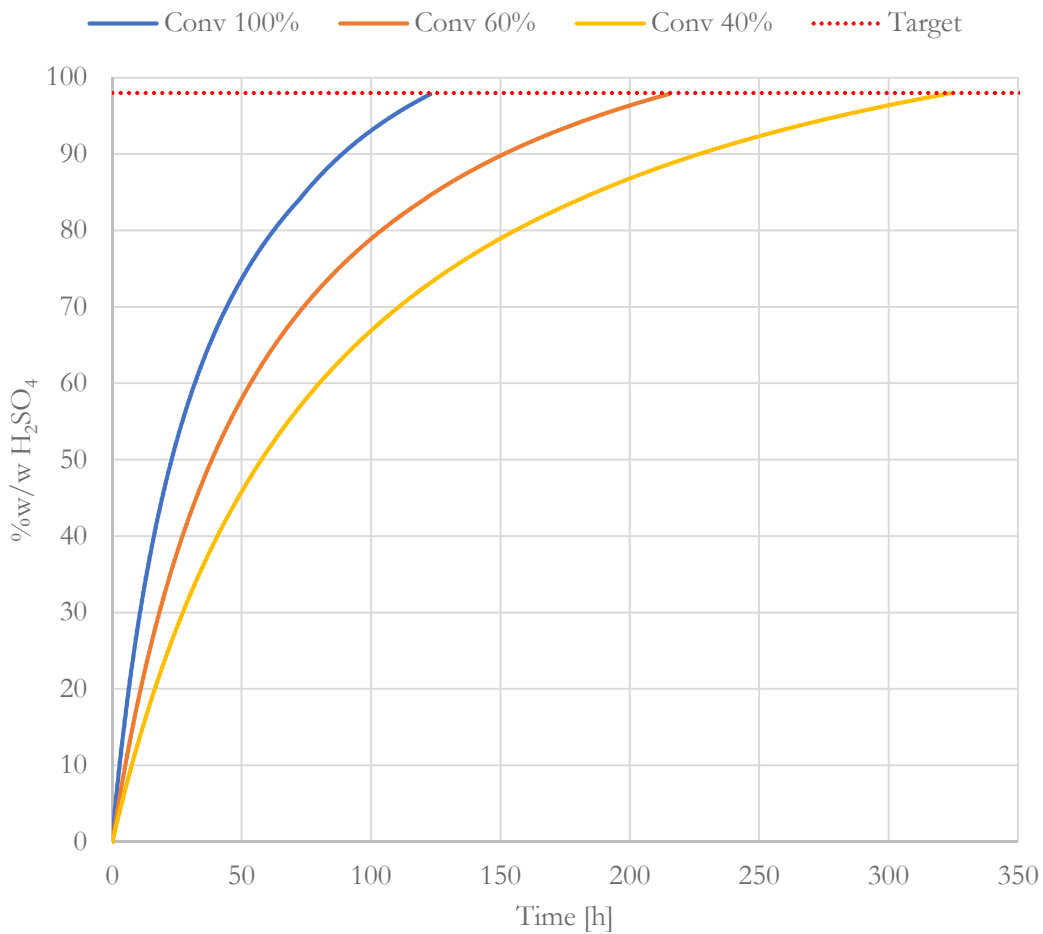
Figure 5. 4 - Sulphuric acid mass fraction profile in time, at different SO_2 conversions
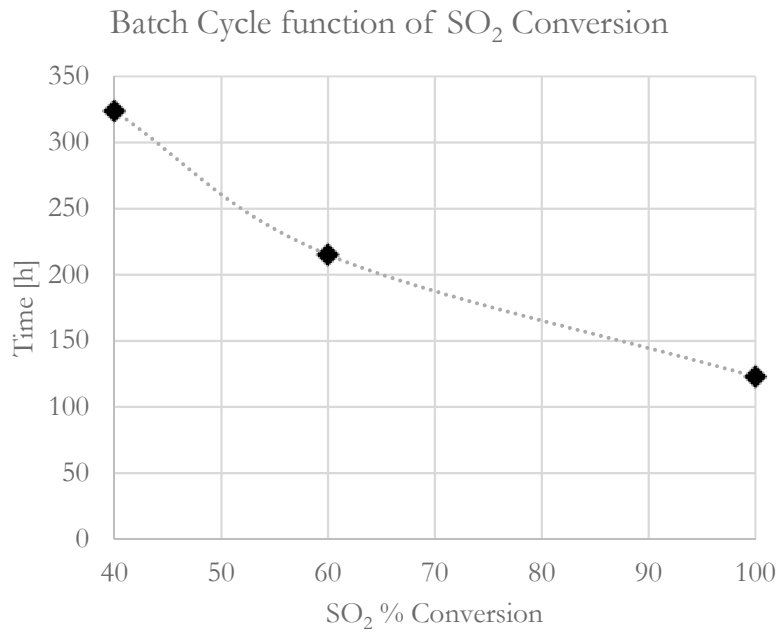
Figure 5. 5 - Batch Cycle function of SO_2 Conversion
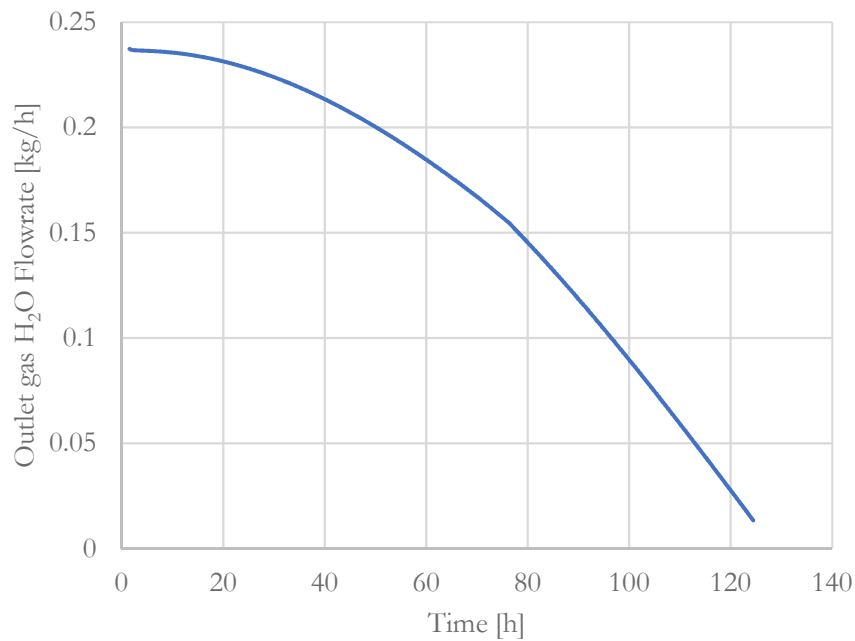
Figure 5. 6 - Outlet gas H_2O flowrate profile in time, 100% SO_2 conversion case

It is worth to analyse also the flowrate of the other components of the outlet gas stream. Please note that Figure 5.6, 5.7, 5.8, 5.9 refers to the same input condition of unitary SO_2 conversion. Figure 5.7 refers to the O_2 flowrate; the value is pretty constant in time compared to water, since the oxygen solubility is almost constant (low solubility) at different acid concentrations.
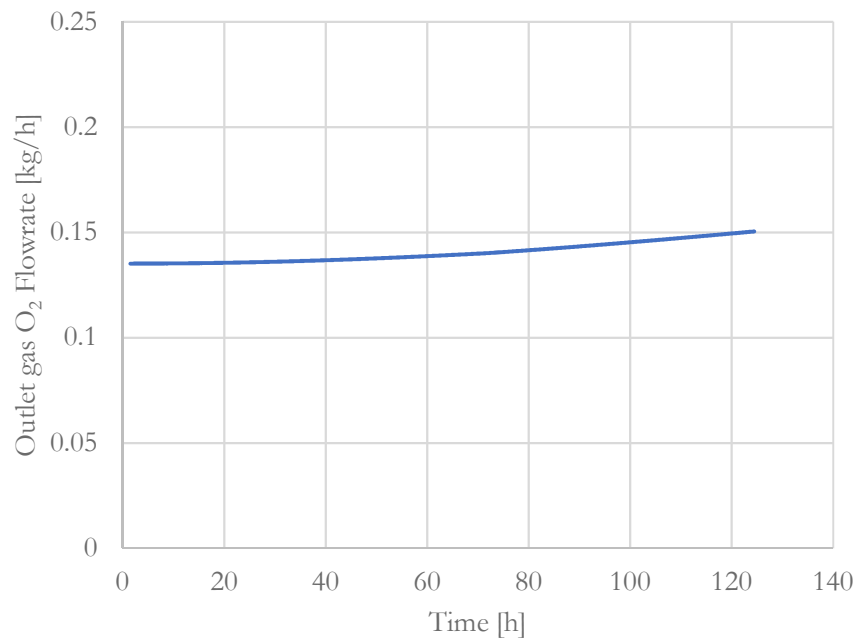
Figure 5. 7 - Outlet gas O_2 flowrate profile in time, 100% SO_2 conversion case

More interesting are the plots of the N_2 flowrate (Figure 5.8) and total flowrate (Figure 5.9). In fact, the amount of nitrogen in the offgas increases with time. The reason is simply link with said above: the solubility of N_2 in the liquid phase decreases with the increase of the H_2SO_4 fraction. However, the overall flowrate is almost constant due to the balance of the different terms.
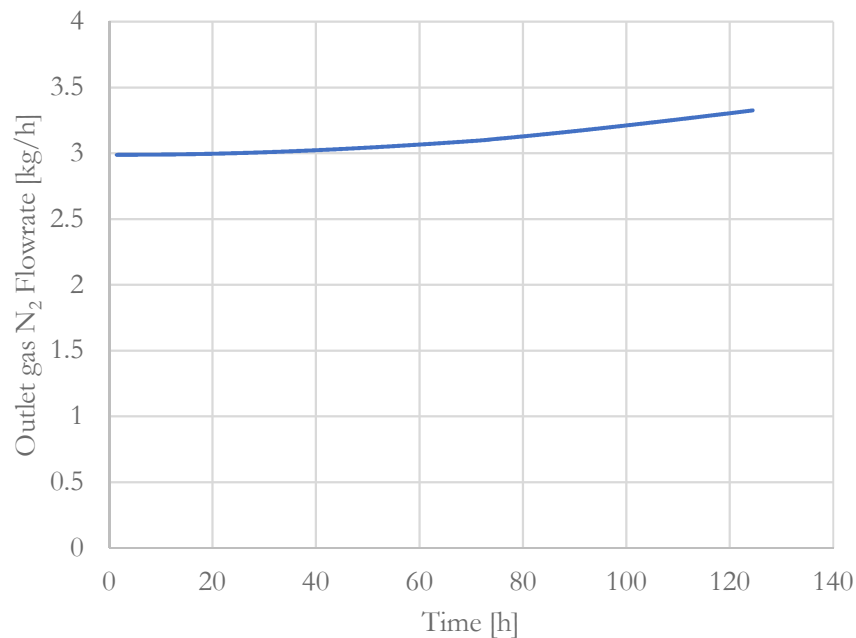
Figure 5. 8 - Outlet gas N_2 flowrate profile in time, 100% SO_2 conversion case
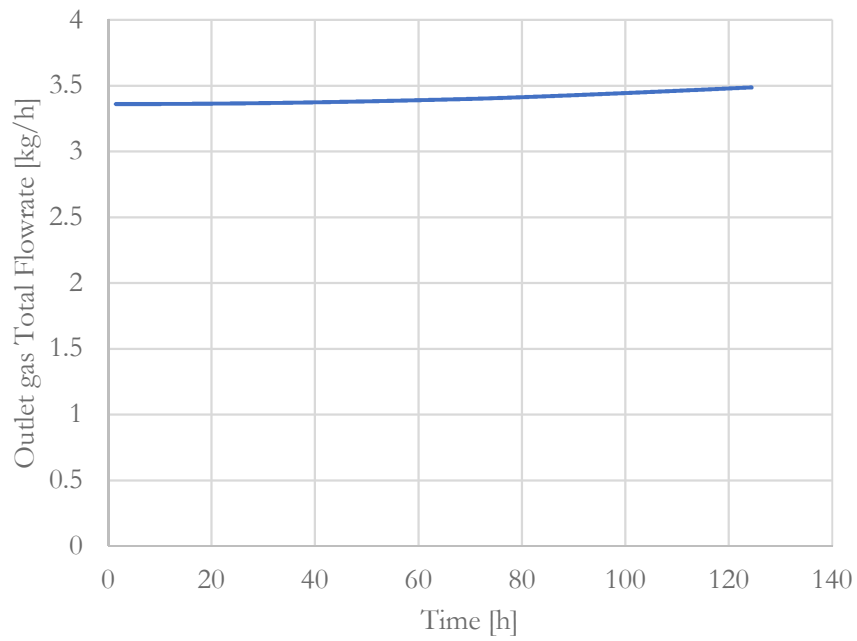
Figure 5. 9 - Outlet gas total flowrate profile in time, 100% SO_2 conversion case

Another variable that is possible to monitor, in order to see the evolution of the batch cycle, is the liquid hold up inside the tank (Figure 5.10). The initial value of this variable is 10 kg of pure water, as imposed by the project specification and it increases up to about 50 kg of H_2SO_4 market grade (98% w/w).
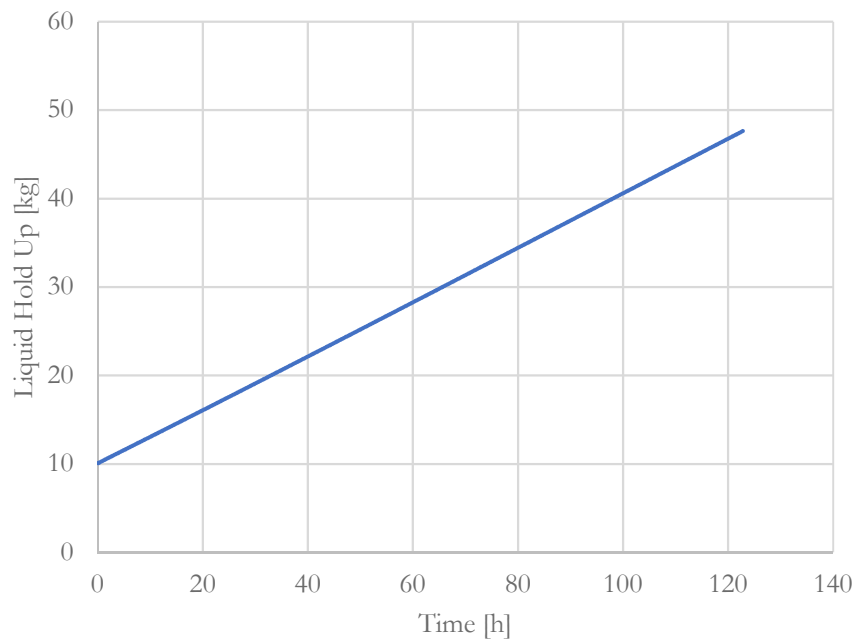
Figure 5. 10 - Liquid hold up profile in time

The last profiles to analyse are the controlled variables, i.e. the gas feed flowrate and the pressure of the tank. The reason to monitor these variable is basically linked to the observation of the stability of the process. It is worth to reaffirm that the simulator starts from a stationary condition and, to avoid a not reasonable initial dynamic, the valves are already opened at a value that guarantee the setpoint. As consequence, the sulphuric acid starts to produce from time zero at the nominal rate. As expected, both the profiles are constant in time (Figure 5.11, Figure 5.12).
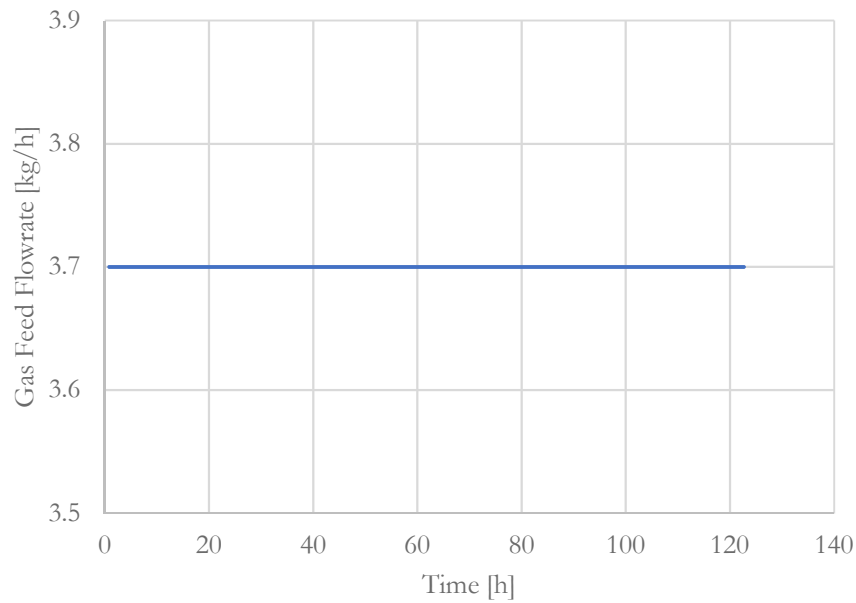
Figure 5. 11 - Gas feed flowrate profile in time
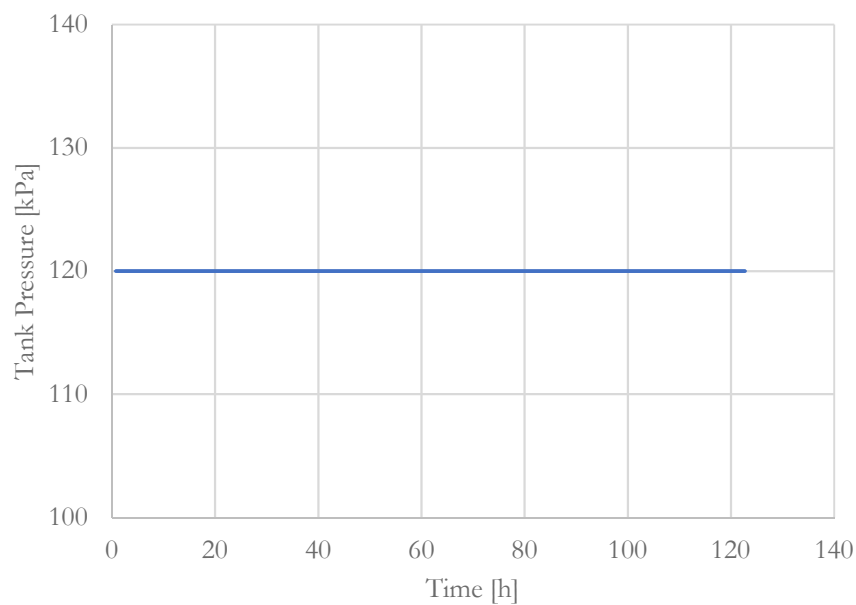
Figure 5. 12 - Tank pressure profile in time

5.2 Experimental Analysis

The experimental analysis starts from the same consideration of what said in Chapter 3. As said, it is not possible to operate, in a separate way, the reactor and the absorption sections. So, they are performed also the measurement of the absorption section. This section is monitored through measure of the density of the liquid that exit from the bottom of the column, measure of temperature of the inlet gas and measure of the recirculated liquid, before and after the intermediate heat exchanger E-201.

In principle, the final output could be the validation of the Aspen HYSYS® simulation with the experimental data. However, the experimental complexity makes until now impossible to perform this comparison. In fact, there are many aspects that makes the real behaviour different from the analysed simulations. All these peculiarities are studied in this section. So, it is possible to say that, as output of the simulation, there is only the verification of the project specifications. It is not present, in Sotacarbo S.p.A. documentations, the specific value of the project time needed for the production of sulphuric acid. The reason is linked with the fact that it was designed a column made with another material, that would have operated at different operative conditions. Despite this, the order of magnitude of hundreds of hours is respected. Moreover, it is possible to say that the experimentations were perform with the objective of the study of the reactor. In fact, the specific tests for the absorption column are expected at the end of the runs of the preliminary design of experiments. It has been stated that the column could be analysed, in order to reduce the hours of experimentation, with batches of sulphuric acid at different concentrations, already purchased from Sotacarbo.

The first and most important variable to analyse is the density profile in time (Figure 5.13), that gives information on the H_2SO_4 mass fraction inside the solution. This plot is taken from the PLC of the day 1 of this year experiments, where run 1 and run 2 of the preliminary design of experiments were performed. Different information can be obtained from this graph. Before starting any kind of explanation, it is worth to say that the different colours represent the different phase of the process. The start-up of the plant is made by two phases: in the first one ("Heating") the liquid pump and the electrical resistances of the reactor section are turned on. For the absorption section the only interesting part is the turning on of the pump. The second phase involves the starting of the nitrogen feed to the system ("Nitrogen"), till the reaching of the nominal reaction temperature. At that moment, the reactant gases are fed to the reactor; in this case two experiments were performed ("Run 1", "Run 2"). The last part ("Shutdown") concern the period in which the electric resistances are turned off and the inerting with nitrogen can start. It is evident the increasing of the density during the reaction phases, due to the absorption of SO_3 in water to get H_2SO_4 (H_2SO_4 is denser than H_2O). It is less evident, however, the increase of density in the other phases. For the heating phase, this increment could be attributed to an evaporative term of H_2O, since the liquid is recirculated at very high rate (0.54 m^3/h). An additional contribution is present during the other two phases: N_2 can strip part of water from the liquid phase. It is reaffirmed the importance of

knowing the composition of the off gases, in order to take into correctly account the passage of water at the top of the column.

Another important phenomenon that occurs, correlated with the presence of water at the exit of the top of the column, is the drag effect of the blower. This equipment is oversized and normally not used for process reasons. But, when it is turned on for safety reasons, it contributes to massively suck the gases, reducing the residence time and to drag liquid water. This aspect is another explanation of the experimental complexity that has to be faced.

The last important aspect that must be noted is the green dot. The "Day 2" tag means that this data is the first density registration of the following day of experimentations. Sotacarbo S.p.A., from one to another day, doesn't change the liquid batch. For this reason, it is reasonable to say the density should be at the same level of the last data of the day before. Since Sotacarbo S.p.A. was interested to understand the explanation of this phenomenon, this work has been extended also for getting an explanation of this evidence. All the dissertation about this aspect is discussed in the dedicated following subsection (5.2.1).
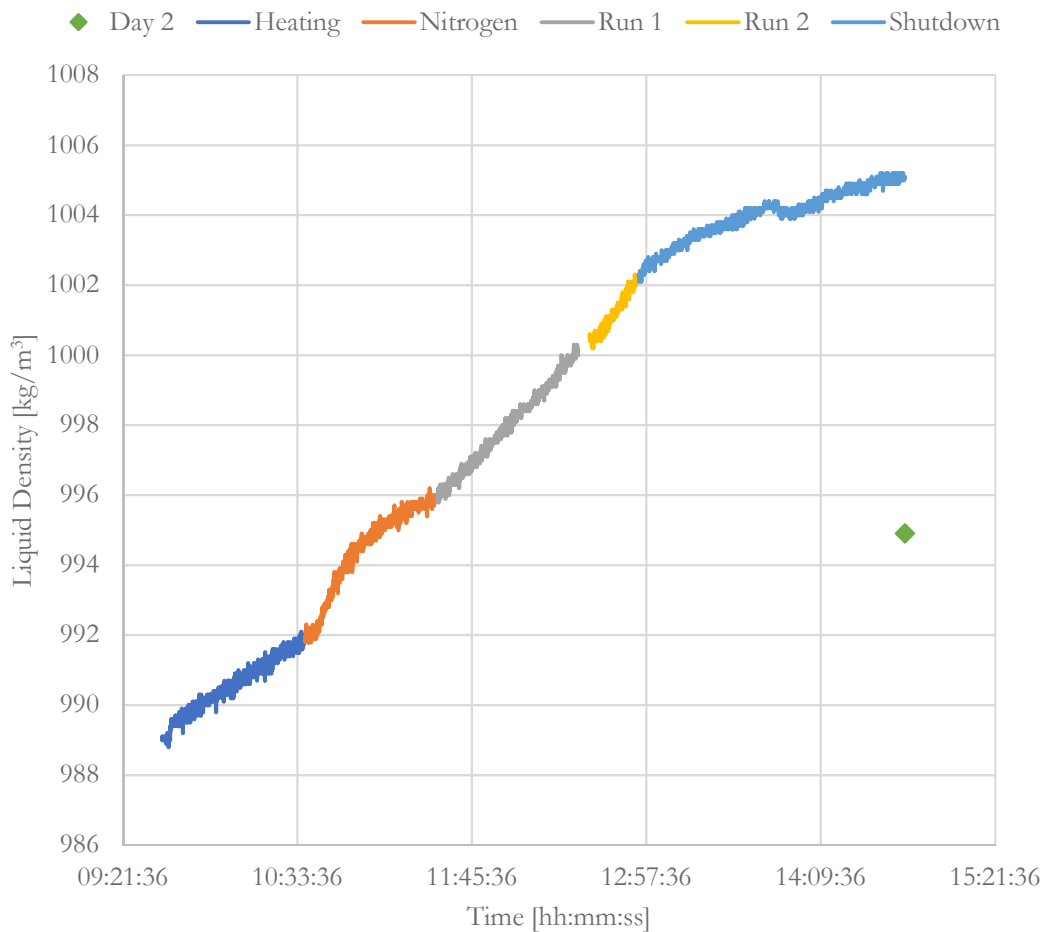
Figure 5. 13 - Liquid density profile in time

The other measured variable is the inlet gas temperature. The outlet gas from the reactor passes through the heat exchanger E-104 (see P&ID). The cooling water is not manipulated in any control loop and, so, the gases are cooled down in an uncontrolled way. It is interesting to look at the temperature profile during the reaction phase. In particular, in Figure 5.14, it is shown the run of the last year (19 September 2016). The reason is simply link with the fact that the inlet flowrate was kept constant, differently from the runs of this year and, so, it is easier to analyse the profiles. This profile is compared with the outlet gas temperature from the reactor. It is evident that the fluctuation in the reactor temperature is reflected on the inlet of the column, due to the uncontrolled logics. However, the oscillations are limited. The profile appears fragmented due to the thermocouple resolution (0.1 °C).
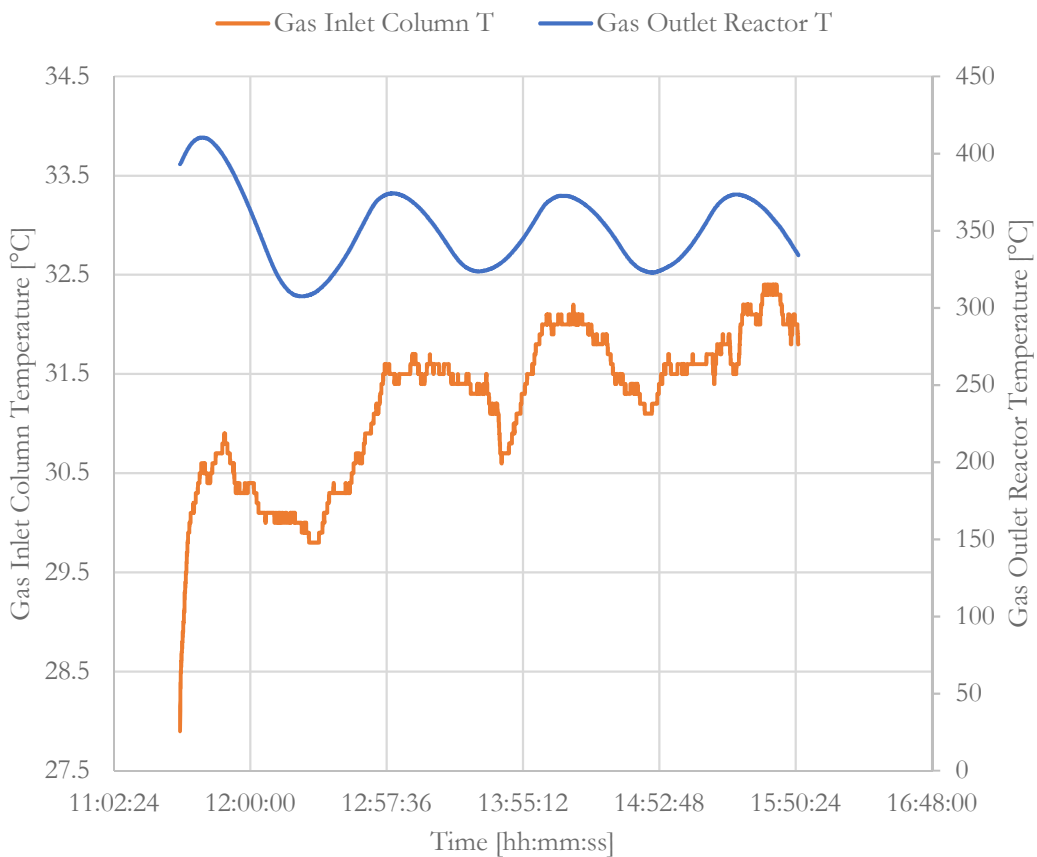
Figure 5. 14 - Temperature comparison between column inlet and reactor outlet, reaction phase

Moreover, the other important variable is the temperature of the recirculated liquid, monitored at the bottom of the column (TT-201) and after the cooling, before re-entering in the column (TT-202). The two different profiles are almost superimposed, due to the high liquid recirculation. It is of interest to analyse one of those profiles (TT-202 for instance) during the different process phases (Figure 5.15); different considerations can be done. First, the temperature does not stabilize around a set point, although the variable is controlled. The simply reason is that, operating the plant for few hours, the

exothermicity of the absorption reaction is too low and the setpoint/project column temperature of 40 °C is not reached. Moreover, it is interested to notice an increase of temperature not only during the reaction phases; the explanations can be multiple. The pump can be an important source of heat for the recirculating liquid; but, also, reasons not directly linked with the process are possible, i.e. the increasing ambient temperature and sun radiation during the day. Furthermore, during the "Nitrogen" phase, the slope changes. Basically, hotter nitrogen is heating the recirculating liquid inside the absorption column.
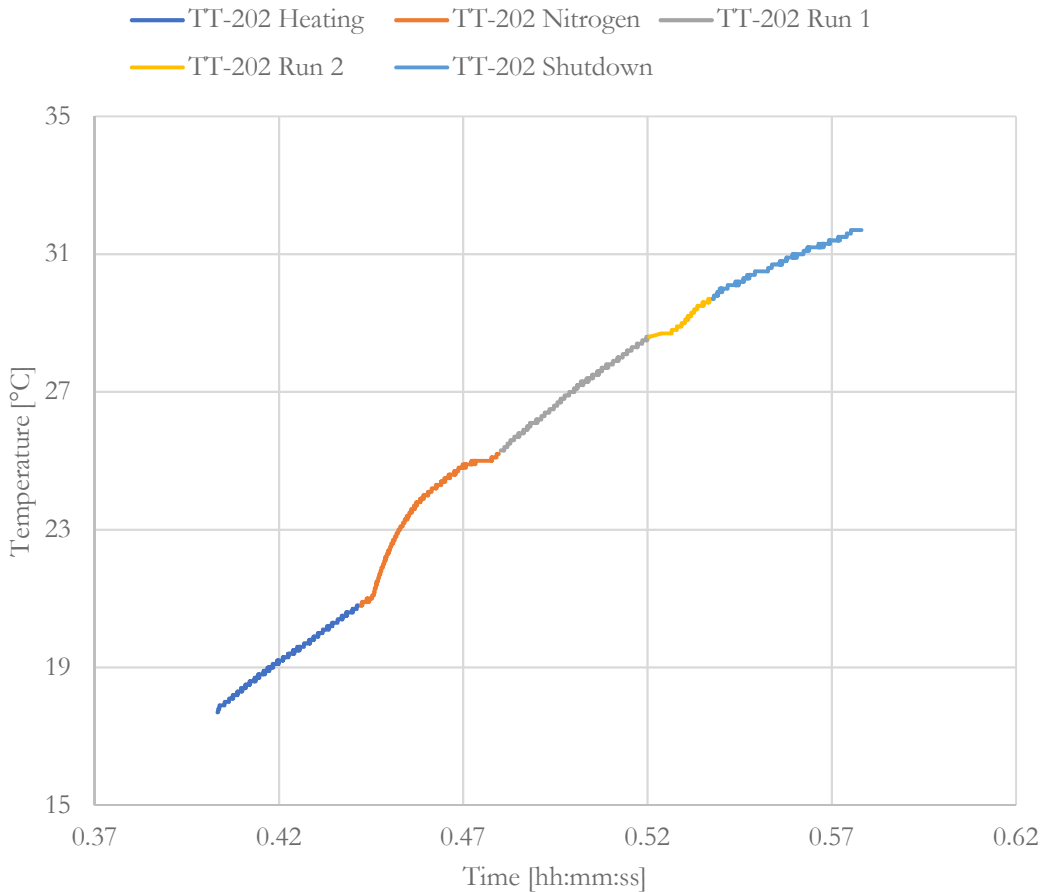
Figure 5. 15 - Recirculating liquid temperature profile in time

5.2.1. Explanation of the Density Trend

Before explaining possible reasons why the density decreases between one day and another one, while the plant is switched off; it is worth to show also the density measures of the last year (Figure 5.16). This plot shows that this phenomenon is systematically present in all the days and, also, at higher liquid density, i.e. at higher sulphuric acid concentration. The abscissa refers to the translation of hours in the form [hh:mm:ss] to a decimal unit; the different runs are not immediately successive, but, as said, they are related to different days.
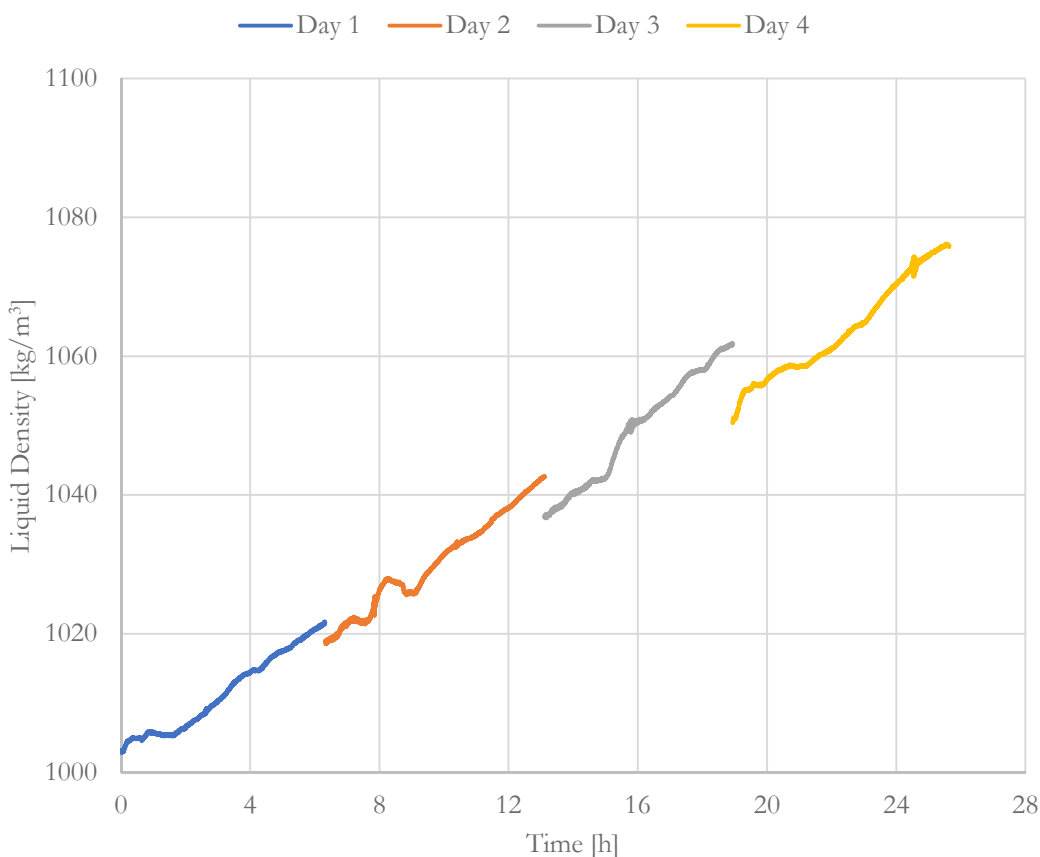
Figure 5. 16 - Liquid density profile in time, different days of experimentation

The evolution of the absorption reaction is also monitored through off-line pH measures. These measurements are done at the beginning and at the end of each experimentation day (Table 5.3). The evidence of the proceeding of the acidification is shown with a pH decreasing, so the reaction is actually occurring. On the other side, the pH increases from the final measure of the first day to the initial measure of the second day. A pH increasing is correlated with a decreasing of the acidity of the solution; this evidence is in trend with the density measure, i.e. less quantity of sulphuric acid.

	Initial pH	Final pH
Day 1	1.88	1.63
Day 2	1.69	1.24

Table 5. 3 - pH measure of the recirculated liquid

They have been identified three possible explanations for this phenomenon. Please note that the following explanations are not mutually exclusive. The proposed explanations concern:

- Dissolved salts effect.
- Circuit effect.
- Atmospheric effect.

Each of these points is discussed and explained in the following sections.

5.2.1.1. Dissolved Salts Effect

Sotacarbo S.p.A. reports that the batch of water is taken from public network. It means that the water is not demineralized and, so, there is a great quantity of dissolved salts inside. These species can react with sulphuric acid, consuming H^+ ions and altering the pH. The high number of dissolved species makes complex any kind of computation on the reaction equilibria. It is only presented, in Table 5.4, the value of the electrical conductivity of the Sardinian public network and a reference value for the demineralized water. In fact, it is reasonable to use this last kind of water to run the absorption reaction (industrial standard). It is evident the enormous value of conductivity with respect to demi water.

	Electrical Conductivity [μS/cm]
Network Water [46]	1251
Demineralized Water for Process Applications [47]	2

Table 5. 4 - Water electrical conductivity comparison

It is clear the need to switch to a production with demi water, even if the salts did not have any effect on the pH and liquid density. It is proposed, for the future experimentation, to complete substitute the current batch of water. After the removal, an alkaline wash of the circuit is needed, to get rid of the fouling eventually present on the packings and, in general, in all the parts of the process circuit.

5.2.1.2. Circuit Effect

The circuit effect means that it could be the possibility of a water loss in a certain point of the plant. In particular, in order to explain the experimental evidence, there would be a passage of water toward the process side. The most probable points are:

- A leakage in the ball valve (BV-101), normally closed, that allows the charging of the water batch at the beginning of the process cycle. This aspect can be simply detected with a valve inspection.
- A leakage in the plate heat exchanger (E-201) that allows the cooling of the recirculating liquid. The cooling fluid is water at 4 barg. The passage of water is possible since the process operates at almost at ambient pressure, consequently the delta pressure is directed toward the process side. This consideration could be verified with a pressure test of E-201. It is possible to connect the two (inlet, outlet) process or utility ports to a nitrogen network. If the outlet pressure, measured on the nitrogen network, is considerably lower that the inlet one; it is possible to conclude that a part of the gas passes to the other side, across a leakage between plates.

5.2.1.3. Atmospheric Effect

The last aspect under investigation is what it has been called atmospheric effect. It refers to a possible interaction between the process and the atmosphere, when the plant is switched off. This is possible since, at the top of the column, the process is directly in contact with the atmosphere, through the chimney. Different types of interaction are possible. First, at the end of the processing, the pipe is full of vapour water that can condensate and, so, acting to dilute the acid. The eventually presence of condensate in the pipeline can be monitored with the inspection of the sampling port installed on the outlet gas line. Moreover, since the sulphuric acid has a strong tendency to dilute, it is possible that the humidity of the atmosphere is absorbed by the liquid, that brings to a reduction of density and to an increase of the pH.

Two distinct actions can be done to face these effects. It is possible to exclude both the effects by the installation of a blind flange at the top of the column. Doing so, the column would be isolated for the entire period of stop, excluding any contact with the external environment. Moreover, it is of interest the analysis of the tendency of the acid solution to absorb the humidity of the air. It was set a specific test to verify this aspect. During the last day of IOSTO experimentation, when the plant was shut down, two samples of liquid solution were taken. The first one was kept in contact with the atmosphere, while the other one was isolated. The results, in term of pH, are shown in Table 5.5.

	pH
Initial Value	0.815
Final Value (Isolated sample)	0.815
Final Value (Sample in contact with the atmosphere)	0.824

Table 5. 5 - pH comparison of the liquid sample at different conditions

It is evident that the hypothesis is validated. In fact, the isolated sample is remained unaltered; while in the other one the pH increases, signal of dilution due the contact with air humidity.

125

Chapter 6
Conclusion and Future Developments

The innovative IOSTO process is at the first stages of developments and a lot of experimental work is programmed for the near future. Despite this, this process seems to be a valid solution that combines different strategic aspects: CO_2 capture; production of electricity, starting from coal with high sulphur content with low emissions; production of sulphuric acid, starting from non-valuable gases. The principal goal of this work was to verify the industrial feasibility of this innovative process, through a series of experimental tests and optimize the process operations for future developments. They were performed several activities concerning: theoretical analysis of the process through literature information, modeling of the plant using commercial software, design of experiments, analysis of data and integration of those data with theoretical studies and model, in order to have a better and coherent picture of the plant behaviour.

In the first part of the work, the preliminary modeling of the plant in Aspen HYSYS® environment was performed, based on literature information. The reactor was modeled, firstly, with an equilibrium reactor, then a with a pseudo-homogeneus 1D model. The last model was also implemented, through the definition of balance equations, in MATLAB®. In this way, it will be possible to substitute the current reactor model with more complex one, since in Aspen HYSYS® only the aforementioned model is present. Moreover, the criteria for the identification of possible transport limitations were applied and, as result, it was demonstrated that the reactor operates in fully chemical regime. In this work phase, they were available the data of the first experimental campaign and, so, those data, concerning both the reactor and absorption sections, were deeply analysed. With the comparison of the simulation results and the first experimental campaign, it was evident that the reactor does not approach the chemical equilibrium condition. Moreover, it was possible to demonstrate that the literature kinetic was not able to predict the IOSTO results. In parallel, the analysis of the experimental data allowed to discover some problems in IOSTO operation and to identify, also with the comparison with the model, a series of tangible actions for the improvement of the plant operation.

The need of experimental validation of the model paved the way to the planning of a series of experimental runs. It was proposed an automatized routine, developed in C++ with the BzzMath library, for the definition of the preliminary experiments (design of experiments). This procedure was compared with the Sotacarbo S.p.A. classical planning of experiments. The results showed that the two different set of experiments were comparable, with a good coverage of the experimental domain.

On the basis of a partial set of experiments, it was performed the fitting of an experimental reaction rate expression. It was developed a procedure to elaborate raw data in order to use them in the regression routine. This step was necessary due to the poor measurement system. A power-law and LHHW expressions were used as kinetic models. The determination of the reaction rate parameters, developed in C++ with the usage of BzzMath library codes, showed that the power-law model works better than the LHHW one, in the studied experimental domain. The power-law model was then validated with additional experimental data, comparing them with the results of Aspen HYSYS®

simulation. The kinetic model, up to now, is only a rough estimation since the experiments are incomplete. For this reason, it was developed the model-based design of experiments, with the aim of finding additional experimental points to investigate, for a better model reliability. This procedure was completely developed in C++ language with a dedicated function of the BzzMath library.

The column, only experimentally analysed in Chapter 3, was studied on a theoretical basis with the development of a dynamic model using commercial simulators. They were tested different solutions (SimSci DYNSIM® and Aspen Hysys® in dynamic mode). At the end, it was selected Aspen Hysys® basically for computational time reasons. The real complexity of the column, combined also with experiments mainly dedicated for the study of the reactor section, made impossible any sort of validation of the dynamic model, currently developed on thermodynamic and literature basis. In the last part of the work, it was performed an important discussion on the explanation of the density profile in time of the liquid acid solution.

The near future developments concern the completion of the planned preliminary tests, combined with all the suggestion of improvement of the micro-pilot plant that are provided throughout the text. All the work was performed in such a way to allow easy modification for future developers. Once the test will be finished and the simulation will be strongly established; it will be possible to perform a process and economic feasibility study of the process. In particular, the feasibility of the process need to be extended also to the dehydration section, with the usage a real feed stream coming the upstream process. Moreover, all the procedure for the scale-up of a new process will be applicable. Particular attention is required from the discontinuous absorption column; in order to find a possible solution for the industrial escalation. Furthermore, it is possible to extend the principle of IOSTO process to other flue gas types, not only correlated with the oxy-combustion flameless processes.

Bibliography:

1. Sperimentazione di una sezione di recupero di acido solforico da fumi di ossicombustione; Frau C., Loria E., Poggi F.; September 2016.
2. Realizzazione della sezione di recupero di H_2SO_4 e prove funzionali; Frau C., Loria E.; September 2016.
3. II Carbone del Sulcis: possibilità di utilizzazione. Bollettino della Società sarda di scienze naturali, Vol. 19; Botteghi C., Conti L., Mansani R.;1979.
4. Flue Gas Desulphurization: The State of the Art; R. K. Srivastava & W. Jozewicz; Journal of the Air & Waste Management Association; 2001.
5. IPCC, http://www.ipcc.ch.
6. BP Energy Outlook; 2017 Edition.
7. Oxy-fuel combustion technology for coal-fired power generation; B.J.P. Buhre, L.K. Elliott, C.D. Sheng, R.P. Gupta, T.F. Wall; Progress in Energy and Combustion Science 31 (2005) 283–307.
8. CO_2 Capture Technologies, Post Combustion Capture (PCC); Global CCS Institute; 2012.
9. Cryogenic Carbon Capture; L. Baxter et al.; Engineering Conferences International; 2016.
10. https://sesinnovation.com/technology/carbon_capture/CFG/.
11. Pre-combustion, post-combustion and oxy-combustion in thermal power plant for CO_2 capture; Mohamed Kanniche et al.; Applied Thermal Engineering 30 53–62; 2010.
12. http://www.iteaspa.it/en/technology/overview/.
13. Flameless Pressurized Oxy-combustion Technology; Sotacarbo Workshop; 2014.
14. Flameless Pressurized Oxy-coal Combustion Technology; G. Benelli et al.; 2013.
15. Flameless Pressurized Oxy-coal, a step ahead in technology development of a ready for CCS competitive and retrofittable carbon capture solution; M. Malavasi; 2015.
16. Sulphuric Acid Manufacture: Analysis, Control and Optimization; G. Daverport, M. J. King; 2006.
17. http://www.essentialchemicalindustry.org/chemicals/sulphuric-acid.html.
18. http://www.mcgroup.com.
19. http://www.marketsandmarkets.com.
20. Argus North America Sulphur and Sulphuric Acid; Argus Media Group; 2017.
21. Best Available Techniques (BAT) Reference Document on the Production of Sulphuric acid; 1999.
22. Technical Documents of IOSTO Process; Sotacarbo S.p.A, HySyTech s.r.l.; from 2015 to 2017.
23. Catalyst Specification Sheet; Clariant; 2012.
24. Kinetics of the Catalytic Oxidation of Sulphur Dioxide; B. Davidson; A.I.Ch.E. Journal; 1964.

25. Experimental and kinetic study of SO$_2$ oxidation on a Pt/γ-Al$_2$O$_3$ catalyst; T. Hamzehlouyan et al.; Applied Catalysis B: Environmental; 2014.
26. Kinetic modeling of sulphur deactivation of Pt/BaO/Al$_2$O$_3$ and BaO/Al$_2$O$_3$ NO$_x$ storage catalyst; J. Dawody; Applied Catalysis B: Environmental; 2007.
27. Calculation of average bed porosity; A. S. Pushnov; Chemical and Petroleum Engineering; 2006.
28. Sulphuric Acid Modeling; C. Bhat et al.; Sulphur Magazine, Vol. 330; 2010.
29. H$_2$SO$_4$ Model; AspenTech; 2014.
30. Aspen Plus Sulphuric Acid Model; AspenTech, 2011.
31. Aspen HYSYS Simulation of Sulphuric Acid Plant; S. T. Sultana et al.; Journal of Chemical Engineering; 2011.
32. Chemical Reactor Analysis and Design; Froment, Bishoff, De Wilde; 2011.
33. Fixed-Bed Reactor Design and Diagnostics; H. F. Rase; 1990.
34. Elements of Chemical Reaction Engineering, fourth ed., Pearson Education Inc.; H. S. Fogler; 2006.
35. Tests for Transport Limitations in Experimental Catalytic Reactors; D. E. Mears; 1971.
36. Temperatures and partial pressures at the surfaces of catalyst particles; F. Yoshida et al.; AIChE Journal, 8; 1962.
37. Perry's Chemical Engineers' Handbook; R.H. Perry; 1999.
38. Dynamic modeling and process optimization of an industrial sulphuric acid plant; A.A. Kiss et al.; 2010.
39. Interpolation and regression models for the chemical engineer; G. Buzzi-Ferraris, F. Manenti; 2010.
40. Statistical methods in research and production; O. L. Davies; 1957.
41. Kinetic Model Development for Dehydration of 2,3-Butanediol to 1,3-Butadiene and Methyl Ethyl Ketone over an Amorphous Calcium Phosphate Catalyst; D. Song; Industrial and Engineering Chemistry Research; 2016.
42. Development of a kinetic model for hydrogen production from phenol over Ni-Co/ZrO$_2$ catalyst; W. Nabgan et al.; Journal of Environmental Chemical Engineering; 2016.
43. Kinetics and mechanistic aspects for CO$_2$ reforming of methane over Ni based catalyst; Y. Kathiraser et al.; Chemical Engineering Journal; 2015.
44. Kinetics of dimethyl ether oxidation over Pt/ZSM-5 catalyst; C. Deng et al.; Catalysis Communications; 2016.
45. Theory of Optimal Experiments; V. V. Fedorov; Academic Press, New York, 1972.
46. http://www.abbanoa.it/distretto-2-iglesias1.
47. Green Oleo S.r.l. Estimates.

Appendix

Appendix 1

Stream	Temperature [°C]	Pressure [barg]	Flowrate [kg/h]	SO2	SO3	H2O	H2SO4	O2	CO2
Stream 1	450	0.2	4.5	2	0	39	0	3	56
Stream 1.1	249	0.2	4.5	2	0	39	0	3	56
Stream 1.2	30	0.2	4.5	2	0	39	0	3	56
Stream 1.3	30	0.2	3.7	3.16	0	3.48	0	4.75	88.61
Stream 1.4	350	0.2	3.7	3.16	0	3.48	0	4.75	88.61
Stream 1.6		0.2	3.7						
Stream 1.7		0.2	3.7						
Stream 8	30	0.2	0.9	0.01	0	99.99	0	0	0
Stream 3	350	0.2	3.7	0.02	3.2	3.54	0	3.22	90.02
Stream 3.1	40	0.2	3.7	0.02	3.2	3.54	0	3.22	90.02
Stream 2.1	40	0.2							
Stream 2.2	40	0.2							
Stream 2.3	40	0.2							
Stream 2.4	40	0.2							
Stream 2.5	40	0.2	3.4	0.01	0	0	0	3.48	96.51
Stream 2.6	40	0.2	3.4	0.01	0	0	0	3.48	96.51
Stream 7	40	0.2	3.4	0.01	0	0	0	3.48	96.51
Stream 2	20	2	50	0	0	100	0	0	0
Stream 6	35	2	50	0	0	100	0	0	0
Stream 9	20	2	50	0	0	100	0	0	0
Stream 10	35	2	50	0	0	100	0	0	0
Stream 11	20	2	100	0	0	100	0	0	0
Stream 12	35	2	100	0	0	100	0	0	0
Stream 4	20	0		0	0	100	0	0	0
Stream 5	40	0		0	0	10	90	0	0

Molar composition [%mol/mol]
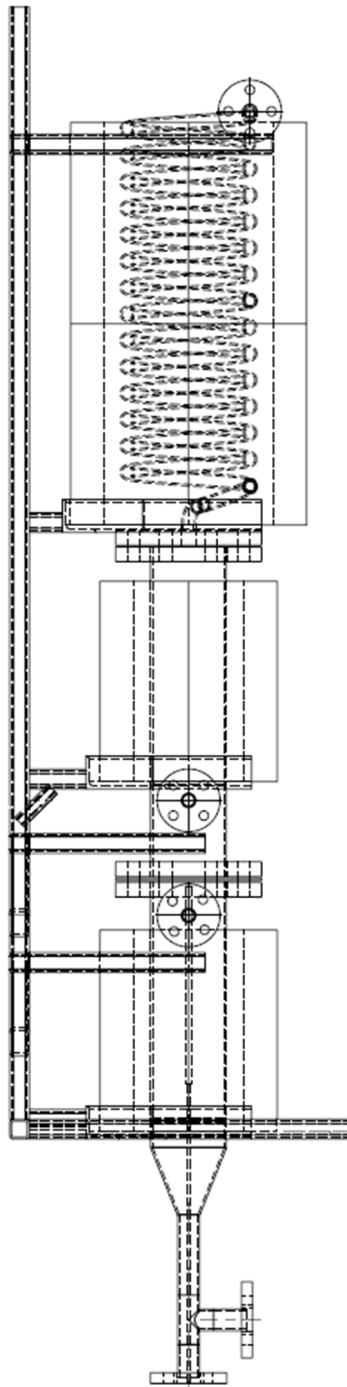
Appendix 2

Appendix 3

N2 Rich				CO2 Rich			
Run	SO2	O2	N2	T [°C]	Run	SO2	O2	CO2	T [°C]
1	0.083304	0.068726	3.54797	350	1	0.053816	0.044398	3.601786	350
2	0.132099	0.108981	3.45892	350	2	0.086103	0.071035	3.542862	350
3	0.254987	0.210364	3.234649	350	3	0.170041	0.140284	3.389675	350
4	0.045029	0.037149	1.917822	350	4	0.029090	0.023999	1.946912	350
5	0.071405	0.058909	1.869686	350	5	0.046542	0.038397	1.915061	350
6	0.137831	0.11371	1.748459	350	6	0.091914	0.075829	1.832257	350
7	0.022515	0.018575	0.958911	350	7	0.014545	0.011999	0.973456	350
8	0.035702	0.029454	0.934843	350	8	0.023271	0.019199	0.957530	350
9	0.068915	0.056855	0.87423	350	9	0.045957	0.037915	0.916128	350
10	0.08338	0.04169	3.57493	350	10	0.053721	0.026860	3.619419	350
11	0.132291	0.066145	3.501564	350	11	0.085859	0.042930	3.571211	350
12	0.255703	0.127851	3.316446	350	12	0.169094	0.084547	3.446359	350
13	0.083439	0.02086	3.595701	350	13	0.053647	0.013412	3.632941	350
14	0.132438	0.03311	3.534452	350	14	0.085673	0.021418	3.592909	350
15	0.256256	0.064064	3.37968	350	15	0.168373	0.042093	3.489534	350
16	0.083304	0.068726	3.54797	410	16	0.053816	0.044398	3.601786	410
17	0.132099	0.108981	3.45892	410	17	0.086103	0.071035	3.542862	410
18	0.254987	0.210364	3.234649	410	18	0.170041	0.140284	3.389675	410
19	0.045029	0.037149	1.917822	410	19	0.029090	0.023999	1.946912	410
20	0.071405	0.058909	1.869686	410	20	0.046542	0.038397	1.915061	410
21	0.137831	0.11371	1.748459	410	21	0.091914	0.075829	1.832257	410
22	0.022515	0.018575	0.958911	410	22	0.014545	0.011999	0.973456	410
23	0.035702	0.029454	0.934843	410	23	0.023271	0.019199	0.957530	410
24	0.068915	0.056855	0.87423	410	24	0.045957	0.037915	0.916128	410
25	0.083304	0.068726	3.54797	450	25	0.053816	0.044398	3.601786	450
26	0.132099	0.108981	3.45892	450	26	0.086103	0.071035	3.542862	450
27	0.254987	0.210364	3.234649	450	27	0.170041	0.140284	3.389675	450
28	0.045029	0.037149	1.917822	450	28	0.029090	0.023999	1.946912	450
29	0.071405	0.058909	1.869686	450	29	0.046542	0.038397	1.915061	450
30	0.137831	0.11371	1.748459	450	30	0.091914	0.075829	1.832257	450
31	0.022515	0.018575	0.958911	450	31	0.014545	0.011999	0.973456	450
32	0.035702	0.029454	0.934843	450	32	0.023271	0.019199	0.957530	450
33	0.068915	0.056855	0.87423	450	33	0.045957	0.037915	0.916128	450

Appendix 4

Run	Inlet First Stage [kg/h]						[K]	Outlet First Stage [kg/h]					
	SO2	O2	SO3	H2O	N2	CO2	T	SO2	O2	SO3	H2O	N2	CO2
1	0.083	0.069	0	0	3.548	0	612.25	0.05606	0.062365	0.03389	0	3.555335	0
2	0.083	0.069	0	0	3.548	0	588.05	0.060481	0.06347	0.028364	0	3.555335	0
3	0.083	0.069	0	0	3.548	0	650.45	0.044992	0.059598	0.047724	0	3.555335	0
4	0.132	0.11	0	0	3.459	0	605.55	0.085777	0.099057	0.059093	0	3.486531	0
5	0.132	0.11	0	0	3.459	0	602.95	0.086877	0.099332	0.057716	0	3.486531	0
6	0.132	0.11	0	0	3.459	0	596.15	0.095781	0.101558	0.046587	0	3.486531	0
7	0.254	0.21	0	0	3.234	0	606.85	0.210509	0.200083	0.056434	0	3.255095	0
8	0.254	0.21	0	0	3.234	0	603.05	0.211119	0.200235	0.055673	0	3.255095	0
9	0.254	0.21	0	0	3.234	0	598.55	0.212207	0.200507	0.054312	0	3.255095	0
10	0.083	0.042	0	0	3.575	0	622.75	0.026391	0.027827	0.070662	0	3.571578	0
11	0.083	0.042	0	0	3.575	0	588.45	0.040703	0.031405	0.052772	0	3.571578	0

```cpp
#define BZZ_COMPILER_3
#include "BzzMath.hpp"

// Number of Experiments
!! MODIIFY IF CHANGE THE NUMBER OF EXPERIMENTS !!
int Nexp = 11;
// Number of Species
int NC = 6;
// Initial conditions of different experiments
[m_SO2 m_O2 m_SO3 m_H2O m_N2 m_CO2 Tin]
// m in [kg/h] T in [K]
BzzMatrix ICtot(Nexp, NC + 1,        0.083, 0.069,
0.000, 0.000, 3.548, 0.000, 612.250,
                                     0.083, 0.069,
0.000, 0.000, 3.548, 0.000, 588.050,
                                     0.083, 0.069,
0.000, 0.000, 3.548, 0.000, 650.450,
                                     0.132, 0.110,
0.000, 0.000, 3.459, 0.000, 605.550,
                                     0.132, 0.110,
0.000, 0.000, 3.459, 0.000, 602.950,
                                     0.132, 0.110,
0.000, 0.000, 3.459, 0.000, 596.150,
                                     0.254, 0.210,
0.000, 0.000, 3.234, 0.000, 606.850,
                                     0.254, 0.210,
0.000, 0.000, 3.234, 0.000, 603.050,
                                     0.254, 0.210,
0.000, 0.000, 3.234, 0.000, 598.550,
                                     0.083, 0.042,
0.000, 0.000, 3.575, 0.000, 622.750,
                                     0.083, 0.042,
0.000, 0.000, 3.575, 0.000, 588.450);

// Matrix of experimental Data [kg/h]  [1bed OUT]
BzzMatrix xMexp(Nexp, NC,            0.056060, 0.062365,
0.033890, 0.000000, 3.555335, 0.000000,
                                     0.060481, 0.063470,
0.028364, 0.000000, 3.555335, 0.000000,
                                     0.044992, 0.059598,
0.047724, 0.000000, 3.555335, 0.000000,
                                     0.085777, 0.099057,
0.059093, 0.000000, 3.486531, 0.000000,
                                     0.086877, 0.099332,
0.057716, 0.000000, 3.486531, 0.000000,
```

```cpp
                                        0.095781, 0.101558,
0.046587, 0.000000, 3.486531, 0.000000,
                                        0.210509, 0.200083,
0.056434, 0.000000, 3.255095, 0.000000,
                                        0.211119, 0.200235,
0.055673, 0.000000, 3.255095, 0.000000,
                                        0.212207, 0.200507,
0.054312, 0.000000, 3.255095, 0.000000,
                                        0.026391, 0.027827,
0.070662, 0.000000, 3.571578, 0.000000,
                                        0.040703, 0.031405,
0.052772, 0.000000, 3.571578, 0.000000);

// First Guess Parameters and Min Max Value
// d.o.f = [alpha beta k0_kin Ea] - POWER LAW
BzzVector P0(4,      1.2,   1.1,  2.32e+6,     4700.);
BzzVector Pmin(4, -20.0, -20.0,        1.,     -100.);
BzzVector Pmax(4,  20.0,  20.0,    1e+15,  1000000.);

// To Define Pact as Global
BzzVector Pact;

// Number of Points along the Reactor
int mMax = 10;
// Length of the Bed [m]
double Lbed = 0.305;
// Pressure [kPa]
double Press = 120.;

// Molecular weight [kg_i/mol_i]
[m_SO2 m_O2 m_SO3 m_H2O m_N2 m_CO2]
BzzVector MW(NC, 64. / 1000., 32. / 1000., 80. / 1000., 18. /
1000., 28. / 1000., 44. / 1000.);

// Area [m2]
double Dint = 0.083;                              //[m]
double A = 0.005410607947645;                     //[m2]

void F2SistDiff(BzzVector &y, double z, BzzVector &dydz);
double F3sse(BzzVector &P);
BzzMatrix &F1odeSol(BzzVector &IC_j, BzzVector &P);

int main()
{
    int maxIter = 10000;
    BzzVector Popt1;
    BzzVector Popt2;
```

```cpp
        BzzVector Popt3;
        BzzVector Popt4;
        BzzVector Popt;

        bzzOpenMP = 0;

        BzzMinimizationRobust fminsearch1(P0, F3sse, Pmin,
        Pmax);
        fminsearch1(maxIter);
        fminsearch1.GetSolution(&Popt1);

        BzzMinimizationRobust fminsearch2(Popt1, F3sse, Pmin,
        Pmax);
        fminsearch2(maxIter);
        fminsearch2.GetSolution(&Popt2);

        BzzMinimizationRobust fminsearch3(Popt2, F3sse, Pmin,
        Pmax);
        fminsearch3(maxIter);
        fminsearch3.GetSolution(&Popt3);

        BzzMinimizationRobust fminsearch4(Popt3, F3sse, Pmin,
        Pmax);
        fminsearch4(maxIter);
        fminsearch4.GetSolution(&Popt4);

        BzzMinimizationRobust fminsearch5(Popt4, F3sse, Pmin,
        Pmax);
        fminsearch5(maxIter);
        /**///**///**///**///**/printf("\n\n%-s%-d\n", "nIterTot =
        ", fminsearch5.GetIterTotal());
        fminsearch5.GetSolution(&Popt);

        FILE *fp;
        fp = fopen("Res.xls", "w");
        fprintf(fp, "%-s\n", "Parameters");
        fprintf(fp, "%f\n %f\n %f\n %f\n", Popt[1], Popt[2],
        Popt[3], Popt[4]);
        fclose(fp);
        /**///**///**///**///**/getchar();
        return 0;
}
double F3sse(BzzVector &P)
{
        BzzMatrix xM;
        double SSEtot = 0.;
        double epsi = 1.e-4;
```

```
        for (int h = 1; h <= Nexp; h++)
        {
                xM = F1odeSol(ICtot.GetRow(h), P);    //[kg/h]

                BzzVector vTemp(NC);
                BzzVector vTempAux(NC);

                for (int l = 1; l <= NC; l++)
                {
                        //[kg/h]
                        vTemp[l] = xM[l][mMax];
                }

                vTempAux = xMexp.GetRow(h);
                vTemp -= vTempAux;

                double SSEh = 0.;

                for (int q = 1; q <= NC; q++)
                {
                        SSEh += fabs(vTemp[q] / (epsi + vTempAux[q]));
                }
                SSEtot += SSEh;
        }
/**//**//**//**//**//**/printf("\n%-s%-1.15E", "SSEtot =
", SSEtot);
        return SSEtot;
}

BzzMatrix &F1odeSol(BzzVector &IC_j, BzzVector &P)
{
        BzzVector IC_j_act(IC_j);
        Pact = P;
        BzzVector w;

        static BzzMatrix xM(NC, mMax);
        BzzOdeStiff ODEsolver(IC_j_act, 0., F2SistDiff);

        double z = 0.;
        double dz = Lbed / mMax;
        for (int m = 1; m <= mMax; m++)
        {
                z += dz;
                w = ODEsolver(z);

                for (int j = 1; j <= NC; j++)
```

```cpp
            {
                xM[j][m] = w[j];
            }
        }
        return xM;
}

void F2SistDiff(BzzVector &y, double z, BzzVector &dydz)
{
        // y [m_SO2 m_O2 m_SO3 m_H2O m_N2 m_CO2 T]
        double T = y[7];

        // Subdivide Elements of P
        // d.o.f = [alpha beta k0_kin Ea] - POWER LAW
        double alpha = Pact[1];
        double beta = Pact[2];
        double k0_kin = Pact[3];
        double Ea = Pact[4];

        BzzVector Fi(NC);
        double Ftot = 0.;
        BzzVector Pi(NC);
        BzzVector yi_mol(NC);

        // Calculations
        for (int ii = 1; ii <= NC; ii++)
        {
            Fi[ii] = y[ii] / MW[ii];         //[mol/h]
        }

        for (int jj = 1; jj <= NC; jj++)
        {
            Ftot += Fi[jj];                  //[mol/h]
        }

        for (int kk = 1; kk <= NC; kk++)
        {
            yi_mol[kk] = Fi[kk] / Ftot;      //[-]
            Pi[kk] = Press * yi_mol[kk];     //[kPa]
        }

        // Reaction Rate y [m_SO2 m_O2 m_SO3 m_H2O m_N2 m_CO2 T]
        double R = 8.314;                        //[J/mol/K]
        double DH0R = -98930;                    //[J/mol]
        double Tref = 298;                       //[K]
        double Keq_Tref = 2.5633e+12;            //[-]
        double k0 = Keq_Tref*exp((DH0R / R)*(1 / Tref));
```

```cpp
    double Keq_T = k0*exp(-DH0R / (R*T));

    // r [mol/m3/h]
    double k_d = (k0_kin*exp(-Ea / T));
    double term_dir = (pow(Pi[1], alpha)*pow(Pi[2], beta));
    double term_inv = ((1 / (10.066*Keq_T))*pow(Pi[1], alpha
    - 1)*pow(Pi[2], beta - 0.5)*Pi[3]);
    double r = k_d * (term_dir - term_inv);

    // Derivatives
    dydz[1] = -r*MW[1] * A;
    dydz[2] = -0.5*r*MW[2] * A;
    dydz[3] = +r*MW[3] * A;
    dydz[4] = 0.;
    dydz[5] = 0.;
    dydz[6] = 0.;
    dydz[7] = 0.;
}
```

```cpp
#define BZZ_COMPILER_3
#include "BzzMath.hpp"

// Number of Experiments
!! MODIIFY IF CHANGE THE NUMBER OF EXPERIMENTS !!
int Nexp = 11;
// Number of Species
int NC = 6;
// Initial conditions of different experiments
[m_SO2 m_O2 m_SO3 m_H2O m_N2 m_CO2 Tin]
// m in [kg/h] T in [K]
BzzMatrix ICtot(Nexp, NC + 1,               0.083, 0.069,
0.000, 0.000, 3.548, 0.000, 612.250,
                                            0.083, 0.069,
0.000, 0.000, 3.548, 0.000, 588.050,
                                            0.083, 0.069,
0.000, 0.000, 3.548, 0.000, 650.450,
                                            0.132, 0.110,
0.000, 0.000, 3.459, 0.000, 605.550,
                                            0.132, 0.110,
0.000, 0.000, 3.459, 0.000, 602.950,
                                            0.132, 0.110,
0.000, 0.000, 3.459, 0.000, 596.150,
                                            0.254, 0.210,
0.000, 0.000, 3.234, 0.000, 606.850,
                                            0.254, 0.210,
0.000, 0.000, 3.234, 0.000, 603.050,
                                            0.254, 0.210,
0.000, 0.000, 3.234, 0.000, 598.550,
                                            0.083, 0.042,
0.000, 0.000, 3.575, 0.000, 622.750,
                                            0.083, 0.042,
0.000, 0.000, 3.575, 0.000, 588.450);

// Matrix of experimental Data [kg/h]  [1bed OUT]
BzzMatrix xMexp(Nexp, NC,                   0.056060, 0.062365,
0.033890, 0.000000, 3.555335, 0.000000,
                                            0.060481, 0.063470,
0.028364, 0.000000, 3.555335, 0.000000,
                                            0.044992, 0.059598,
0.047724, 0.000000, 3.555335, 0.000000,
                                            0.085777, 0.099057,
0.059093, 0.000000, 3.486531, 0.000000,
```

```cpp
                                          0.086877, 0.099332,
0.057716, 0.000000, 3.486531, 0.000000,
                                          0.095781, 0.101558,
0.046587, 0.000000, 3.486531, 0.000000,
                                          0.210509, 0.200083,
0.056434, 0.000000, 3.255095, 0.000000,
                                          0.211119, 0.200235,
0.055673, 0.000000, 3.255095, 0.000000,
                                          0.212207, 0.200507,
0.054312, 0.000000, 3.255095, 0.000000,
                                          0.026391, 0.027827,
0.070662, 0.000000, 3.571578, 0.000000,
                                          0.040703, 0.031405,
0.052772, 0.000000, 3.571578, 0.000000);

// First Guess Parameters and Min Max Value
// d.o.f = [A_d Ea_d A_SO2 Ea_SO2 A_O2 Ea_O2 A_SO3 Ea_SO3] -
SSE
BzzVector P0(8,  3.8506,  -6.4349, 9.2649, -1.7200, 1.2783,  -
1.08, 9.0718,  -1.64);      // First Guess
BzzVector Pmin(8,    0.,  -20e+5,     0.,   -2e+5,      0.,  -
2e+5,     0.,  -2e+5);
BzzVector Pmax(8,  2e+5,    20e+5,  100.0,   2e+5,   100.0,
2e+5,  100.0,   2e+5);

// To Define Pact as Global
BzzVector Pact;

// Number of Points along the Reactor
int mMax = 10;
// Length of the Bed [m]
double Lbed = 0.305;
// Pressure [kPa]
double Press = 120.;

// Molecular weight [kg_i/mol_i]
[m_SO2 m_O2 m_SO3 m_H2O m_N2 m_CO2]
BzzVector MW(NC, 64. / 1000., 32. / 1000., 80. / 1000., 18. /
1000., 28. / 1000., 44. / 1000.);

// Area [m2]
double Dint = 0.083;                              //[m]
double A = 0.005410607947645;                     //[m2]

void F2SistDiff(BzzVector &y, double z, BzzVector &dydz);
double F3sse(BzzVector &P);
```

```cpp
BzzMatrix &F1odeSol(BzzVector &IC_j, BzzVector &P, bool
&status);

int main()
{
    int maxIter = 10000;
    BzzVector Popt1;
    BzzVector Popt2;
    BzzVector Popt3;
    BzzVector Popt4;
    BzzVector Popt;

    bzzOpenMP = 0;
    bzzWarningWindow = 0; // No Show of Warning Window

    BzzMinimizationRobust fminsearch1(P0, F3sse, Pmin,
    Pmax);
    fminsearch1(maxIter);
    fminsearch1.GetSolution(&Popt1);

    BzzMinimizationRobust fminsearch2(Popt1, F3sse, Pmin,
    Pmax);
    fminsearch2(maxIter);
    fminsearch2.GetSolution(&Popt2);

    BzzMinimizationRobust fminsearch3(Popt2, F3sse, Pmin,
    Pmax);
    fminsearch3(maxIter);
    fminsearch3.GetSolution(&Popt3);

    BzzMinimizationRobust fminsearch4(Popt3, F3sse, Pmin,
    Pmax);
    fminsearch4(maxIter);
    fminsearch4.GetSolution(&Popt4);

    BzzMinimizationRobust fminsearch5(Popt4, F3sse, Pmin,
    Pmax);
    fminsearch5(maxIter);
    /**//**//**//**//**/printf("\n\n%-s%-d\n", "nIterTot =
    ", fminsearch5.GetIterTotal());
    fminsearch5.GetSolution(&Popt);

    FILE *fp;
    fp = fopen("Res.xls", "w");
    fprintf(fp, "%-s\n", "Parameters");
```

```
        fprintf(fp, "%f\n %f\n %f\n %f\n %f\n %f\n %f\n %f\n",
        Popt[1], Popt[2], Popt[3], Popt[4], Popt[5], Popt[6],
        Popt[7], Popt[8]);
        fclose(fp);
        /**//**//**//**//**/getchar();
        return 0;
}

double F3sse(BzzVector &P)
{
        BzzMatrix xM;
        double SSEtot = 0.;
        double epsi = 1.e-4;
        bool status;

        for (int h = 1; h <= Nexp; h++)
        {
                xM = F1odeSol(ICtot.GetRow(h), P, status); //[kg/h]
                // In case the ODE system cannot be solved with a
                certain set of kinetic parameters, the routine
                doesn't stop but, with the "status" function, it
                assigns a huge value for the SSE. In this way the
                optimization routine is obliged to re-start again
                with another first guess of the kinetic parameters
                if (status == 1)
                {
                        SSEtot = DBL_MAX;
                        return SSEtot;
                }

                BzzVector vTemp(NC);
                BzzVector vTempAux(NC);

                for (int l = 1; l <= NC; l++)
                {
                        //[kg/h]
                        vTemp[l] = xM[l][mMax];
                }

                vTempAux = xMexp.GetRow(h);
                vTemp -= vTempAux;

                double SSEh = 0.;

                for (int q = 1; q <= NC; q++)
                {
                        SSEh += fabs(vTemp[q] / (epsi + vTempAux[q]));
```

```cpp
            }
            SSEtot += SSEh;
        }
        /**//**//**//**//**//**/printf("\n%-s%-1.15E", "SSEtot =
        ", SSEtot);
        return SSEtot;
}

BzzMatrix &F1odeSol(BzzVector &IC_j, BzzVector &P, bool
&status)
{
        BzzVector IC_j_act(IC_j);
        Pact = P;
        BzzVector w;

        static BzzMatrix xM(NC, mMax);
        BzzOdeStiff ODEsolver(IC_j_act, 0., F2SistDiff);

        double z = 0.;
        double dz = Lbed / mMax;
        for (int m = 1; m <= mMax; m++)
        {
            z += dz;
            w = ODEsolver(z);
            if (ODEsolver.GetCalculationState() != 1 &&
            ODEsolver.GetCalculationState() != 2) //If problems
            in ODE resolution
            {
                xM = 0.;          // Need, in all the cases, to
                provide an output value
                status = 1;
                return xM;
            }
            for (int j = 1; j <= NC; j++)
            {
                xM[j][m] = w[j];
            }
        }
        status = 0;
        return xM;
}

void F2SistDiff(BzzVector &y, double z, BzzVector &dydz)
{
        // y [m_SO2 m_O2 m_SO3 m_H2O m_N2 m_CO2 T]
        double T = y[7];
```

```
// Subdivide Value of P
// d.o.f = [A_d Ea_d A_SO2 Ea_SO2 A_O2 Ea_O2 A_SO3
Ea_SO3] - LHHW
double A_d_norm = Pact[1];
double Ea_d_norm = Pact[2];
double A_SO2_norm = Pact[3];
double Ea_SO2_norm = Pact[4];
double A_O2_norm = Pact[5];
double Ea_O2_norm = Pact[6];
double A_SO3_norm = Pact[7];
double Ea_SO3_norm = Pact[8];

// Parameters at their original dimension
double A_d = A_d_norm*1E+6;
double Ea_d = Ea_d_norm*1E+3;
double A_SO2 = A_SO2_norm*1E-09;
double Ea_SO2 = Ea_SO2_norm*1E+04;
double A_O2 = A_O2_norm*1E-05;
double Ea_O2 = Ea_O2_norm*1E+04;
double A_SO3 = A_SO3_norm*1E-09;
double Ea_SO3 = Ea_SO3_norm*1E+04;

BzzVector Fi(NC);
double Ftot = 0.;
BzzVector Pi(NC);
BzzVector yi_mol(NC);

// Calculations
for (int ii = 1; ii <= NC; ii++)
{
    Fi[ii] = y[ii] / MW[ii];          //[mol/h]
}

for (int jj = 1; jj <= NC; jj++)
{
    Ftot += Fi[jj];                   //[mol/h]
}

for (int kk = 1; kk <= NC; kk++)
{
    yi_mol[kk] = Fi[kk] / Ftot;       //[-]
    Pi[kk] = Press * yi_mol[kk];      //[kPa]
}

// Reaction Rate y [m_SO2 m_O2 m_SO3 m_H2O m_N2 m_CO2 T]
double R = 8.314;                     //[J/mol/K]
double DH0R = -98930;                 //[J/mol]
```

```cpp
    double Tref = 298;                      //[K]
    double Keq_Tref = 2.5633e12;            //[-]
    double k0 = Keq_Tref*exp((DH0R / R)*(1 / Tref));
    double Keq_T = k0*exp(-DH0R / (R*T));

    // r [mol/m3/h]
    // d.o.f = [A_d Ea_d A_SO2 Ea_SO2 A_O2 Ea_O2 A_SO3
    Ea_SO3] - LHHW
    double k_d = (A_d*exp(-Ea_d / T));
    double term_dir = Pi[1] * pow(Pi[2], 0.5);
    double term_inv = (1/(10.066*Keq_T))*Pi[3];
    double k_SO2 = A_SO2*exp(-Ea_SO2 / T);
    double k_O2 = A_O2*exp(-Ea_O2 / T);
    double k_SO3 = A_SO3*exp(-Ea_SO3 / T);
    double den = ( (k_SO2*Pi[1]) + (k_O2*pow(Pi[2], 0.5)) +
    (k_SO3*Pi[3]) + 1 );
    double r = (k_d * (term_dir - term_inv))/pow(den,2);

    // Derivatives
    dydz[1] = -r*MW[1] * A;
    dydz[2] = -0.5*r*MW[2] * A;
    dydz[3] = +r*MW[3] * A;
    dydz[4] = 0.;
    dydz[5] = 0.;
    dydz[6] = 0.;
    dydz[7] = 0.;

}
```

Appendix 7
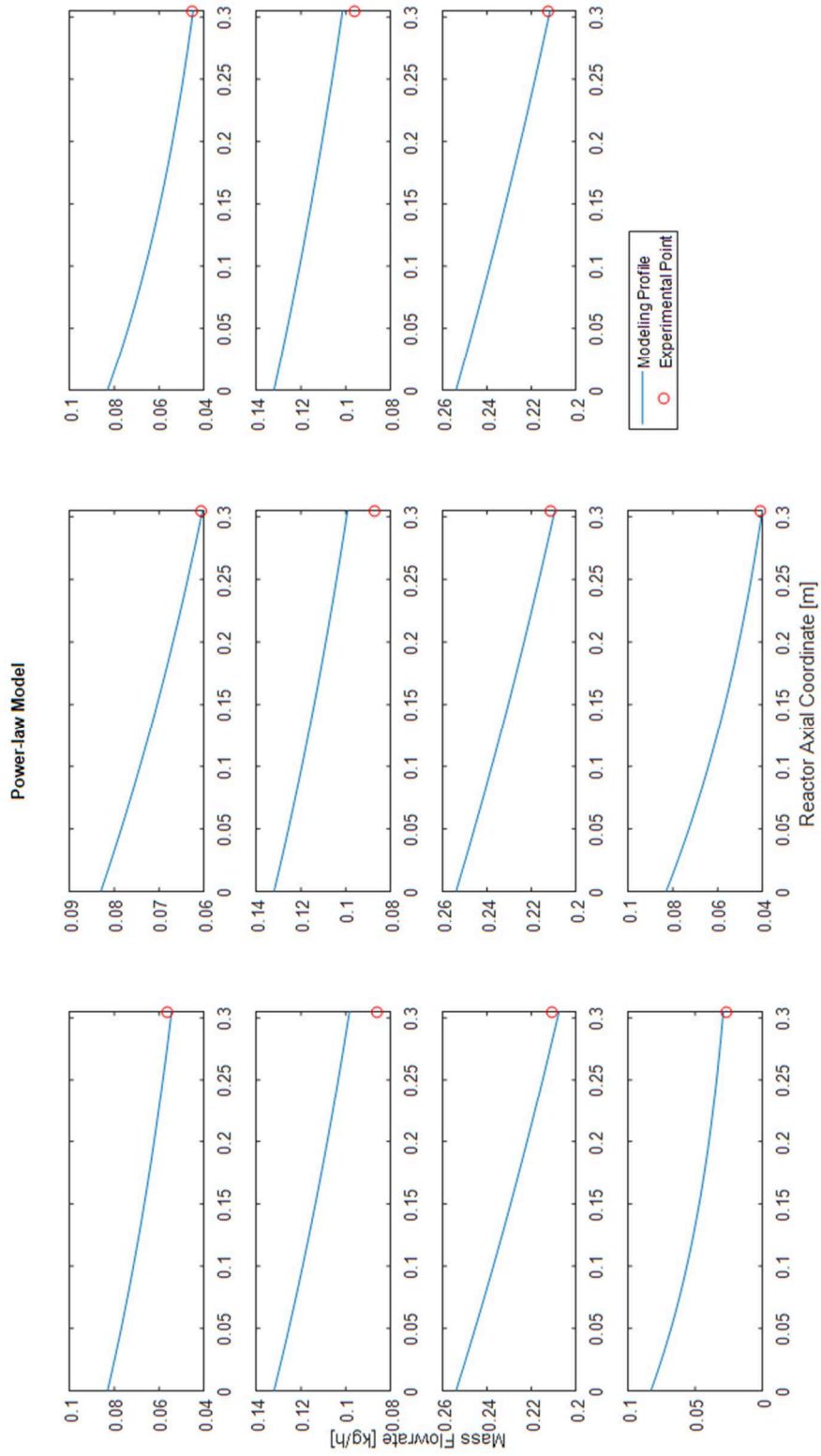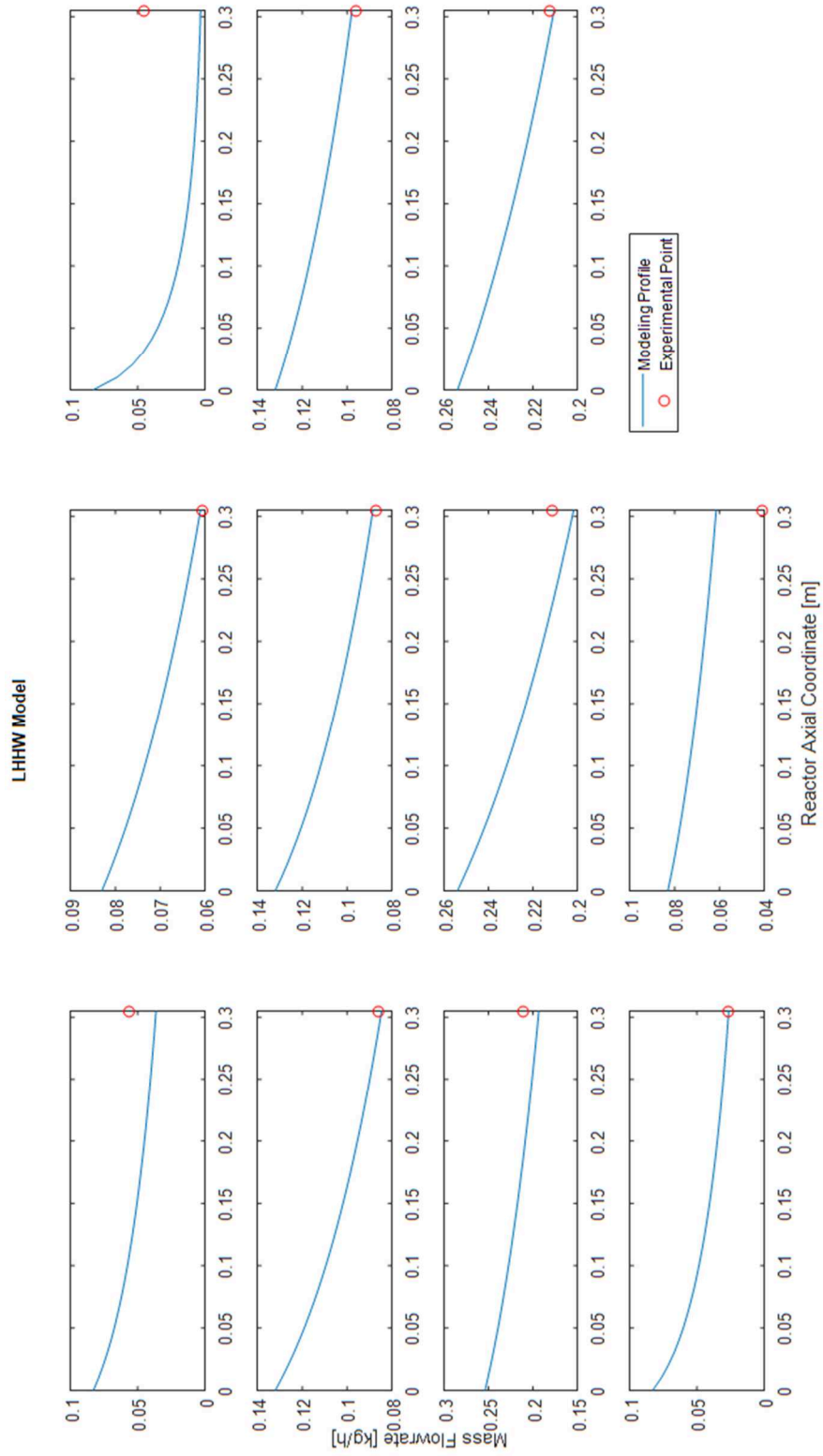
	Inlet First Stage [kg/h]			[°C]		
Run	SO2	O2	N2	Inlet T	Outlet T	Conversion
12	0.083	0.069	3.548	322.8	343.2	0.36578
13	0.083	0.069	3.548	338.2	316.3	0.35275
14	0.08300	0.04200	3.57500	325.5	346.7	0.66847
15	0.08300	0.04200	3.57500	319.3	343.1	0.64194
16	0.08300	0.04200	3.57500	345.5	322.1	0.54900
17	0.08300	0.04200	3.57500	348.1	322.6	0.53572

Appendix 8

```cpp
#define BZZ_COMPILER_3
#include <iostream>
#include <fstream>
#include <sstream>
#include <iomanip>
#include <stdlib.h>
#include <stdio.h>
#include <string>
#include <vector>
#include "BzzMath.hpp"

using namespace std;

// Number of Experiments
!! MODIIFY IF CHANGE THE NUMBER OF EXPERIMENTS !!
int Nexp = 11;
// Number of Species
int NC = 6;
// Initial conditions of different experiments
[m_SO2 m_O2 m_SO3 m_H2O m_N2 m_CO2 Tin]
// m in [kg/h] T in [K]
BzzMatrix ICtot(Nexp, NC + 1,                    0.083, 0.069,
0.000, 0.000, 0.3548, 0.000, 0.612250,
                                                 0.083, 0.069,
0.000, 0.000, 0.3548, 0.000, 0.588050,
                                                 0.083, 0.069,
0.000, 0.000, 0.3548, 0.000, 0.650450,
                                                 0.132, 0.110,
0.000, 0.000, 0.3459, 0.000, 0.605550,
                                                 0.132, 0.110,
0.000, 0.000, 0.3459, 0.000, 0.602950,
                                                 0.132, 0.110,
0.000, 0.000, 0.3459, 0.000, 0.596150,
                                                 0.254, 0.210,
0.000, 0.000, 0.3234, 0.000, 0.606850,
                                                 0.254, 0.210,
0.000, 0.000, 0.3234, 0.000, 0.603050,
                                                 0.254, 0.210,
0.000, 0.000, 0.3234, 0.000, 0.598550,
                                                 0.083, 0.042,
0.000, 0.000, 0.3575, 0.000, 0.622750,
                                                 0.083, 0.042,
0.000, 0.000, 0.3575, 0.000, 0.588450);
```

```cpp
// Matrix of experimental Data [kg/h]  [1bed OUT]
BzzMatrix xMexp(Nexp, NC,                    0.056060, 0.062365,
0.033890, 0.000000, 3.555335, 0.000000,

                                             0.060481, 0.063470,
0.028364, 0.000000, 3.555335, 0.000000,

                                             0.044992, 0.059598,
0.047724, 0.000000, 3.555335, 0.000000,

                                             0.085777, 0.099057,
0.059093, 0.000000, 3.486531, 0.000000,

                                             0.086877, 0.099332,
0.057716, 0.000000, 3.486531, 0.000000,

                                             0.095781, 0.101558,
0.046587, 0.000000, 3.486531, 0.000000,

                                             0.210509, 0.200083,
0.056434, 0.000000, 3.255095, 0.000000,

                                             0.211119, 0.200235,
0.055673, 0.000000, 3.255095, 0.000000,

                                             0.212207, 0.200507,
0.054312, 0.000000, 3.255095, 0.000000,

                                             0.026391, 0.027827,
0.070662, 0.000000, 3.571578, 0.000000,

                                             0.040703, 0.031405,
0.052772, 0.000000, 3.571578, 0.000000);

/// First Guess Parameters and Min Max Value
// d.o.f = [alpha beta k0_kin Ea] - POWER LAW
BzzVector P0(4,    2.006, -1.682,  1.5225,  4.6024);
BzzVector Pmin(4,    -1.,    -3.,      0.01,     0.1);
BzzVector Pmax(4,     4.,     2.,      10.,      10.);

// To Define as Global
BzzVector Pact(4);

// Number of Points along the Reactor
int mMax = 1;
// Length of the Bed [m]
double Lbed = 0.305;
// Pressure [kPa]
double Press = 120.;

// Molecular weight [kg_i/mol_i] m_SO2 m_O2 m_SO3 m_H2O m_N2
m_CO2
BzzVector MW(NC, 64. / 1000., 32. / 1000., 80. / 1000., 18. /
1000., 28. / 1000., 44. / 1000.);

// Area [m2]
double Dint = 0.083;                                      //[m]
```

```cpp
    double A = 0.005410607947645;                        //[m2]

//Function Declaration//

void RegressionText(int model, int ex, BzzVector &b, BzzVector
&x, BzzVector &y);
void F2SistDiff(BzzVector &y, double z, BzzVector &dydz);

int main()
{
    int numModels = 1; // Number of models

    BzzNonLinearRegression nonLinReg(numModels, ICtot,
    xMexp, RegressionText);
    nonLinReg.InitializeModel(1, P0, Pmin, Pmax);
    nonLinReg.SelectCriterion(1);

    BzzVector xMin(NC + 1, 0.022514599, 0.018574544, 0., 0.,
    0.0874229541, 0., 0.588);
    BzzVector xMax(NC + 1, 0.256255993, 0.210364014, 0., 0.,
    0.3595701198, 0., 0.72315);

    //BzzVector xMin(NC + 1, 0.083, 0.042, 0., 0., 0.3234,
    0., 0.588);
    //BzzVector xMax(NC + 1, 0.254, 0.210, 0., 0., 0.3575,
    0., 0.65045);

    nonLinReg.LeastSquaresAnalysisAndExperimentsSearch(xMin,
    xMax);
    nonLinReg.BzzPrint("risultati");

    BzzVector a;
    a = nonLinReg.GetParameters(1);
    a.Save("Parameters.xls");
    return 0;
}

void RegressionText(int model, int ex, BzzVector &b, BzzVector
&x, BzzVector &y)
{
    BzzVector IC_j_act(x);
    //Return to correct dimension
    IC_j_act[5] = IC_j_act[5] * 10;
    IC_j_act[7] = IC_j_act[7] * 1000;
    Pact = b;
    BzzVector w;
```

```
        static BzzMatrix xM(NC, mMax);
        BzzOdeStiff ODEsolver(IC_j_act, 0., F2SistDiff);

        double z = 0.;
        double dz = Lbed / mMax;
        for (int m = 1; m <= mMax; m++)
        {
                z += dz;
                w = ODEsolver(z);

                for (int j = 1; j <= NC; j++)
                {
                        xM[j][m] = w[j];
                }
        }

        BzzVector vTemp(NC);

        for (int l = 1; l <= NC; l++)
        {
                //[kg/h]
                vTemp[l] = xM[l][mMax];
        }
        y = vTemp;
}

void F2SistDiff(BzzVector &y, double z, BzzVector &dydz)
{
        // y [m_SO2 m_O2 m_SO3 m_H2O m_N2 m_CO2 T]
        double T = y[7];

        // Subdivide Value of P
        // d.o.f = [alpha beta k0_kin Ea] - POWER LAW
        double alpha_norm = Pact[1];
        double beta_norm = Pact[2];
        double k0_kin_norm = Pact[3];
        double Ea_norm = Pact[4];

        //Return to correct dimension
        double alpha = alpha_norm;
        double beta = beta_norm;
        double k0_kin = k0_kin_norm*1e6;
        double Ea = Ea_norm*1e3;

        BzzVector Fi(NC);
        double Ftot = 0.;
        BzzVector Pi(NC);
```

```
    BzzVector yi_mol(NC);

    // Calculations
    for (int ii = 1; ii <= NC; ii++)
    {
        Fi[ii] = y[ii] / MW[ii];            //[mol/h]
    }

    for (int jj = 1; jj <= NC; jj++)
    {
        Ftot += Fi[jj];                     //[mol/h]
    }

    for (int kk = 1; kk <= NC; kk++)
    {
        yi_mol[kk] = Fi[kk] / Ftot;         //[-]
        Pi[kk] = Press * yi_mol[kk];        //[kPa]
    }

    // Reaction Rate y [m_SO2 m_O2 m_SO3 m_H2O m_N2 m_CO2 T]
    double R = 8.314;                       //[J/mol/K]
    double DH0R = -98930;                   //[J/mol]
    double Tref = 298;                      //[K]
    double Keq_Tref = 2.5633e+12;   //[-]
    double k0 = Keq_Tref*exp((DH0R / R)*(1 / Tref));
    double Keq_T = k0*exp(-DH0R / (R*T));

    // r [mol/m3/h]
    double k_d = (k0_kin*exp(-Ea / T));
    double term_dir = (pow(Pi[1], alpha)*pow(Pi[2], beta));
    double term_inv = ((1 / (10.066*Keq_T))*pow(Pi[1], alpha
    - 1)*pow(Pi[2], beta - 0.5)*Pi[3]);
    double r = k_d * (term_dir - term_inv);

    // Derivatives
    dydz[1] = -r*MW[1] * A;
    dydz[2] = -0.5*r*MW[2] * A;
    dydz[3] = +r*MW[3] * A;
    dydz[4] = 0.;
    dydz[5] = 0.;
    dydz[6] = 0.;
    dydz[7] = 0.;
}
```